Engineered Microsystems and their application in the culture and characterization of *3-Dimensional* Breast Tumor Models

Nidhi Menon

Dissertation submitted to the Faculty of the
Virginia Polytechnic Institute and State University
in partial fulfillment of the requirements for the degree of

Doctor of Philosophy
in
Translational Biology, Medicine, and Health

Caroline N. Jones, Chair
Blake N. Johnson
Carla V. Finkielstein
Jennifer E. Vaughn
Christopher B. Lawrence

April 30, 2021
Blacksburg, Virginia

Keywords: Breast cancer, Tumor microenvironment, Tumor Extracellular Matrix (ECM), 3D-tumor models, Biomaterials, Hydrogels, Fungal Endophytes, Drug Discovery, Biosensors, FRET

Engineered Microsystems and their application in the culture and characterization of *3-Dimensional* Breast Tumor Models

Nidhi Menon

(ABSTRACT)

Microsystems are a broad category of engineered technologies in the micro and nano scale that have a diverse range of applications. They are emerging as a powerful tool in the field of biomedical research, drug discovery, as well as clinical diagnostics and prognostics, especially with regards to cancer. One of the major challenges in precision and personalized medicine in cancer lies in the technical difficulties of *ex-vivo* cell culture and propagation of the limited number of primary cells derived from patients. Therefore, our aims are to 1. Develop a biologically relevant platform for culturing cancer cells and characterize how it influences the cell growth and phenotype compared to conventional 2-dimensional(2D) cell culturing techniques, 2. Isolate secondary metabolites from endophytic fungi and screen them on the platform for potential anticancer properties in a preliminary drug discovery pipeline, 3. Design and develop biosensors for quantifying cell responses in real-time within these systems.

Several biomaterial scaffolds with microscale architectures have been utilized for engineering the tumor extracellular matrix, but very few studies have thoroughly characterized the phenotypic changes in their cell models, which is critical for translational applications of biomaterial systems. The overall objective of these studies is to engineer a biomimetic platform for the culture of breast cancer cells *in vitro* and to quantify and profile their phenotypic changes. In order to do this, we first evaluated a blank-slate matrix consisting of thiolated collagen, hyaluronic acid and heparin, cross-linked chemically via Michael addition reaction using diacrylate functionalized poly (ethylene glycol). The hydrogel network was used with

triple-negative breast cancer cells and showed significant changes in characteristics, with cells self-assembling to form a 3D spheroid morphology, with higher viability, and exhibiting significantly lower cell death upon chemotherapy treatment, as well as had a decrease in proliferation. Furthemore, the transcriptomic changes quantified using RNA-Seq and Next-Gen Sequencing showed the dramatic changes in some of the commonly targeted pathways in cancer therapy. Furthermore, we were able to show the importance of our biomimetic platform in the process of drug discovery using fungal endophytes and their secondary metabolites as the source for potential anticancer molecules. Additionally, we developed gold nanoparticle and antibody-based (ICAM1 and CD11b) sensors to quantify cell responses spatiotemporally on our platform. We were able to show quenching of the green fluorescent fluorophores due to the Förster Resonance Energy Transfer mechanism between the fluorophore and the gold nanometal surface. We also observed antigen-dependent recovery of fluorescence and inhibition of energy transfer upon the antibody binding to the cell-surface receptors. Future efforts are directed towards incorporating the hydrogel system with antigen-dependent sensors in a conceptually-designed microfluidic platform to spatiotemporally quantify the expression of surface proteins in various cells of the tumor stroma. This includes the migration,infiltration, and polarization of specific immune cells. This approach will provide further insight into the heterogeneity of cells at the single-cell resolution in defined spaces within the 3D microfluidic platform.

Engineered Microsystems and their application in the culture and characterization of *3-Dimensional* Breast Tumor Models

Nidhi Menon

(GENERAL AUDIENCE ABSTRACT)

Microsystems are a broad category of engineered technologies in the micro and nano scale that have a diverse range of applications. They are emerging as a powerful tool in the field of biomedical research, drug discovery, as well as clinical diagnostics and prognostics, especially with regards to cancer. However, a major challenge in being able to offer personalized medicine to cancer patients comes from the difficulty of growing cells from the patient's tumor biopsy in a laboratory for further screening and analysis. There are also limited resources available for real-time expression of proteins on cell-surfaces, that could be potential biomarkers and targets for treatment.

Various natural and synthetic polymers are biocompatible and have been used widely in engineering the tumor extracellular matrix. However, the effect of hydrogels derived from these polymers on the specific tumor cells are not always well characterized. Our studies explore the influence of a biohybrid hydrogel on breast cancer cells and our results show that the microscale architecture of the hydrogel platform works as a suitable scaffold for recapitulating the 3-dimensional(3D) breast tumor microenvironment, and can also be employed in the drug discovery process. Additionally, we developed a nano-scale biosensor to enable the quantification of specific cell-surface proteins in real-time. Ongoing and future efforts are focused on designing and fabricating a microfluidic device with precise control over the design of space and special chambers for cell culture. These will be used for studying interactions of various cells in the tumor microenvironment that influence cancer progression. Integrating these micro-scale systems, including sensors will allow researchers to quantify cell behavior

in response to the variable factors they are exposed to, as well as provide insight to answer fundamental questions about cancer biology that are limited by the conventional 2D cell culture systems.

Dedication

To my family, for their unconditional love and support, especially my parents Kala Menon and Nandakumar Menon. Thank you.

Acknowledgments

I would like to thank my advisor, Dr. Caroline N. Jones for mentoring me over the many years, and for her support and kindness. I also want to thank the members of my committee: Dr. Blake N. Johnson, Dr. Carla V. Finkielstein, Dr. Jennifer E. Vaughn, and Dr. Christopher B. Lawrence. I am grateful for all their support, encouragement and advice. Thank you for taking the time to discuss my projects with me and thank you for helping me grow as a scientist. Thank you also to Dr.Liwu Li and Dr. Luke Achenie for allowing me to rotate in their labs, and to help me hone my molecular biology and computational skills.

I want to take this opportunity to also thank my professors at Purdue University. My undergraduate education was invigorating. It further inculcated in me the inquisitiveness to quench my thirst for knowledge and to pursue my PhD. I want to name and personally thank some of the most inspiring teachers I have had at this institution- Dr. Ganesan Narsimhan, Dr. Osvaldo Campanella, Dr. Martin Okos, Dr. Nathan Mosier, Dr. Priyam Patel, Dr. Kari Clase, and Dr. Jenna Rickus.

My love for science and zest for learning goes all the way back to my young days. I fondly think about my teachers from my days in school for always encouraging me to do better- Dr. Shunila Joy Chauhan, Banshidhar Thakur, Naghma Shaikh, Pradnya Sharma, Sangeeta Varma, Janvi Mehta, and Sarita Pinto.

To my colleague, and friend, Udaya Sree Datla, I am grateful for your kindness, supportive presence, and generosity. This would not have been possible without you. I also want to

thank Maryam Moarefian and Naya Eady, past members of the Jones lab for being great colleagues and friends, as well as Xin He of Dr. Lawrence's lab for being a wonderful neighbor to share science with. It has been my pleasure to mentor undergraduate members of the lab: Trisha Deshmukh, Molly Richelle Thornberg, and Kristina East, and I want to thank them for giving me the opportunity. Thank you also to all the members of the Graduate Program in Translational Biology, Medicine, and Health for all your support. I want to express my gratitude to the administrative and cleaning staff of Life Sciences I, for their hard work in ensuring a safe and clean environment. Special thanks to Dr. Birgit Scharf for her unwavering support and kindness. Thank you also to Dr. Helm for agreeing to support and be involved in my project. Additionally, I want to thank members of the Nikon team-Jacob and Clay, and also Don Leber (Microelectronics facilities manager), and Kristy DeCourcy (Confocal Microscope Facilities Manager) for training me and answering my unending questions.

To my partner and best friend, Shraman Kadapa, thank you for your constant love, support, and encouragement. I would not have been here without you. To my friends, Vidhi Pansari and Craig Dias, thank you for listening to me go on for the last 15 years. I am glad to have you both in my life. Puja Banerjee and Katie Schwartz, thank you for letting me complain about all my failed experiments, and for always lifting my spirits. You guys are my rock! To my friends Chandani Shrestha and Ayaan Kazerouni, thank you for making Blacksburg so much more warm and memorable. I will always cherish our time together. Udaya, Bharath, Edgar, and Poorna, thank you for noticing me during our TBMH orientation and deciding to be my friends. Happy to have had your support over the years. Last but not least, a debt of gratitude to my family for being my source of strength, for being the first people to inspire me and help me develop a sense of curiosity, for their sacrifices in letting me pursue my dreams, and for their unconditional love. Special shout-out to Ruby, my late furry friend and the best sibling I could ask for growing up.

Attributes

Chapter 2 was published in February 2020, in the Royal Society of Chemistry journal Biomaterials Science. Nidhi Menon planned and executed the experiments, carried out data analysis, and wrote the manuscript. Ha X. Dang assisted with the genomic data analysis. Udaya Sree Datla assisted with carrying out the ELISA experiments and analysis. Maryam Moarefian helped with creating the mesh for the COMSOL Computational fluid dynamics simulation. Christopher B. Lawrence, Christopher A. Maher provided valuable feedback and suggestions to improve the manuscript, and Caroline N. Jones supervised the project and guided the overarching direction of the manuscript.

Chapter 3 is a manuscript in preparation for submission. Nidhi Menon planned and executed the experiments, carried out data analysis, and wrote the manuscript. Sebastian Wellford, Molly Richelle Thornberg, and Kristina East assisted with collecting plants, isolating fungi, and purifying extracts. Richard Helm provided the equipment and guided the solid-phase extraction process. Christopher B. Lawrence and Caroline N. Jones directed the project.

Chapter 4 is a manuscript in preparation for submission. Nidhi Menon planned and executed the experiments, carried out data analysis, and wrote the manuscript. Yang Liu helped with brainstorming and carried out preliminary experiments and data analysis for the initial stages of the project. Trisha Deshmukh assisted with microarray experiments and optimization. Blake N. Johnson and Caroline N.Jones co-supervised the project and provided valuable feedback and direction.

Contents

List of Figures

List of Tables

List of Abbreviations

Ab Antibody

AuNP Gold nanoparticle

ECM Extracellular Matrix

EGF Epidermal Growth Factor

FRET Förster Resonance Energy Transfer

GF Growth Factor

HP-B Heparin-based

MCS Multicellular spheroid

NSET Nanometal Surface Energy Transfer

PDA Potato Dextrose Agar

PDB Potato Dextrose Broth

PEG Poly(ethylene glycol)

TME Tumor Microenvironment

TNBC Triple-negative breast cancer

Chapter 1

Introduction

1.1 The Breast Tumor Microenvironment

Breast cancer is the most commonly diagnosed cancer in women. Despite an improvement in overall survival rates, metastatic breast cancer and recurrent disease has a poor prognosis[1]. The breast tumor microenvironment (TME) is a complex architecture composed of diverse range of cells present in the tumor stroma. The earliest studies investigating this complex milieu of cells were able identify a diverse host of cell immune cells as a common component of the tumor archetype[2, 3]. We now know that cells interacting in, and infiltrating the tumor microenvironment are beyond plenty, and include fibroblasts, T and B cell lymphocytes, neutrophils, macrophages, Natural killer cells, dendritic cells, Myeloid derived suppressor cells, adipocytes, and have their own blood vasculature supported by pericytes and vascular endothelial cells[4]. Extensive studies have revealed how the cells of the tumor stroma can be polarized by the intricate signals in the microenvironment and contribute to tumor growth, progression, angiogenesis, metastasis, and drug resistance[1, 4, 5, 6, 7, 8]. While the endogenous and exogenous signaling is critical, these are further influenced by the presence of the tumor extracellular matrix(ECM)[9]. Some of the components of the breast tumor ECM include collagens, glycosaminoglycans, proteoglycans, fibronectin, elastin, tenascin, and a plethora of matrix metalloproteinases[10, 11, 12, 13]. The intricacies of the tumor

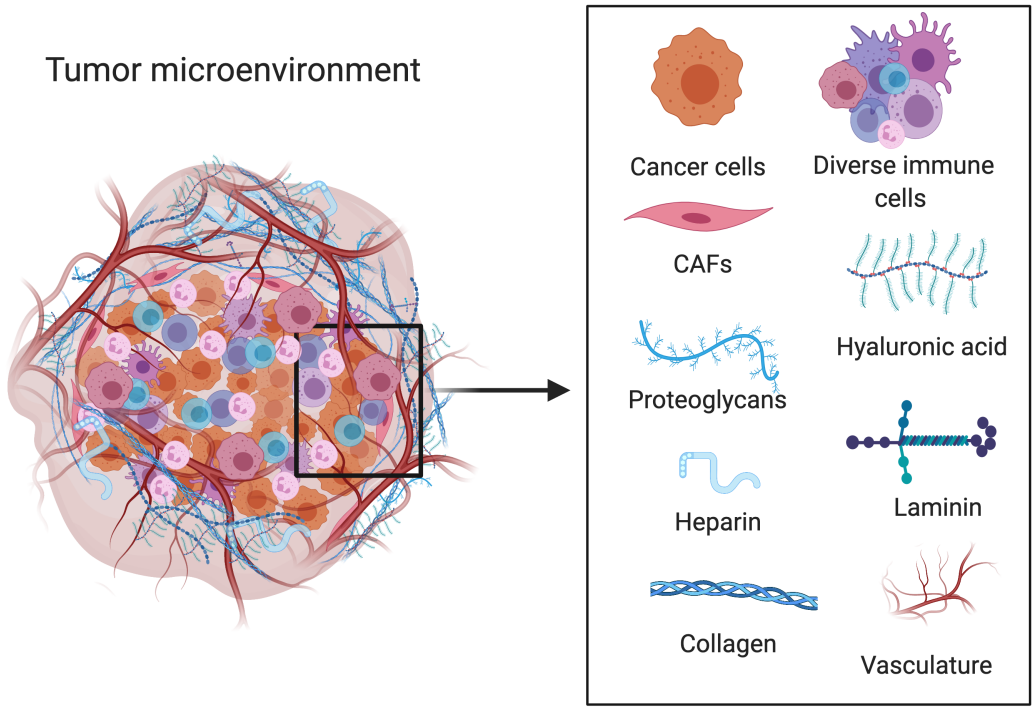

Figure 1.1: **Components of the Tumor Microenvironment.** Apart from cancer cells, the tumor microenvironment is also home to a diverse range of tissue-resident cells. These include cancer-associated fibroblasts (CAFs),immune cells such as T cells, B cells, macrophages, neutrophils, dendritic cells, and natural killer (NK) cells, among others. The tumor ECM architecture plays a critical role in the tumor microenvironment, and is a diverse mixture of various structural and fribrillar proteins, glycosaminoglycans, as well as proteoglycans. Additionally, there is also a complex network of vasculature running through the system.

microenvironment are shown in Figure 1.1 below.

1.1.1 Biomaterials for engineering tumor extracellular matrix

Since gaining a deeper understanding of the tumor tissue architecture, a significant amount of attention has been diverted to engineering the extracellular matrix using a range of biomaterials. Biomaterials, primarily hydrogels have been used in this attempt to mimic tissue

mechanics and biology. Hydrogels are hydrophilic 3D networks of polymers that can be tuned to obtain the desired properties for its application and response to environmental interactions. There is a plethora of physical and chemical crosslinking mechanisms for synthesis of the polymer networks[14, 15]. Chemical methods include thiol-based reactions, using Thiol-ene or Michael-addition reactions. Aldehyde functionalized monomers can also be used for Schiff-based cross-linking with amine groups. Diel's Alder based click chemistry is often used with diene and dienophile functionalized polymers. Photoinitiated polymerization can happen either under visible light or UV-exposure in the presence of photo-reactive molecules. Enzyme-catalyzed reactions can initiate cross-linking by formation of specific linkages between functional groups. Physical cross-linking mechanisms can be based on electrostatic, hydrophobic interactions, hydrogen bonding, as well as via thermal, shear and pH responsive materials[16]. The design and components of the hydrogel vastly influence diffusion and mass transfer in the system, as well as cell morphology, phenotype, and drug resistance. [17, 18]. The various hydrogels tried and tested for engineering the extracellular matrix of the tumor microenvironment have ranged from natural, semi-synthetic to synthetic. Figure 1.2 gives a brief summary of the types of hydrogels and crosslinking mechanisms.

Natural hydrogels

Naturally derived hydrogels have protein or polysaccharide-based backbones[19]. Some of the protein-based hydrogels in the market include collagen, gelatin, elastin, fibrin, silk fibroin, laminin. Some of the polysaccharide-derived hydrogels are glycosaminoglycans like hyaluronic-acid, heparin, alginate, and chitosan[20]. Additionally, there are ECM-based hydrogels derived from decellularized tissue, like the widely used Matrigel (a natural reconstituted basement matrix derived from Engelbreth-Holm-Swarm mouse sarcoma)[21].

Synthetic hydrogels

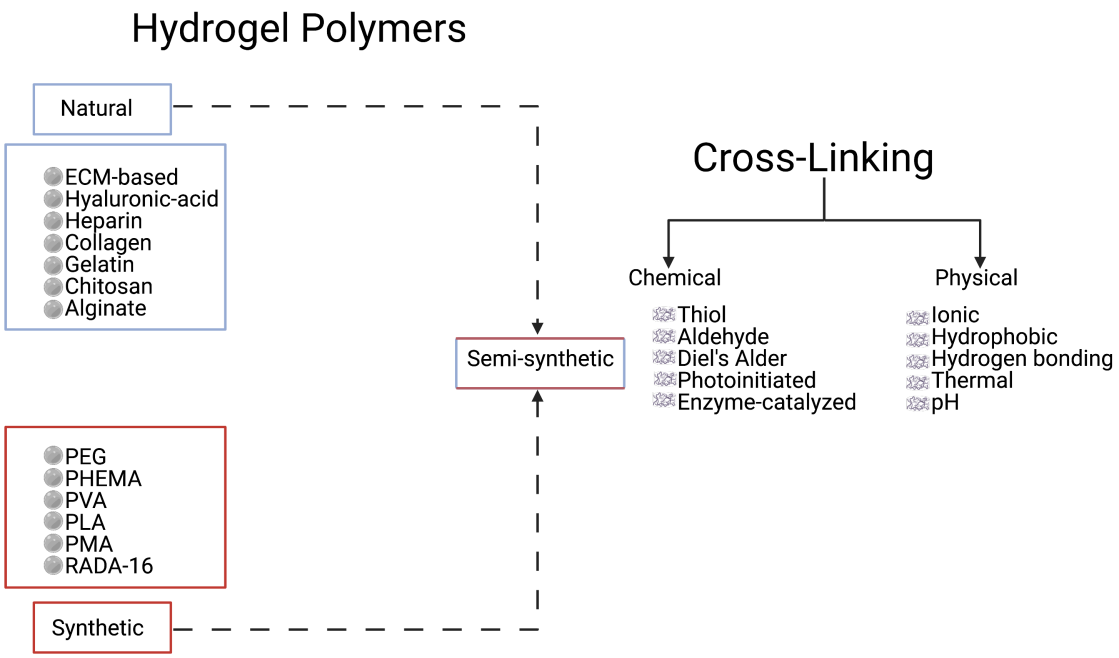

Figure 1.2: **Hydrogel polymer networks and cross-linking strategies.** Various natural and synthetic polymers can be used for applications in engineering the tumor extracellular matrix, cross-linked using one of the diverse chemical or physical means, to obtain the desired biochemical and mechanical properties.

Some of the prominent synthetic hydrogel networks are derivatives of non-natural polymers like poly (ethylene glycol) (PEG), poly(hydroxyethyl methacrylate) (PHEMA), poly (methyl acrylate) (PMA), poly(vinyl alcohol) (PVA), poly(lactic acid) (PLA)[22, 23]. While natural polymers have the biomimetic advantage, synthetic hydrogels provide more control over properties, and have better durability due to slower degradation[24].

Semi-synthetic hydrogels

Biohybrid hydrogels consist of a balance of natural and synthetic polymers to provide a holistic environment for cells, along with being able to control some of the critical rheological characteristics[22]. This is done by incorporating specific binding moieties, structural proteins, or other ECM proteins for a more tunable hydrogel and to avoid the unquantifiable effects from the variability observed from natural derivatives[25].

1.1.2 Solid-phase presentation of growth-factors in the tumor extracellular matrix

Choosing a suitable microenvironment for a cell model from the abundant options for engineering hydrogels is a daunting task. Hyaluronic acid and collagen have been widely used to engineer the hydrogel scaffolds for *in vitro* cancer cell culture due to their abundance in the tumor extracellular matrix[26, 27]. While there has been previous emphasis on the importance of heparin sulfate proteoglycans in the breast tumor microenvironment, especially with respect to growth factor binding and delivery, very few hydrogels have characterized a holistic biomimetic hydrogel with heparin as a critical component[28]. Therefore, the ability to present endogenous and exogenous signals in the microenvironment in solid-phase by the integral components of the ECM are critical for mimicking the *in vivo* tumor microenviron-

ment.

Biomaterial scaffolds that recapitulate the tumor microenvironment in its presentations of signals, providing the right mechanical stiffness for *in vitro* cell culture are not always thoroughly characterized for the cell models they are used with. The differences during initial seeding of cells in 2D and 3D models are not well understood, especially during the self-assembly and formations of multicellular spheroids (MCSs). To add to this, stimulating cells with GFs in 2D vs 3D cell model systems have shown considerable changes in phenotype. However, these have not been well documented in popular breast cancer cell models.

1.2 *In vitro* screening for cancer therapies

Potential anticancer drugs have close to a 7% rate of translation into approval[29]. Engineering biomimetic *in vitro* tumor models have become increasingly important in order to improve this low rate of conversion from discovery through approval, especially due to the high costs incurred from entering ineffective drugs into clinical trials. As aforementioned, engineering the tumor extracellular matrix and developing complex microfluidic devices to capture the interactions of the tumor stroma have been on the rise. Several of these microscale platforms have specifically been used for applications in drug screening. Studies have shown repeatedly the importance of using 3D models of tumors compared to 2D models for applications in drug discovery and screening[30, 31]. Additionally, microfluidics devices have been developed to study combinatorial drugs treatments with these tumor models[32, 33]. There has also been a growth in the use of 3D models using *ex-vivo* culture of patient-derived tumors for personalized treatment. One study used a 3D hydrogel, VersaGel, to screen clinical treatments for Glioblastoma using cells from 5 patients, and found that the platform

predicted clinical outcomes for treatment with temozolomide for all of them[34]. Several new companies have emerged in the last few years that are now working on providing services for personalized treatment to cancer patients using *ex vivo* models.

1.2.1 Natural Products in Drug Discovery

Natural products and their derivatives have long been used in drug discovery, having contributed close to 35% of the approved drugs in the market[35]. Approximately 41% of the drugs approved for anti-tumor therapy have been credited to natural sources[35]. Some of the prominent sources are plants, which constitute for about 75% of the naturally inspired drugs approved[36]. Other natural sources include marine and other animals, microbes, such as bacteria and fungi. The biological diversity provides for abundant natural sources. However, the abundance also points to the prospects of undiscovered compounds with potential health benefits that are yet to be explored.

1.2.2 Fungal Endophytes in Drug Discovery

Fungal endophytes are a class of symbiotic fungi that reside in the internal tissues of plants. Individual plants can be host to hundreds of endophytic fungi that could be found in tissues of various parts of the plant[37]. Secondary metabolites from endophytic fungi have shown promising outcomes in the treatment of various disease pathologies, including cancer[38]. Plant endophytes offer several advantages in drug discovery over their pathogenic fungal counterparts due to its co-inhabiting properties, rarely adversely affecting its host[39]. Since the discovery of Paclitaxel in Northwest Pacific yew endophyte, endophytes have contributed

significantly to the discovery of novel anticancer compounds[40]. Despite the plethora of endophytes inhabiting the several thousand species of plants, and their highly potential medicinal properties, they continue to remain largely under-studied. Therefore, there is a huge untapped opportunity to isolate and discover novel natural compounds from secondary metabolites with pharmaceutical benefits, especially in the fight against cancer. Screening natural compounds in the appropriate *in vitro* cancer models will provide a better understanding of their efficacy.

1.3 Quantifying cell responses *in vitro*

Cell-based assays that quantify changes at the genomic or proteomic level usually rely on end-point experimental data or are used for cell-separation in the beginning of studies. While these provide important information during their respective time-points, critical information is lost during the time-frame of the study due to lack of biosensors that can provide real-time quantification. This is especially important when studying cell-cell interactions or during drug screening applications. Monitoring cell behavior during assays *in vitro* can provide incredibly valuable information.

1.3.1 Conventional Immunoassays and Molecular Biology Techniques

The most widely used techniques for specific protein detection and quantification are immunohistochemistry, immunofluorescence(IF) staining, flow cytometry, ELISA, and western

blot. These antibody-based assays are the gold-standards and have been used for decades as such. The limitations of these assays include the lack of temporal quantification, as well as in some cases requires the fixation or lysis of cells to obtain the required information. Similarly, in case of molecular biology techniques, like the different types of PCR, and Next-Gen Sequencing methods, extraction of genomic material from cells is necessary. While massive amounts of information can be obtained at the genomic levels using these techniques, it is not compatible for monitoring cell responses spatially and over time.

1.3.2 Biosensors for real-time sensing and quantification

There is a range of biosensors that have been developed for analyte detection. They are composed of a bioelement, such as an antibody, enzyme, or nucleic acids. They also consist of a sensing mechanism or sensor element that can be based on optical, fluorescent, electric current, electric potential, electrical conductance, impedance, temperature, mass, or viscosity changes[41]. Most sensors today have high sensitivity and detection range, but generally require immobilization of the detecting element and target analyte[42, 43, 44]. Additionally, most of these sensors require complex methods for design as well as downstream signal calibration and quantification. In order to detect cell-surface proteins during live cell imaging, different types of optical sensors have been developed. Fluorescence is the dominant analytical method used for detection and has a lower cost of design and fabrication[45].

1.3.3 Applications of Förster Resonance Energy Transfer (FRET) in biosensing

Förster Resonance Energy Transfer (FRET) is a process of nonradiative energy transfer through long-range dipole-dipole coupling, via energy transfer between a fluorescent donor and acceptor molecule[46]. This mechanism of energy transfer has been utilized in sensing with luminescent quantum dots, bioelements conjugated with fluorophores and metal acceptors, and several other donor-acceptor interactions for applications in cell biology imaging[47, 48, 49]. More recently, there has been an interest in quenching-based approach and antigen-dependent recovery of fluorescence. A complex engineering of antibody probes, called quenchbodies, utilizes FRET between the fluorophore and tryptophan residues in the variable region interface[50]. However, due to the complex engineering of the probe, similar quenching approaches have now been utilized with fluorophores and metal nanoparticles as acceptors[51]. This donor-acceptor complex between fluorophores and nanometal surfaces can be exploited to develop simple, yet effective fluorescence biosensors to detect cell-surface antigens.

1.4 Conclusions

Engineering microsystems for the culture and characterization of 3D tumor models are beneficial for several applications in biomedical research. Recapitulating the tumor microenvironment is critical for applications in drug screening and developing micro-scale biosensing technologies to be used in conjunction with these platforms will enable quantification of bi-

ological changes spatiotemporally in these tumor model systems. Currently, the solid-phase presentation of GFs due to ECM proteins in the tumor microenvironment are not well studied. Additionally, there is a lack of simple, real-time sensors to quantify phenotypic changes in 3D systems and for studying their interactions with other cells in the tumor stroma.

The goal of the studies that follow are to evaluate the influence of a heparin, hyaluronic acid and collagen- based semi-synthetic blank-slate matrix (cross-linked with PEG) on triple-negative breast cancer cell line MDA-MB-231. The ECM components are prominent in the breast tumor microenvironment and function as growth-factor binding moieties. The model is then used in a preliminary drug discovery process using promising fungal endophyte extracts with potential anticancer properties. Following which, an optical, FRET-based biosensor is developed to measure spatiotemporal changes of receptor expressions on cell-surfaces. Ultimately, the aim is to mimic the breast tumor microenvironment *in vitro* and quantify phenotypic changes in various cells of the tumor stroma using real-time biosensors within microfluidic platforms. This is to shed light on the degree of heterogeneity observed in the tumor stroma at a single-cell resolution. The studies provide insight into breast tumor compatible hydrogels and their application in drug discovery, as well as the development of a simple, effective biosensor for measuring expression of cell-surface proteins.

Chapter 2

Heparin-based hydrogel scaffolding alters the transcriptomic profile and increases the chemoresistance of MDA-MB-231 triple-negative breast cancer cells

2.1 Abstract

The tumor microenvironment plays a critical role in the proliferation and chemoresistance of cancer cells. Growth factors (GFs) are known to interact with the extracellular matrix (ECM) via heparin binding sites, and these associations influence cell behavior. In the present study, we demonstrate the ability to define signals presented by the scaffold by pre-mixing growth factors, such as epidermal growth factor, into the heparin-based (HP-B) hydrogel prior to gelation. In the 3D biomimetic microenvironment, breast cancer cells formed spheroids within 24 hours of initial seeding. Despite higher number of proliferating cells in 2D cultures, 3D spheroids exhibited a higher degree of chemoresistance after 72

hours. Further, our RNA sequencing results highlighted the phenotypic changes influenced by solid-phase GF presentation. Wnt/β-catenin and TGF-β signaling were upregulated in the cells grown in the hydrogel, while apoptosis, IL2-STAT5 and PI3K-AKT-mTOR signaling were downregulated. With emerging technologies for precision medicine in cancer, this nature of fine-tuning the microenvironment is paramount for cultivation and downstream characterization of primary cancer cells and rare circulating tumor cells (CTCs), and effective screening of chemotherapeutic agents.

2.2 Introduction

The tumor microenvironment is a result of tumor-derived signals, interactions with the extracellular matrix (ECM) and the surrounding tissue and is known to play a critical role in tumor initiation, progression, and chemoresistance[52, 53, 54, 55]. Interactions between the cell and its extracellular environment and neighboring cells are vital for survival, growth, and differentiation[56]. Conventional two-dimensional (2D) monolayer cultures are incapable of reproducing the characteristic features of tumors *in vivo*. While 2D cell culture experiments have contributed significantly to our understanding of cancer, they are unable to provide key insights into the features of the tumor interactions with the surrounding microenvironment. Recent statistics estimate approximately 90% of chemotherapies and immunotherapies fail when translated to *in vivo* solid tumors, despite promising *in vitro* experiments[57].

The hanging-drop method[58], the use of non-adhesive substrates[59], and orbital shaking[60] have been previously used to form spheroids in aqueous culture. However, none of these methods encourage self-assembly, but are rather focused on external physical stimuli to encourage cell aggregation. The use of hydrogels as a biomimetic niche have shown notable

changes in cell behavior[61, 62, 63, 64, 65, 66, 67, 68]. While previous studies have introduced novel natural and synthetic materials for controlling biological and mechanical properties, they are limited in their molecular characterization of tumor cells in their microenvironment. Moreover, there is minimal control over GF presentation and delivery, which is essential for optimal cell response[69]. In contrast, hyaluronic acid and heparin-based hydrogels have proven to be potent scaffolds for primary cell culture and mimic the slow, controlled release of GFs *in vivo*[69, 70, 71, 72, 73, 74, 75, 76, 77, 78]. Epidermal growth factor (EGF) plays a vital role in controlling breast tumor cell growth and differentiation. Overexpression of the EGF receptor (EGFR) has been well documented in breast carcinogenesis[79]. In order to test the capacity of the HP-B hydrogel system for cultivation of breast tumor cells, EGF was used to study the strength of heparin as a GF binding moiety. Furthermore, EGF stimulation was used as a model for studying the differences between localized stimulation using HP-B hydrogel versus aqueous stimulation in growth media. Identifying the genotypic and phenotypic differences between 2D cultures and 3D spheroid cultures are essential for studying tumor response to drugs and to further scrutinize underlying mechanisms conferring adaptive resistance to tumors *in vivo*.

Our study investigated the use of HP-B hydrogel as a biomimetic scaffold for the solid-phase presentation of EGF as well as GFs and endogenous signaling molecules (Figure 2.1). A triple-negative breast cancer (TNBC) cell line (MDA-MB-231) was used as a model. Due to a lack of targeted therapies for this aggressive breast cancer subtype, chemotherapy remains the standard source of treatment. Paclitaxel promotes mitotic arrest and cell death by binding to microtubules and has shown promising results in the triple-negative cohort[80]. Therefore, Paclitaxel was used to study the chemoresistance in these cells. Cells were grown in four conditions; (1) control in a glass dish, (2) EGF supplemented in solution (EGF (aq)) in a glass dish, (3) HP-B hydrogel and (4) HP-B hydrogel pre-mixed with EGF in solid-phase

(HP-B hydrogel + EGF (s)). Viability, proliferation and chemoresistance to paclitaxel were quantified. Additionally, to quantify the genotypic and phenotypic changes observed from sequestration and presentation of solid-phase GFs to breast tumor cells, RNA Sequencing was carried out on cells grown in the conditions mentioned above. This study shows that the microenvironment significantly alters the transcriptomic profile of MDA-MB-231 and increases chemoresistance to paclitaxel.

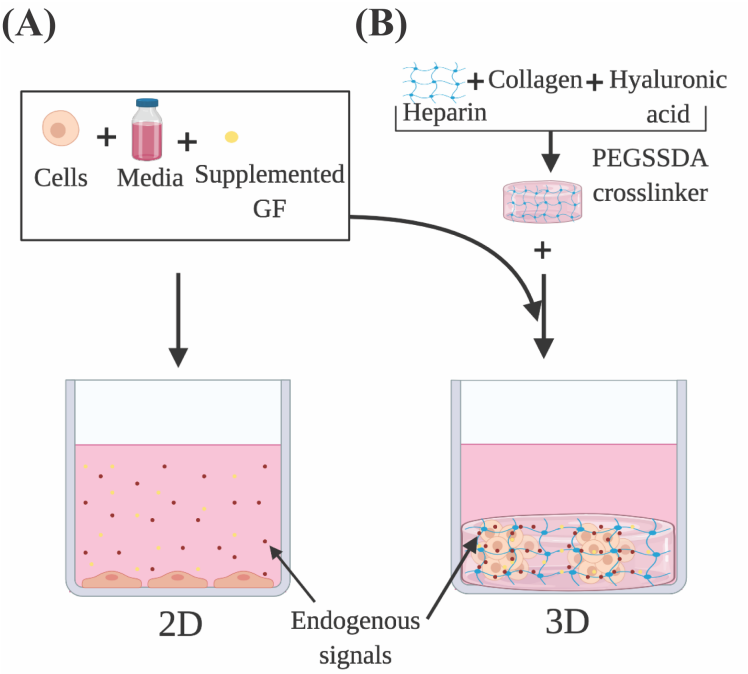

Figure 2.1: **Heparin-based (HP-B) hydrogel for 3D cell culture vs. standard 2D culture in a glass-bottom dish.** In this study, we demonstrate that HP-B hydrogel promotes spheroid formation in breast cancer cells and significantly alters the transcriptomic profile and phenotype of cells compared to standard culture conditions. **(A)** The presentation of growth factors and endogenous signals in aqueous media cannot be precisely controlled. The cells are adherent to the surface, have a flattened morphology and form a 2D monolayer. **(B)** Heparin-based hydrogel acts as a biomimetic tumor niche and promotes solid-phase presentation of growth factors and endogenous signals secreted by the cells, as depicted. The presence of extracellular matrix proteins encourages self-assembly into a spheroid morphology.

PI3K-AKT-mTOR signaling is one of the most commonly targeted pathways for cancer

therapy. However, a study highlighted the aberrant changes in Wnt/β-catenin signaling in response to PI3K inhibitors and implies crosstalk between the two signaling pathways to confer resistance to PI3K inhibitors. Furthermore, dual inhibition of PI3K and Wnt signaling pathways *in vivo* and *in vitro* had a higher synergistic effect compared to inhibition of PI3K alone[81]. Tumor Necrosis Factor Alpha (TNFA) signaling via NF- B is another multifunctional pro-inflammatory pathway that has been known to negatively affect EGFR activation[82]. Another important pathway, TGF-β signaling, has been studied extensively in solid-tumors. It is known to function as a potent immunosuppressor, affecting normal lymphocyte proliferation and maturation in the tumor microenvironment[83, 84]. IL2-STAT5 signaling is also critical for T-cell development and IL2 has been approved for cancer immunotherapy in treating metastatic renal cell carcinoma and metastatic melanoma[85]. IL2 suppression is also known to be mediated by TGF-β[86]. Our results highlight changes in these cancer hallmark pathways, observed in the different microenvironments. HP-B hydrogel is a promising biomimetic scaffold, critical for initial screening and successful translation of novel, targeted therapies to overcome resistance in triple-negative breast cancer.

2.3 Materials and Methods

2.3.1 MDA-MB-231 cell culture

Triple-negative breast cancer cell line MDA-MB-231 (American Type Cell Culture HTB-26) was cultured in Gibco™ Dulbecco's Modified Eagle's Medium F-12 (DMEM/F-12) containing high glucose and GlutaMAX™, supplemented with 10% fetal bovine serum (FBS) and 100 units per ml penicillin and 0.1 mg ml−1 streptomycin. The cells were maintained in

vented T-25 or T-75 flasks (corning) at 37°C and 5% CO2. Media was changed every 48 hours. Using 0.05% Trypsin-EDTA for detachment, cells were harvested for experiments at 80–90% confluency.

2.3.2 Heparin hydrogel preparation

HyStem-HP Hydrogel Kit with PEGSSDA (ESI BIO GS315P) was used to prepare heparin hydrogel with a collagen I background. The kit is comprised of lyophilized solids of Heprasil® (thiol-modified sodium hyaluronate with thiol-modified heparin), Gelin-S® (thiol-modified gelatin), PEGSSDA™ (disulfide containing polyethylene glycol diacrylate), and degassed deionized water (DG Water). All vials are allowed to reach room temperature. Heprasil® and Gelin-S® are reconstituted in DG water to form 1% (w/v) solution, and PEGSSDA™ is reconstituted in DG water to form 2% (w/v) solution. Heprasil® and Gelin-S® vials are placed horizontally in a shaker for 40 minutes for complete dissolution. Solutions of Heprasil® and Gelin-S® are mixed in a 1 : 1 volume ratio. PEGSSDA™ works as a crosslinker and is mixed in a 1 : 4 volume ratio with the Heprasil® and Gelin-S® mixture to initiate gelation. Time for complete gelation is dependent on the volume and surface area occupied by the gel and is approximately 4 hours per ml.

2.3.3 Quantification of EGF retention in HP-B hydrogel

HP-B hydrogel was pre-mixed with 50 ng ml^{-1} EGF. 1.5 mL of this pre-mixed hydrogel was added to a 12-well plate (n = 3) and allowed to gelate for about 4 to 5 hours at room temperature. Following this, 1.5 mL of serum-free, EGF-free growth media was added on top

of the hydrogel in each of the wells and incubated at 37°C. The supernatant was collected, and the wells were replenished with 1.5 ml of fresh serum-free, EGF-free media every 24 hours for a total of 72 hours. The collected supernatants were analyzed for total EGF content, using EGF Human ELISA kit (Invitrogen, KHG0061). Previous studies have validated a normalization factor to account for the degradation of the protein in heparin-based hydrogel, that was used to post-process our data from ELISA[87].

2.3.4 Simulation of EGF retention in HP-B hydrogel

COMSOL Multiphysics® 5.2 was used to simulate the diffusion of EGF through the heparin hydrogel porous media and determine heparin-EGF binding. To reflect the experimental setup, the dimensions of the 1.5 ml hydrogel and media were based on the 12-well plate. The diffusion coefficient of EGF in water [(D_{EQ}) was calculated using the semiempirical eqn (2.1) of Polson[88] shown below. The diffusion coefficient was corrected for heparin-EGF binding (D_{EH}) using eqn (2.2) governing diffusion when protein binding is present[88]. Fick's first law of diffusion, inbuilt in the software was used to run the simulation, taking into consideration the porosity (69%) of the gel.

$$D_{EW} = \frac{9.410x10^{15}(T)}{\mu(M_E)^{\frac{1}{3}}} \tag{2.1}$$

wherein T (37°C) is the temperature, (6.913×10^{-4} Pa.s) is the viscosity of water and ME(6.2 kDa) is the molecular weight of EGF.

$$D_{EH} = D_{EW}(1 - 1.81x10^{-3}c_H)\left[\left(\frac{\%FreeE}{100}\right) + D_H\left(\frac{\%BoundE}{100}\right)\right] \quad (2.2)$$

wherein c_H is the concentration of heparin and hyaluronic acid (4 kg m^{-3}), D_H is the diffusion coefficient of heparin, assumed to be 0 in the hydrogel, due to the crosslinking of the matrix.

2.3.5 Characterization of viability and chemoresistance

Cells were grown in 96-well plates (Cellvis P96-1.5H-N) (n = 3) with a low seeding density of 1000 cells per well. Cells were grown in four different conditions: (1) 100 l of complete growth media (control), (2) 100 l of complete growth media supplemented with 50 ng ml^{-1} EGF (Sigma E9644) in solution (EGF (aq)), (3) 50 l HP-B hydrogel topped with 100 l of complete growth media (HP-B hydrogel), (4) 50 l HP-B hydrogel pre-mixed with 50 ng ml^{-1} EGF (HP-B hydrogel + EGF(s)). Media (100 μl) was replenished every 24 hours. At the end of 72 hours, a live and dead cell assay (Abcam, ab115347) was performed to assess the viability of cells. In order to quantify chemoresistance, cells were allowed to grow for 48 hours prior to the addition of 100 l of 100 nM paclitaxel. The cells were treated for 24 hours and images were taken at the 72-hour mark using the live and dead cell assay. Images of live (labeled green) and dead (labeled red) cells were taken on the Zeiss LSM 880 confocal microscope at 40× magnification. A manual cell counter on the open source software ImageJ/Fiji [89] was used to count the live and dead cells in the image frame. ANOVA and Tukey's honest significant difference was used to compare the mean percentage of dead cells in all the groups.

2.3.6 Proliferation assay

MDA-MB-231 cells were cultured on cover slips (1.5, 0.16 mm) embedded in 12-well plates (MatTek) (n = 3) for immunohistochemistry experiments. The cells were grown in the same four aforementioned conditions. The coverslip was coated with 50μ l of the hydrogel for the two HP-B hydrogel samples. Cells were seeded at 1000 cells per well. Media was changed every 24 hours and cells were allowed to grow for 72 hours. Cells were fixed with 4% formaldehyde (Sigma 818708) and permeabilized using 0.5% Triton™ X-100 (Sigma ×100). 1% BSA was used as the blocking solution and the specimens were incubated for 30 min. Samples were then incubated overnight at 4 °C with primary rabbit monoclonal anti-Ki-67 (abcam ab16667). Cells were then washed with PBS before incubating with the secondary goat anti-rabbit IgG H&L conjugated with Alexa Fluor® 488 (abcam ab150077) for 1 hour in the dark. Images were taken using the Zeiss confocal microscope (Zeiss LSM 880) at 40× magnification. ANOVA and Tukey's honest significant difference was used to compare the mean percentage of Ki-67 stained cells in all the groups.

2.3.7 RNA sequencing

Cells were grown in 12-well plates (n = 2) with a density of 2.5 × 104 cells per well in 1.5 ml of complete growth media. Cells were grown in the same aforementioned conditions listed in 2.5, except 1.5 ml of the hydrogel was used as a platform for the wells subjecting cells to HP-B hydrogel. Media was replenished every 24 hours. Total RNA was isolated from cells after allowing the cells to grow for 72 hours. For cells grown on the plate, cells were retrieved using trypsin whereas for cells encapsulated within the hydrogel, liquid nitrogen was used to

flash freeze the gel and a mortar and pestle were used to powder the frozen gel. All samples were then processed with Trizol reagent (Life technologies 15596026). Chloroform (Fisher BP1145-1) was added for phase separation, which was carried out using centrifugation at 12x000g at 4°C for 5 minutes. The aqueous phase was then processed using the RNeasy mini kit (Qiagen 74104) according to the manufacturer's instructions. Eluted RNA was stored in −80 °C. Quality of total RNA was checked on Agilent Tapestation 2200 (Agilent Technologies, Santa Clara CA). 100 ng of total RNA was processed with New England Biolabs (NEB) Next rRNA Depletion Kit (NEB E6310X) to produce rRNA depleted RNA for RNA sequencing. RNA Seq Library preparation was performed with NEBNext Ultra II Directional RNA Library Prep Kit for Illumina (NEB E7760L) and individual samples/libraries were indexed separately using the NEBNext Multiplex Oligos for Illumina (NEB E6609S) for sequencing on the Illumina NextSeq 500/550 High Output kit V2 (75 cycles) (P/N FC-404-2005) to 1×75 (400 million clusters). 13 cycles of PCR enrichment were used to amplify Adapter Ligated DNA. The 300 bp libraries generated are validated using Agilent 2200 Tapestation and quantitated using Quant-iT dsDNA HS Kit (Invitrogen, Q33120) and qPCR. The Illumina NextSeq Control Software v2.1.0.32 (http://illumina.com) with Real-Time Analysis RTA v2.4.11.0 was used to provide the management and execution of the NextSeq 500 and to generate BCL files. The protocol is outlined in the schematic in Supplementary Figure 2.7.

2.3.8 RNA sequencing data analysis

We obtained 21.3 million reads per sample. Raw RNA-Seq reads were trimmed to remove adaptors and demultiplexed using bcl2fastq Conversion Software v2.20 (http://illumina.com). Reads were aligned to the human reference genome Grch38/hg38 using Hisat2[90] and

Bowtie2[91]. Average alignment rate was 95%. FeatureCounts[92] was used to count reads aligned to genes using Gencode annotation v27[93]. Raw read counts were used for subsequent TMM normalization and differential expression analysis using negative binomial model with edgeR v3.22,3[94]. False discovery rate (FDR) was estimated to correct for multiple hypothesis test using Benjamini–Hochberg procedure. Normalized gene expression was used in gene set enrichment analysis (GSEA)[95] to identify cancer hallmark pathways/gene signature altered in EGF (aq), HP-B hydrogel, and HP-B hydrogel + EGF (s) compared with the control group. All statistical analysis and visualization were performed using the R software package v3.5.1[96].

2.4 Results

2.4.1 HP-B hydrogel for long-term, solid-phase EGF presentation

The cumulative percentage release of EGF was less than 5% of the initial bound EGF over a period of 3 days. $96.73 \pm 0.53\%$ of the EGF was retained in the HP-B hydrogel over 72 hours (Figure 2.2**(A)**). Furthermore, to calculate the heparin-EGF binding, a COMSOL model was used to simulate the system (refer to methods for COMSOL Simulation) (Figure 2.2**(B)**). A 99.5% or higher binding rate corroborated the experimental data and resulted in 96% of the EGF being retained over the 72-hour period. The time-lapse simulation demonstrates the high retention of EGF from HP-B hydrogel (Video Reference 2.9).

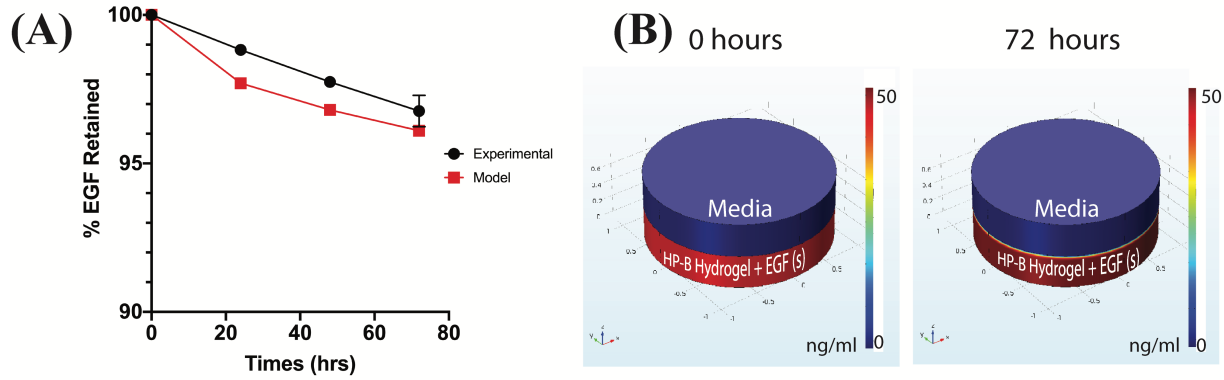

Figure 2.2: **Quantification of EGF release from HP-B hydrogel.(A)** Results from ELISA demonstrate the high retention of EGF in the HP-B hydrogel and this is confirmed by the protein-binding diffusion model. Over 95% of the initial EGF is retained at the end of 72 hours. **(B)** COMSOL multiphysics graphs of the diffusion model illustrate the minimal release of EGF observed after 72 hours.

2.4.2 HP-B hydrogel induces spheroid formation in breast cancer cells and keeps them more viable

MDA-MB-231 cells in the hydrogel formed multicellular (<100 cells) spheroids (100 m) within 24 hours of initial seeding. The cell viability was measured at 72 hours using a live and dead cell assay (Figure 2.3**(A)**). Cell viability in 2D showed a higher variability of viability. At 72 hours, cells in the control condition had 12.9 $\pm$ 4.074% dead cells whereas cells encapsulated in the HP-B hydrogel had only 1.048 $\pm$ 0.24% dead cells. Cells supplemented with aqueous EGF had 13.06 $\pm$ 4.046% dead cells unlike the cells grown in HP-B hydrogel with solid-phase EGF, which had a 1.107 $\pm$ 0.39%. Both hydrogel groups had a significant improvement in viability (*p $<$ 0.05) compared to the control and supplemented EGF (aq) conditions.

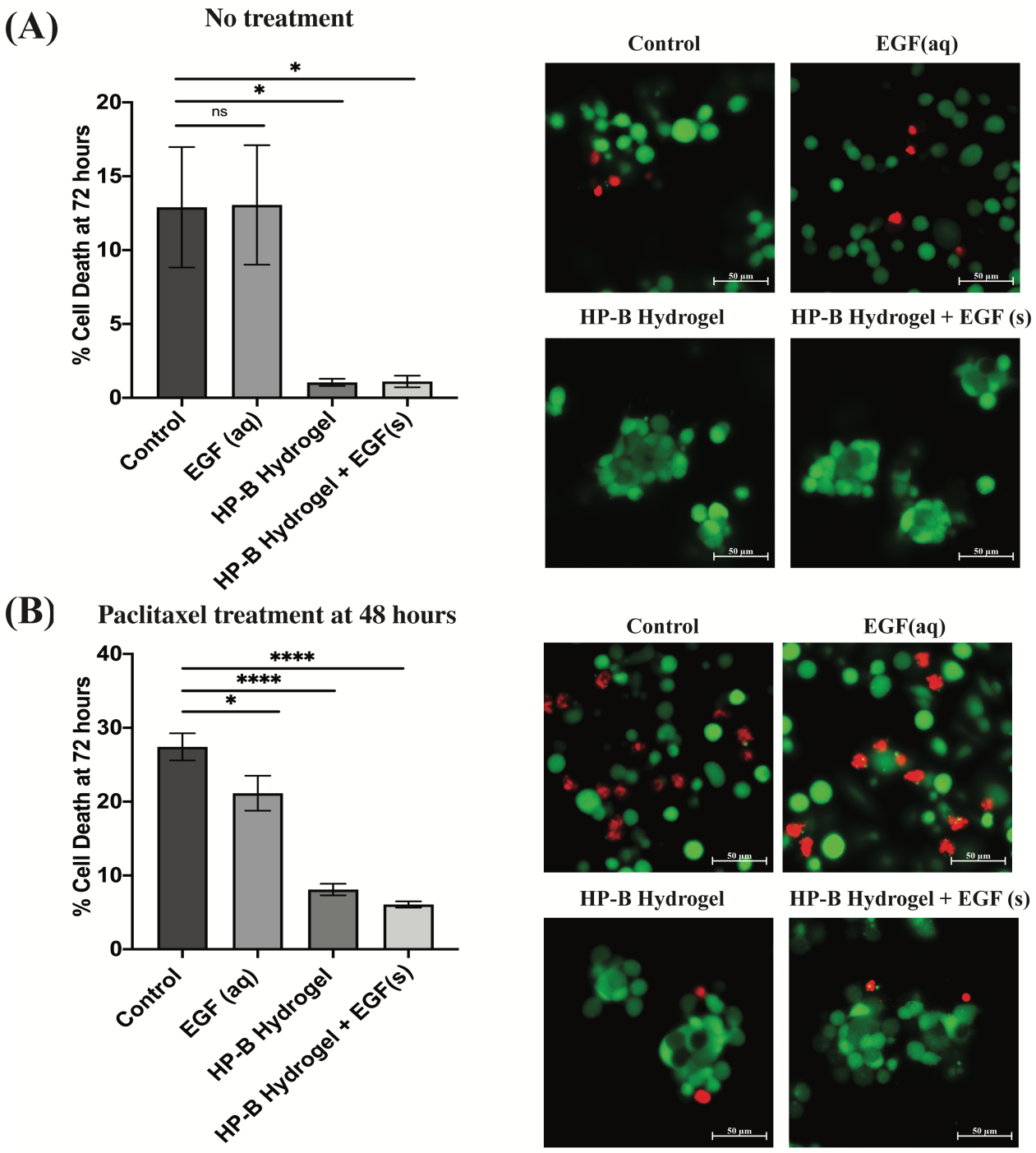

Figure 2.3: **Heparin-based (HP-B) hydrogel increases viability and chemoresistance. (A)** The percentage of dead cells after 72 hours was significantly (*$p < 0.05$) higher in both control and aqueous EGF conditions compared to HP-Bhydrogels, both with and without EGF. **(B)** A 24-hour treatment with paclitaxel prior to the live and dead cell assay at 72 hours increased the percentage of dead cells in all the conditions. However, the difference was significantly higher (*$p < 0.05$, ****$p < 0.0001$) in both 2D conditions compared to the HP-B hydrogels. Data is represented as mean ± standard error of mean (SEM).

2.4.3 3D spheroids exhibit lower cell death post chemotherapy treatment

MDA-MB-231 cells were treated with paclitaxel [100 nM] at 48 hours post initial seeding and viability was assessed at 72 hours (Figure 2.3**(B)**). Cells in the control group had 27.40 ± 1.84% dead cells whereas EGF (aq) supplemented cells had 21.14 ± 2.38% dead cells. However, cells in the HP-B hydrogel had only 8.1 ± 0.79% dead cells and cells HP-B hydrogel + EGF(s) had 6.08 ± 0.42%. The percentage of dead cells in 3D morphology was significantly (****$p < 0.0001$) lower than in 2D.

2.4.4 HP-B hydrogel reduces cell proliferation

Proliferating MDA-MB-231 cells were determined by calculating the percentage of Ki-67 stained nuclei (Figure 2.4). Cells in control had 85.17 ± 4.2% Ki-67 positive nuclei compared to 97.75 ± 1.54% with EGF (aq) stimulation. 3D cultures induced lower proliferation rates in MDA-MB-231 cells. HP-B hydrogel encapsulated cells had 79.97 ± 3.68% proliferating cells, significantly (**$p < 0.005$) lower than EGF (aq) stimulated cells. Similarly, HP-B hydrogel with EGF(s) was significantly (***$p < 0.0005$) lower than EGF (aq) stimulated cells with only 73.56 ± 4.31% proliferating cells.

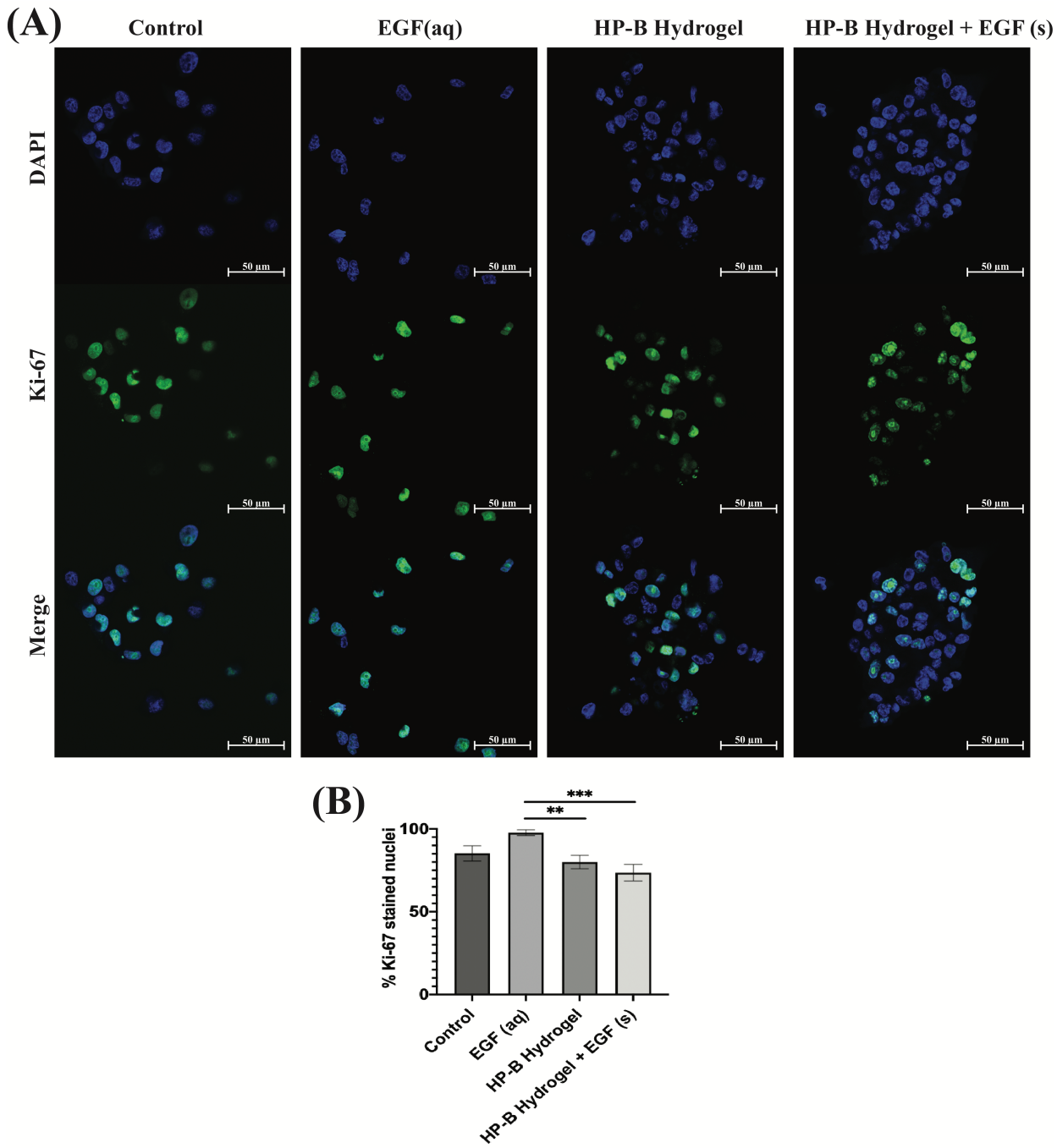

Figure 2.4: **Heparin-based (HP-B) hydrogel decreases breast cancer cell proliferation.(A)** Cells were stained for Ki-67 after 72 hours of cell culture. **(B)** Interestingly, the percentage of Ki-67 positive cells were fewer in 3D spheroids. Aqueous EGF stimulation significantly (**p $<$ 0.005, ***p $<$ 0.0005)" increased proliferation compared to the other conditions. Data is represented as mean $\pm$ SEM.

2.4.5 HP-B hydrogel alters the transcriptomic profile of human breast cancer cells

We identified differentially expressed genes in cells grown with EGF (aq) stimulation (267 genes), HP-B hydrogel (2048 genes) and HP-B hydrogel grown with pre-mixed EGF(s) stimulation (1219 genes) compared to the control group (Figure 2.5**(A)**). Cells grown under the two hydrogel conditions showed significantly different gene expression profiles compared to cells grown under the EGF (aq) and control (Figure 2.5**(B)**). To further investigate the signaling pathways affected by the growth conditions, we performed Gene Set Enrichment Analysis (GSEA) comparing all growth conditions with the control. GSEA was run using the Hallmark gene sets in the Molecular Signature Database (MSigDB). This particular gene set allows for a robust analysis of the most relevant gene expression changes and relates them to specific biological processes. This better facilitates follow-up analysis in the context of the disease phenotype[97]. We identified prominent Hallmark pathways influenced by aqueous EGF stimulation and presence of a 3D microenvironment and solid-phase GF presentation (Figure 2.5**(C)**). Some of these critical pathways are highlighted in Table 2.1. Interestingly, the PI3K-AKT-mTOR signaling pathway was downregulated in both the hydrogel conditions (Figure 2.6**(A)**). The results corroborate previous studies reporting similar downregulation of the PI3K-AKT-mTOR pathways when cells are grown as 3D spheroids[98]. However, AKT1, involved in several signaling pathways regulating cell proliferation, survival and metabolism was upregulated in the hydrogel and PTEN, known to function as a tumor suppressor and promote apoptosis had lower expression levels on both the hydrogel platforms (Supplementary Figure 2.8**(A)**). Furthermore, canonical Wnt/β-catenin signaling was upregulated in the cells grown in HP-B hydrogel and HP-B hydrogel + EGF (s) (Figure 2.6**(B)**). Transcription factors LEF1 and TCF7, downstream mediators of the canonical Wnt/β-catenin signaling

pathway were upregulated in the cells grown in the 3D environment (Supplementary Figure 2.8**(B)**)[99, 100]. TNFA signaling via NF- B, however, was downregulated with both aqueous and solid-phase EGF presentation but upregulated in HP-B hydrogel (Figure 2.6**(C)**). NF- B and TNF mRNA levels were also higher in the control and HP-B hydrogel cultures without EGF stimulation, both aqueous and solid (Supplementary Figure 2.8**(C)**). Both HP-B hydrogel environments also downregulated IL2-STAT5 signaling pathway (Supplementary Figure 2.9**(A)**) and upregulated TGF-β signaling (Supplementary Figure 2.9**(B)**). The full GSEA for the datasets is available in the ESI.

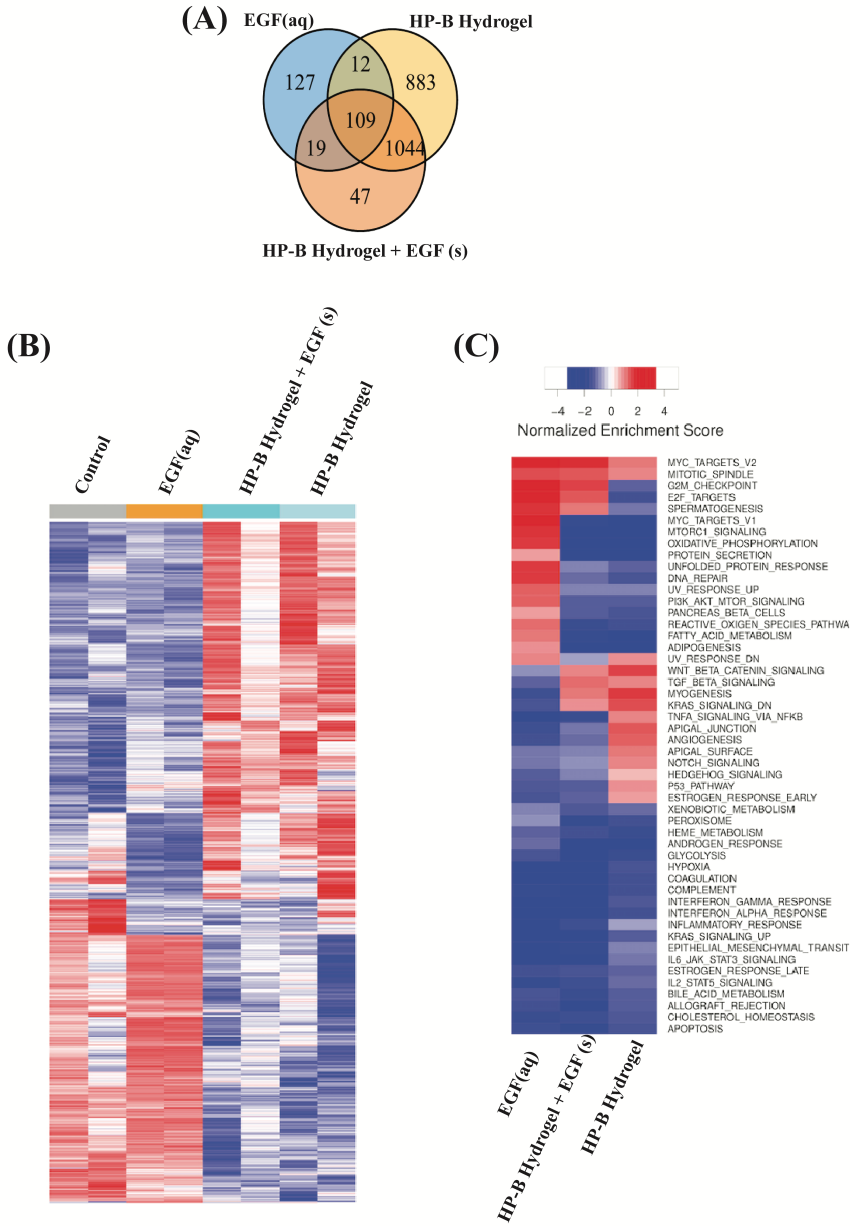

Figure 2.5: **Differential gene expression between 2D versus 3D heparin hydrogel cultivated breast cancer cells.(A)** The Venn diagram represents the differentially expressed genes in the culture conditions compared to the control group. The highest changes were observed in the 3D hydrogel environments. **(B)** Heat map shows gene expression in the four different groups. The control and EGF (aq), or the cells grown on a dish are aligned similarly with slightly stronger expression in the EGF (aq) samples. Likewise, cells grown on HP-B hydrogel with and without solid-phase EGF showed similar alignment reads. **(C)** Heatmap shows normalized enrichment scores for cancer hallmark gene sets. Critical pathways are significantly altered with aqueous and solid-phase presentation.

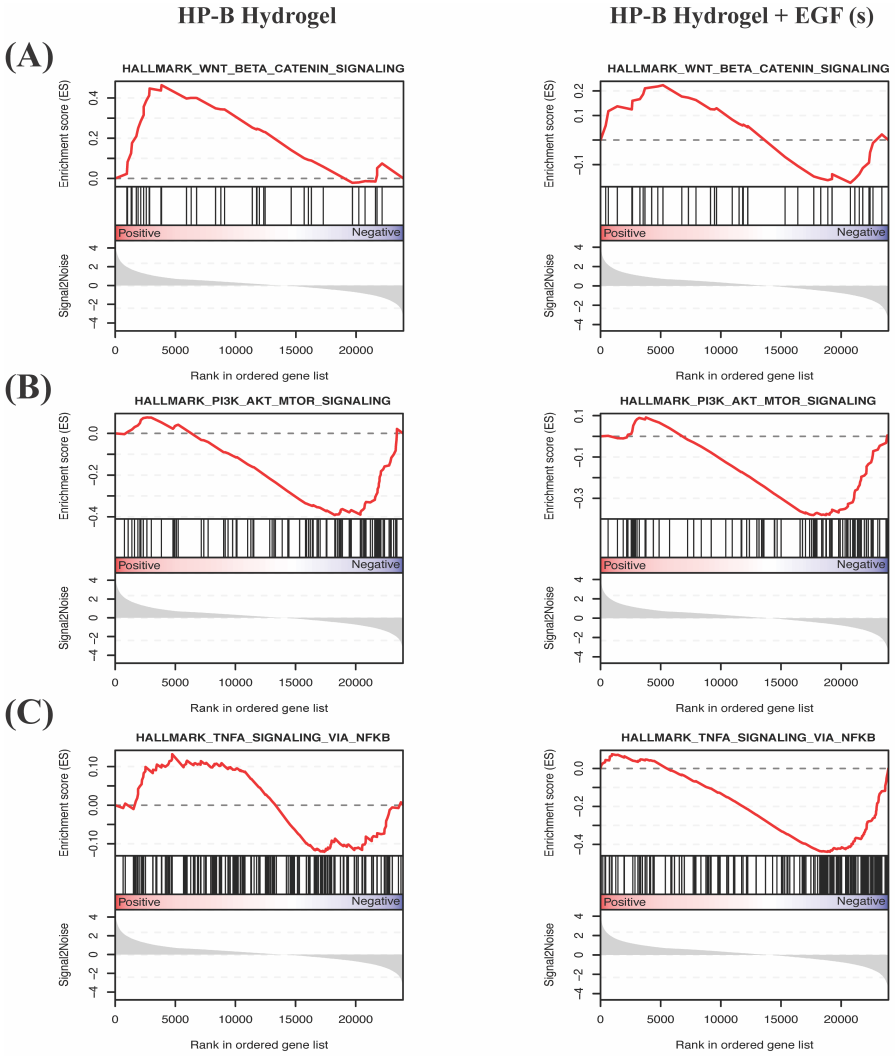

Figure 2.6: **Enrichment plots of differential expression of hallmark pathways.**Normalized gene expression was used in gene set enrichment analysis (GSEA) to identify cancer hallmark pathways/gene signature altered in EGF (aq), HP-B hydrogel, and HP-B hydrogel + EGF (s) compared with the control group. Vertical black lines on the central x-axis correlate with the genes from the pathway and is correspondingly mapped to the dataset. Genes that are positively correlated with the phenotype are on the left (indicated by red), whereas genes that are negatively correlated with the phenotype are on the right (indicated by blue). The degree of positive and negative correlation to the phenotype is determined by where it ranks on the ordered gene list. The enrichment score records hits from the sample to the specific phenotype and the more the number of genes encountered in the sample, the higher the enrichment score. **(A)** Wnt/β-catenin signaling is upregulated in HP-B hydrogel (*p < 0.05) as well as HP-B hydrogel with EGF(s). **(B)** PI3K-AKT-mTOR signaling is interestingly downregulated (*p < 0.05) in both HP-B hydrogel conditions. **(C)** TNFA signaling via NF- B is influenced by the presence of EGF(s) stimulation and is downregulated (**p < 0.005) versus upregulated in HP-B hydrogel without supplemented EGF(s).

Table 2.1: **Enriched cancer hallmark genes signature in breast cancer cells grown with supplemented aqueous EGF, HP-B hydrogel and HP-B hydrogel with solid-phase EGF compared to control.**Pathways are significantly (*p $<$ 0.05, **p $<$ 0.005, ***p $<$ 0.0005) altered with and without solid-phase GF presentation

Hallmark pathways	**EGF (aq)**	**HP-B hydrogel**	**HP-B hydrogel + EGF (s)**
PI3K-AKT-mTOR signaling	Upregulated	Downregulated*	Downregulated*
Wnt/β-catenin signaling	Downregulated	Upregulated*	Upregulated
TNFA signaling pathway via NF-κB	Downregulated**	Upregulated	Downregulated**
IL-2 STAT5 signaling	Downregulated	Downregulated***	Downregulated***
TGF-β	Downregulated	Upregulated	Upregulated
Apoptosis	Downregulated**	Downregulated***	Downregulated***
Oxidative phosphorylation	Upregulated***	Downregulated***	Downregulated***

2.5 Discussion

HP-B hydrogel enables controlled presentation of GFs and endogenous signals and can serve as an effective biomimetic *in vitro* microenvironment for the culture of breast cancer cells. The EGF diffusion study in the HP-B hydrogel was able to confirm the association and dissociation between the GFs and heparin chains that limited the free diffusion of EGF in the pores of the hydrogel. This kind of a slow and sustained release of GFs from the HP-B hydrogel matrix bio-mimics the release of GFs from ECM *in vivo*[101], unlike traditional cell culture where the cells are directly exposed to a high initial concentration of the GFs in soluble form in the media. The spatiotemporal modulation of GFs not only keeps cells more viable but also helps differentiation (tissue-specific). Despite fewer proliferating cells in 3D spheroids, cells remained significantly more viable. Consistent with previous studies, drug resistance can be attributed to cells entering and exiting dormancy in 3D cultures to evade paclitaxel toxicity[102]. Several of the transcriptomic changes influenced by microenvironmental stimulus could be responsible for this phenomenon and the high degree of chemoresistance observed in 3D spheroids.

EGF stimulation in solid-phase revealed a phenotypic profile that differs significantly from EGF stimulation in an aqueous phase. HP-B hydrogel with no EGF stimulation also revealed changes in cell behavior compared to the control group. The 3D environment specifically showed changes in critical pathways regulating cancer progression and metastasis. The gene expression changes seen in the key regulators of PI3K-AKT-mTOR and Wnt/β-catenin signaling pathways convey the importance of studying biomimetic platforms and their influence on the molecular biology of cells. A previous study demonstrated that inhibition of the PI3K-AKT-mTOR in MDA-MB-231 increased Wnt/β-catenin signaling[81]. However, the molecular mechanisms conferring adaptive resistance to tumors *in vivo* have not been fully understood. Our results from RNA sequencing revealed similar trends, wherein PI3K-AKT-mTOR signaling was downregulated, and Wnt/β-catenin signaling was upregulated in the 3D environment. Although, cells grown on the dish with aqueous GF presentation showed the opposite trend. A low cell seeding density and interactions with the ECM environment may be responsible for the switch in the phenotype of the cells grown in the hydrogel environment in this short period of time. Despite the downregulation of the PI3K-AKT-mTOR signaling pathway, cells in the 3D environment had significantly higher viability and adaptive resistance to chemotherapy compared to cells grown in 2D, including the EGF (aq) stimulated cells.

Our study also highlights the importance of specific GF stimulations in the local tumor niche. EGF stimulation in both aqueous and solid-phase led to the downregulation of TNFA signaling via NF-βB. Recent studies suggest a cross-talk between EGFR and TNFA[103]. Another study observed the inhibition of EGFR in lung cancer cells increased TNFA levels as an adaptive response[104]. Further scrutinizing the crosstalk between signaling pathways, specifically in response to their environmental signals in essential to avoid failure of novel drug contenders in clinical testing. Immune-regulating pathways such as IL2-STAT5 signaling

were downregulated in both 3D environments, whereas TGF-β signaling was upregulated. TGF-β signaling has been studied extensively in solid-tumors and is known to function as a potent immunosuppressor, affecting normal lymphocyte proliferation and maturation in the tumor microenvironment[83, 84]. As aforementioned, IL2-STAT5 signaling plays a crucial role in T-cell development and IL2 has been approved for cancer immunotherapy in treating metastatic renal cell carcinoma and metastatic melanoma[85]. IL2 suppression is also known to be mediated by TGF-β[86]. Therefore, the mechanisms underlying immune evasion *in vivo* need to be studied thoroughly to avoid failure of promising immunotherapies. Cocktail therapies may be the key to treating tumors for successful remission.

Our results reaffirm that the rewiring of pathways during cancer proliferation, metastasis and colonization are highly dependent on the local niche[105]. The use of HP-B hydrogel allows for manual fine-tuning of the microenvironment that can be modulated for tissue-specific cell responses[76]. Our study emphasizes the need to use more sophisticated 3D platforms to study tumor dynamics *in vitro* to better represent the interactions between tumor cells and their microenvironment. In the future, HP-B hydrogel can serve as a platform for co-cultures based on the tissue of interest. Studies including organ specific stromal cells may be essential to further validate the need for heparin incorporation to control autocrine and paracrine signaling. This is especially important when evaluating the effects of chemotherapy and immunotherapy *in vitro* to avoid the variability observed between pre-clinical models and clinical trials[106]. The scaffold has applications in the cultivation of low numbers of primary cells and CTCs, as demonstrated by relatively low seeding densities used in our experiments.

Additionally, heparin, in particular, is often administered as an anticoagulant to cancer patients receiving chemotherapy[107]. Heparin-induced thrombocytopenia in cancer patients has been previously documented[108]. The side-effects of heparin, in the context of changes

in the transcriptomic profile, have not been well studied. Results from our study have highlighted that protein-binding moieties, such as heparin and hyaluronic acid can alter the phenotypic profile of cells, leading to increased chemoresistance. Conflicting reports currently exist on whether heparin affects overall survival of patients[109, 110, 111]. Our study further stresses on the need for long-term studies on the influence of heparin content in the tumor microenvironment and its influence on chemoresistance.

2.6 Conclusions

Heparin-based hydrogel was a suitable scaffold for solid-phase epidermal growth factor presentation and to support the formation of breast cancer cell spheroids. Furthermore, MDA-MB-231 cells cultured in HP-B hydrogel were shown to proliferate less and exhibit a higher degree of chemoresistance compared to cells cultured in standard dishes. RNA Seq data illustrates the dramatic differences in transcriptomic profiles of human breast cancer cells cultured in HP-B hydrogel driving these phenotypic changes. This study shows that cell culture biomaterial designs are critical when running *in vitro* assays, including drug screening tests. Future studies are now required to investigate the effects of different growth factors presented via HP-B hydrogels on the survival, differentiation and proliferation of cells.

2.7 Acknowledgments

We would like to thank Carla Finkielstein for her thoughtful discussions on experimental design and RNA seq data analysis. Research reported in this publication was supported

by The National Institute of General Medical Sciences of the National Institutes of Health under award number R35GM133610.

2.8 Conflicts of Interest

There are no conflicts to declare.

2.9 Supplementary Information

Supplementary Video Simulation of the diffusion of EGF.COMSOL Multiphysics is used to model the diffusion of EGF in the porous HP-B hydrogel environment. 50 ng ml^{-1} of pre-mixed EGF with less than 0.05% free EGF in the gel shows cumulative release over time corresponding the experimental data. The video file gives a visual representation of the minimal release of EGF in the HP-B hydrogel.

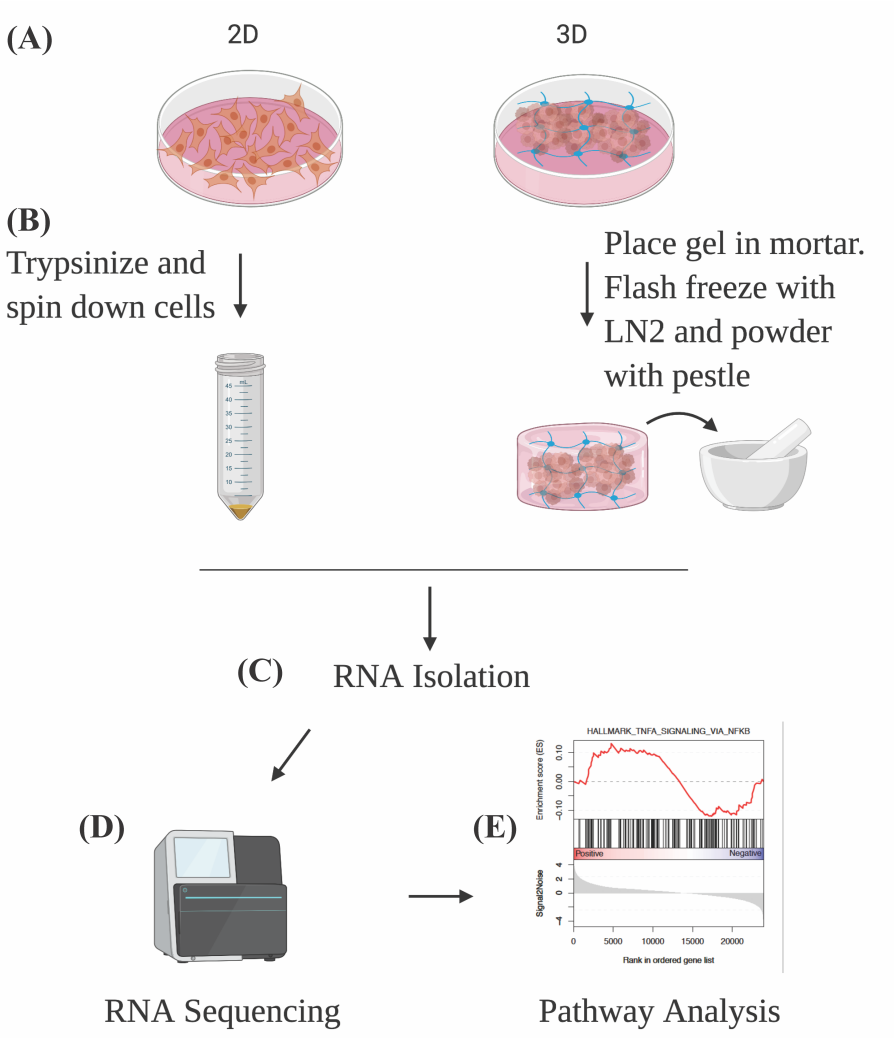

Figure 2.7: **RNA seq protocol to quantify transcriptomic differences in 2D and 3D cultures.** Cells were grown in their respective microenvironments: **(A)**) Cells in 2D culture include both the control group and the EGF (aq) stimulated group on dish, whereas both hydrogel groups with and without EGF(s) are represented by the 3D culture. **(B)** Adherent cells grown on the dish were detached using trypsin and spun down to collect the cells. Whereas the gel was retrieved from the wells and transferred to a mortar. Liquid nitrogen (LN2) was used to flash freeze the gel and the encapsulated cells. The pestle was then used to powder the gel. **(C)** All the samples were processed using Trizol reagent. Chloroform was used for phase separation.RNeasy Mini kit was used to isolate whole RNA. **(D)** Whole RNA was then sent to the sequencing center. Sequencing was done on the Illumina NextSeq 500/550 High Output kit V2 and the raw data files were obtained. **(E)** The data was aligned to the genome to quantify gene expression.Further analysis on differential gene expression and hallmark pathways was carried out.

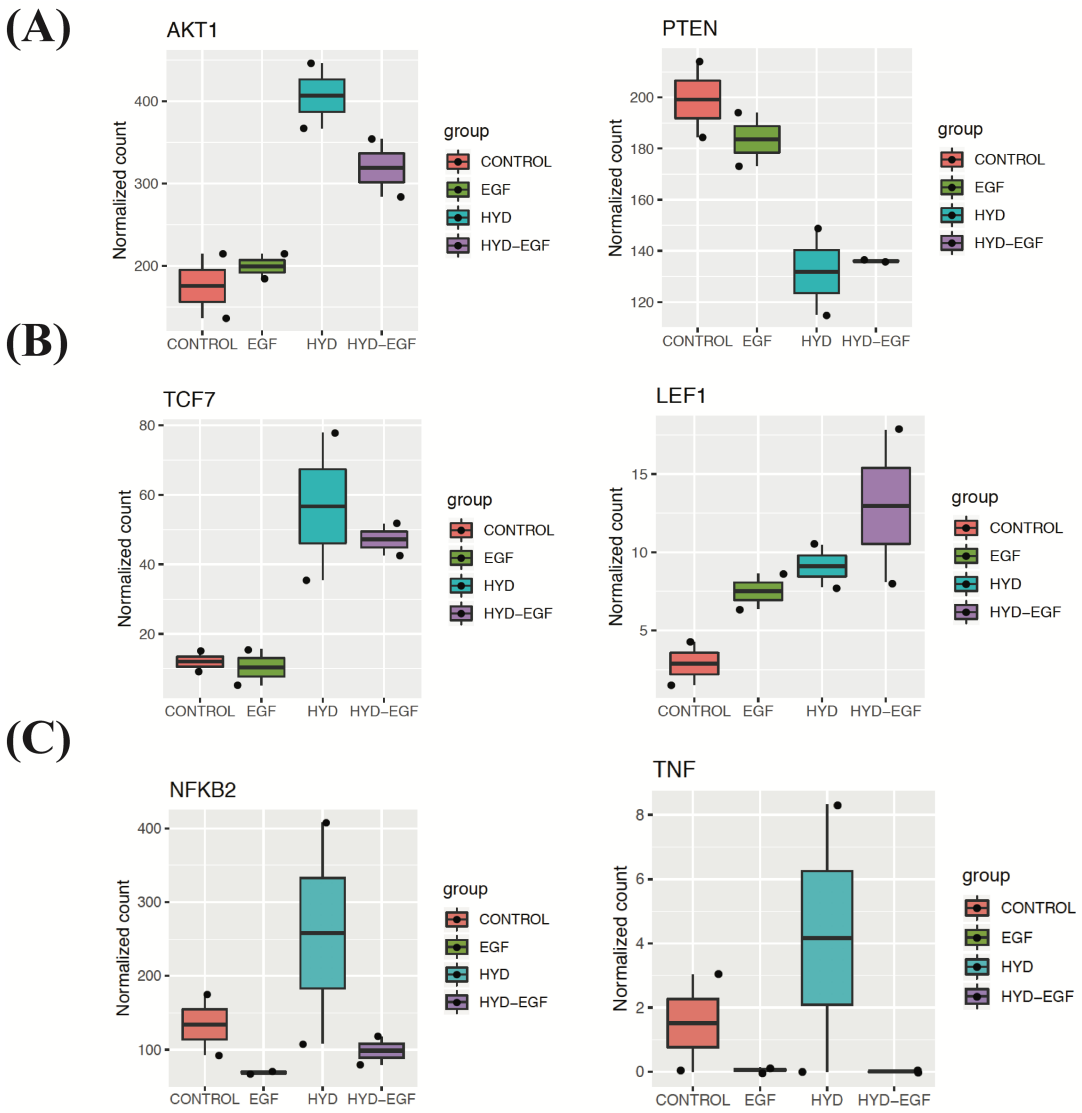

Figure 2.8: **Differentially expressed genes regulating critical pathways** Cells were grown in their respective microenvironments: **(A)**AKT1 levels in the 3D environments remained high despite overall downregulation of the PI3KAKT-MTOR signaling. PTEN levels were also lower in 3D environments.**(B)** TCF7 and LEF1 are upregulated in the 3D microenvironment and are key regulators of the canonical Wnt/β-catenin signaling pathway. **(C)** TNF and NF-βB2 are upregulated in conditions without supplemented EGF, both aqueous and solid-phase.

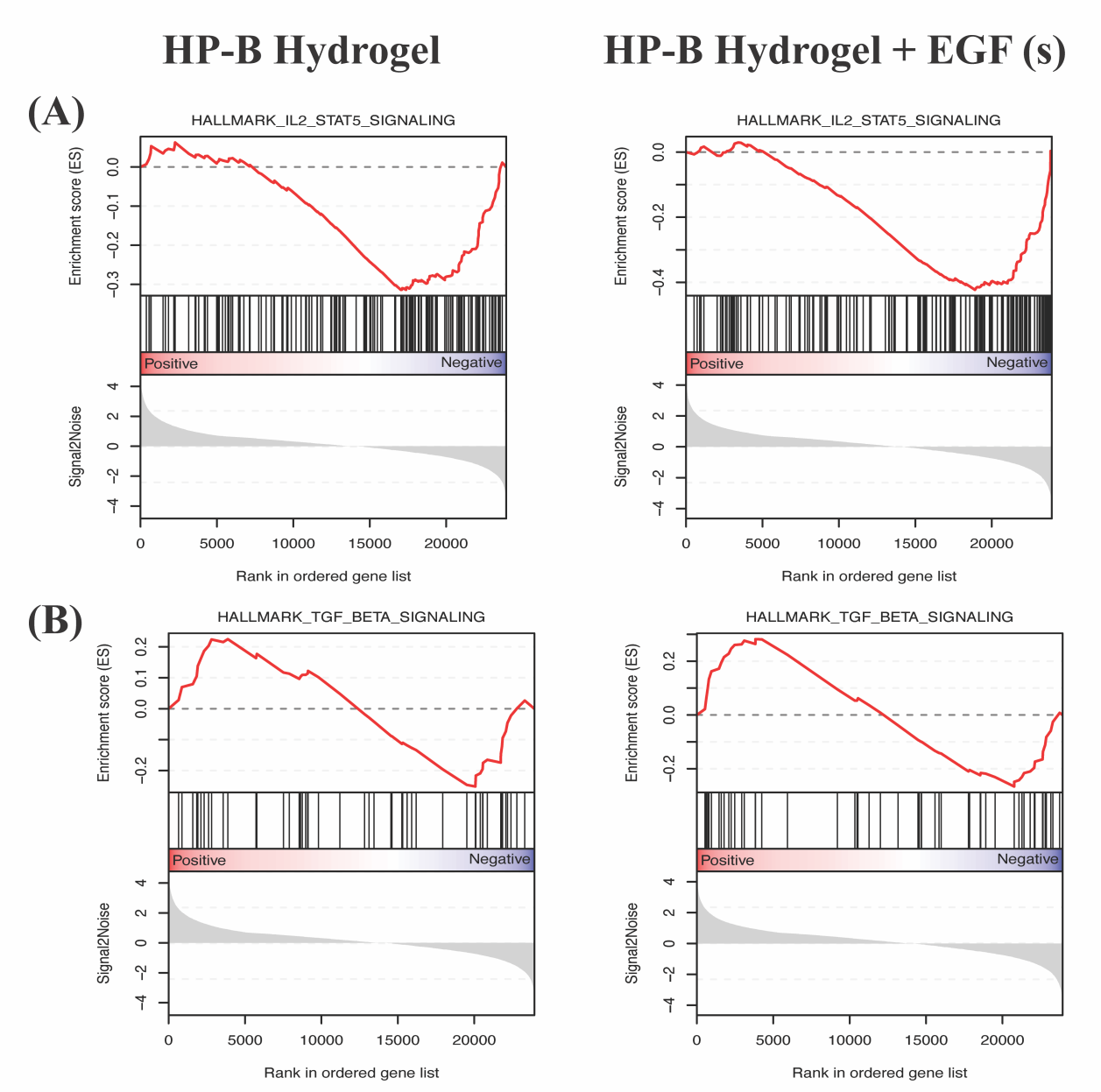

Figure 2.9: **Hallmark Pathways involved in immune response regulation.** **(A)** IL2-STAT5 signaling is downregulated in both HP-B hydrogel groups. **(B)** TGF-β signaling, is upregulated in both HP-B hydrogel environments.

Chapter 3

Secondary metabolites derived from endophytic fungi exhibit high levels of cytotoxic activity against triple-negative breast cancer cells

3.1 Abstract

Breast cancer is one of the leading causes of death among women. Fungal endophytes have been on the forefront of several secondary metabolites that have previously shown anti-breast cancer properties. Despite a third of the cancer therapies being derived from natural products, very few studies have focused on exploring the avenue for drug discovery. Some of the reasons include the cost and labor associated with screening the huge number of compounds derived from natural sources, and the poor rate of translation of these drugs into clinics. To bridge this gap, we collected plants from the New Rivery Valley in VA, USA, and isolated individual endophytic fungi from various parts of the plants. The fungi were then grown and their extracts screened on triple-negative breast cancer cells. Viability assays showed high cytotoxicity against breast cancer cells and a comparable or better result when

compared to standard chemotherapy agent Paclitaxel, also derived from natural sources. Solid-phase extraction of the extracts further helped to narrow down the sources of the active secondary metabolite(s). These were screened in both 2D and 3D breast cancer cell models, with the fractions exhibiting significantly different cell death in both platforms. Introducing new cell models prior to clinical screening and animal models could save the industry a significant amount of time and money, and provide a more realistic insight into the function of the natural compounds.

3.2 Introduction

Breast cancer has the highest record of cases in women and is the second leading cause of death among women, after lung cancer [80]. Triple-negative breast cancer (TNBC) is an aggressive form of breast cancer, lacking estrogen, progesterone and human epidermal growth factor 2 receptors[80, 112]. Conventional breast cancer treatments rely on these specific markers for targeted hormonal therapy. Current treatments rely on surgery and chemotherapy. However, patients with TNBC have a poor prognosis and high rates of relapse[112, 113]. Taxane-based chemotherapies, such as paclitaxel have been widely studied and regarded to be successful in TNBC cohorts[80].

Paclitaxel, widely used to treat several types of cancer, was also first discovered in nature, and is produced by Pacific Yew trees, or Taxus brevifolia [114]. Interestingly, endophytic fungi growing on the Yew trees also produce the same secondary metabolite[115]. Since then, several studies have reported endophytic fungal metabolites to have anticancer, antibacterial and antiviral properties[116, 117, 118]. Identifying endophytic fungal sources of existing and novel anticancer metabolites has the potential to offer better treatment alternatives and to

increase metabolite production synthetically from multiple sources.

The current rate of translation for anticancer drugs, from Phase I trials to FDA approval, stands less than 10%, with an average time of approval being over 10 years[119]. Far worse is the approval of oncology drugs from preclinical discovery to Phase I clinical trials, which is less than 7%[120]. These numbers reflect the massive time and economic investment that do not ultimately yield in desired outcomes. While initial drug discovery has conventionally happened in 2D monolayer cell lines, it is now known that 3D tumor microenvironments can alter phenotypic responses and increase drug resistance in engineered microphysiological breast tumor models[121, 122, 123]. A previous study from our group highlighted the transcriptomic changes that could contribute to significantly lower cell death in a TNBC cell line cultured in a heparin and hyaluronic-acid based blank-slate matrix[124]. To avoid the labor and cost-intensive process of testing anticancer drugs that are likely not to succeed in preclinical animal models, it is imperative to have engineered platforms that recapitulate *in vivo* tumor microenvironments.

We collected plant samples from the New River Valley and cultured fungal endophytes to study their antitumor activity in the TNBC cell line, MDA-MB-231. Preliminary screening was performed using 347 fungal extracts, with duplicates in 96 well plates and paclitaxel as a positive control. 23 of the extracts were found exhibiting promising anticancer activity. The first five promising hits from the initial screen were fractionated to narrow down the source of the active metabolite. The fractions were tested against both the 2D and engineered 3D models of the TNBC cell line.

3.3 Materials and Methods

3.3.1 Metabolite extraction

Endophytic fungi were harvested by collecting plant samples from the New River Valley. Plants segments were separated by organ (stem(S), root(R), Leaf (L), Flower (F)), sterilized with ethanol on the exterior, sliced open, and placed on separate potato dextrose agar (PDA) plates. Plates were incubated for 5 days at 27°C. Multiple fungi typically grew out of each segment onto the plate. Individual fungi were isolated by cutting a square from a single colony and transferring to a new PDA plate.

Initial screening was carried out after growing fungal cultures in 5 mL potato dextrose broth (PDB). The cultures were incubated at 27°C for 3 days on a shaker at 150 rpm. The cultures were incubated at 27°C for 10 days on a shaker at 150 rpm. Samples were then centrifuged at 6000 rpm for 5 minutes. A 10 mL syringe was used to aspirate the media containing the metabolites from the fungi. The sample was then passed through a 0.22-micron filter to remove cells.

To obtain extracellular fungal metabolites for further analysis, the fungal culture was scaled-up. Individual squares were then cut from each fungal culture and placed in 200 mL PDB. The cultures were incubated at 27°C for 10 days on a shaker at 150 rpm. Samples were then centrifuged at 6000 rpm for 5 minutes. A 20 mL syringe was used to aspirate the media containing the metabolites from the fungi. The sample was then passed through a 0.22-micron filter to remove cells.

3.3.2 Solid-phase Extraction

A 3cc Oasis PRiME HLB cartridge was conditioned with 1 mL MeOH followed by 1 mL water with a hose vacuum and cartridge holder system. The fungal metabolite extract was added to the cartridge and slowly eluted. Cartridge was washed with water to make first fraction (Fraction 1). Additional elution with 10% MeOH (Fraction 2), 50% MeOH (Fraction 3), and 100% MeOH (Fraction 4) created the next set of fractions. The water fractions were frozen in liquid nitrogen and freeze-dried overnight using a freeze drier. The methanol fractions are concentrated using a rotavapor, and further concentrated using a centrifugal vacuum concentrator. Following this, the samples are flash frozen and evaporated to dryness on the high vacuum line. The samples were stored in -20°C until further use for experimentation.

3.3.3 Cell culture

Triple-negative breast cancer cell line MDA-MB-231 (American Type Cell Culture HTB-26) was cultured in GibcoTM Dulbecco's Modified Eagle's Medium F-12 (DMEM/F-12) containing high glucose and GlutaMAX™, supplemented with 10% fetal bovine serum (FBS) and 100 unitsml^{-1} penicillin and 0.1 mgml^{-1} streptomycin. The cells were maintained in vented T-25 or T-75 flasks (Corning) at 37°C and 5% CO2. Media was changed every 48 hours. Using 0.05% Trypsin-EDTA for detachment, cells were harvested for experiments at 80-90% confluency.

3.3.4 Initial Screening Process

Cells were grown in 96-well plates with 5000 cells per well (2D). Duplicates (n=2) were run for each of the extracts. 100 nM paclitaxel was used as positive control. Cells without treatment were considered as the negative control. A manual cell counter on the open source software ImageJ/Fiji [89] was used to count the live and dead cells.

3.3.5 Fraction Screening and Viability Assay

Cells were grown in 96-well plates with 5000 cells per well, with and without the hydrogel scaffolding. In order to quantify cell response to the metabolites, cells were allowed to grow for 48 hours prior to the addition of 200 μl (Dry samples were reconstituted in 60 μl DMSO and further reconstituted 1140 l of media) of fungal fractions (n=3) and 200 l of 100 nM paclitaxel as positive control. Untreated cells were considered as negative control. The cells were then treated for 24 hours and a live and dead cell assay was performed (Abcam, ab115347). Images of live (labeled green) and dead (labeled red) cells were taken on the Nikon Ti-E microscope. A manual cell counter on the open source software ImageJ/Fiji [89] was used to count the live and dead cells in the image frame. One-way ANOVA and Šídák's multiple comparisons test was used to analyze the differences in cell death observed in 2D and 3D models of TNBC cells. Dunnett's multiple comparisons test was used to compare the response to paclitaxel within 2D and 3D models.

3.4 Results

3.4.1 Screening of Fungal Endophytic Extracts show promising anti-breast cancer properties

Plants were collected from the New River Valley, and the process of extract preparation is shown in Figure 3.1. Of more than 300 extracts screened initially, Supplementary Figure **??** shows the results from the screening of the first 5 hits chosen for further analysis. While most of the extracts show comparable results to Paclitaxel treatment, Figure 3.2 shows the plant and the fungi that these 5 extracts were derived from. Some of the plants were able to be identified and the Broad ID, genus and species are listed in Table 3.1.

3.4.2 Further screening was able to detect fractions with high metabolite activity

The extracts were fractionated using solid-phase extraction and the process is outlined in Figure 3.3. Viability of the cells treated with the four fractions of Extracts 19(S6S3), 24(S7S1), 33(S9L2), 40(S10F3), and 53(K1-6) were quantified and are graphed in Figure 3.4(A)-(E). All treatments were compared to the paclitaxel control within 2D and 3D groups using Dunnett's multiple comparisons test. The 2D and 3D responses were compared using Šídák's multiple comparisons test for each group of fractions from a single extract. Fractions with higher levels of activity can be distinguished in each of the endophytic extracts. While many of the fractions are active and significantly perform better than Paclitaxel, significant dif-

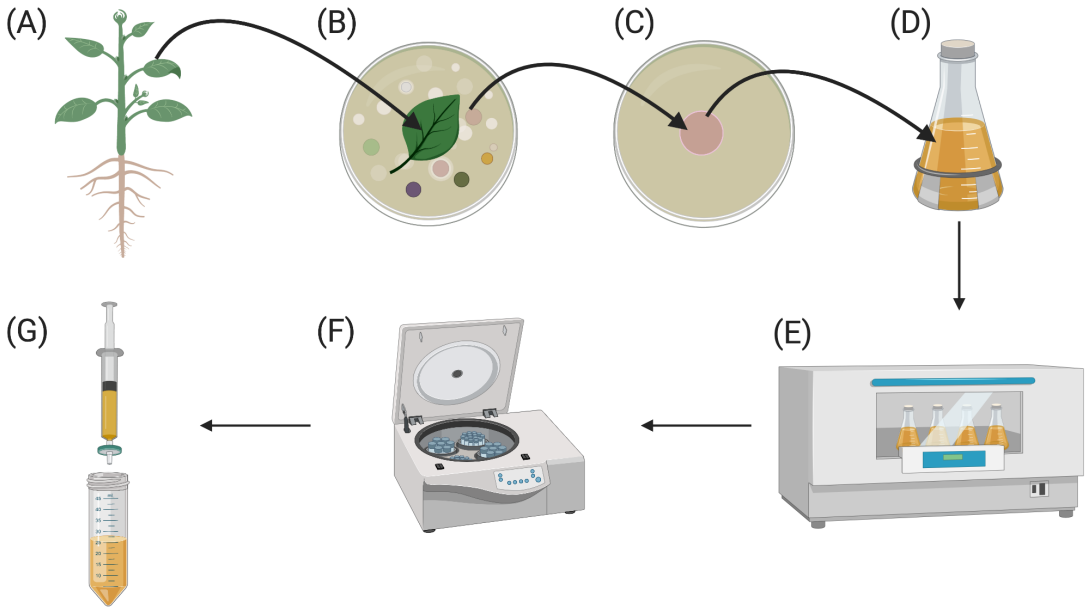

Figure 3.1: **Fungal Extract Preparation from Plants collected in the New River Valley, VA. (A)**All Plants were collected in the New River Valley area of Virginia and brought back to laboratory. **(B)** Plants were separated by organ, sterilized by ethanol on the exterior, cut open and placed on separate PDA plates.Plates were incubated at 27°C for 5 days and several fungi typically grew out of each segment.**(C)** Individual fungi were then isolated by cutting a square from a single colony and placed on a fresh PDA plate.**(D)**Following enough growth, typically 3-4 days, an individual square was cut from each fungi and placed in PDB.**(E)** The cultures were incubated at 27°C on a shaker at 150 rpm. **(F)** Samples were then centrifuged at 6000 rpm for 5 minutes.**(G)** A syringe was used to aspirate the media and passed through a 0.2 micron filter to separate the metabolites from the fungi and the spores.

ferences were often observed between the cell death in the 2D monolayer and 3D spheroid model.

In case of Extract 19 (S6S3), fractions 1,2, and 4 showed significantly (****$p<0.0001$) lower cell death in the 3D spheroid model. However, only fractions 1, 3, and 4 had a better response compared to the paclitaxel control. For Extract 24 (S7S1), fractions 2 and 3 showed significantly(****$p<0.0001$) fewer dead cells in the 3D spheroids model. All four fractions, however, performed significantly better than paclitaxel in 2D and 3D models. Fraction 2 in Extract 33 (S9L2) showed a similar response in 3D spheroids compared to 2D mono-

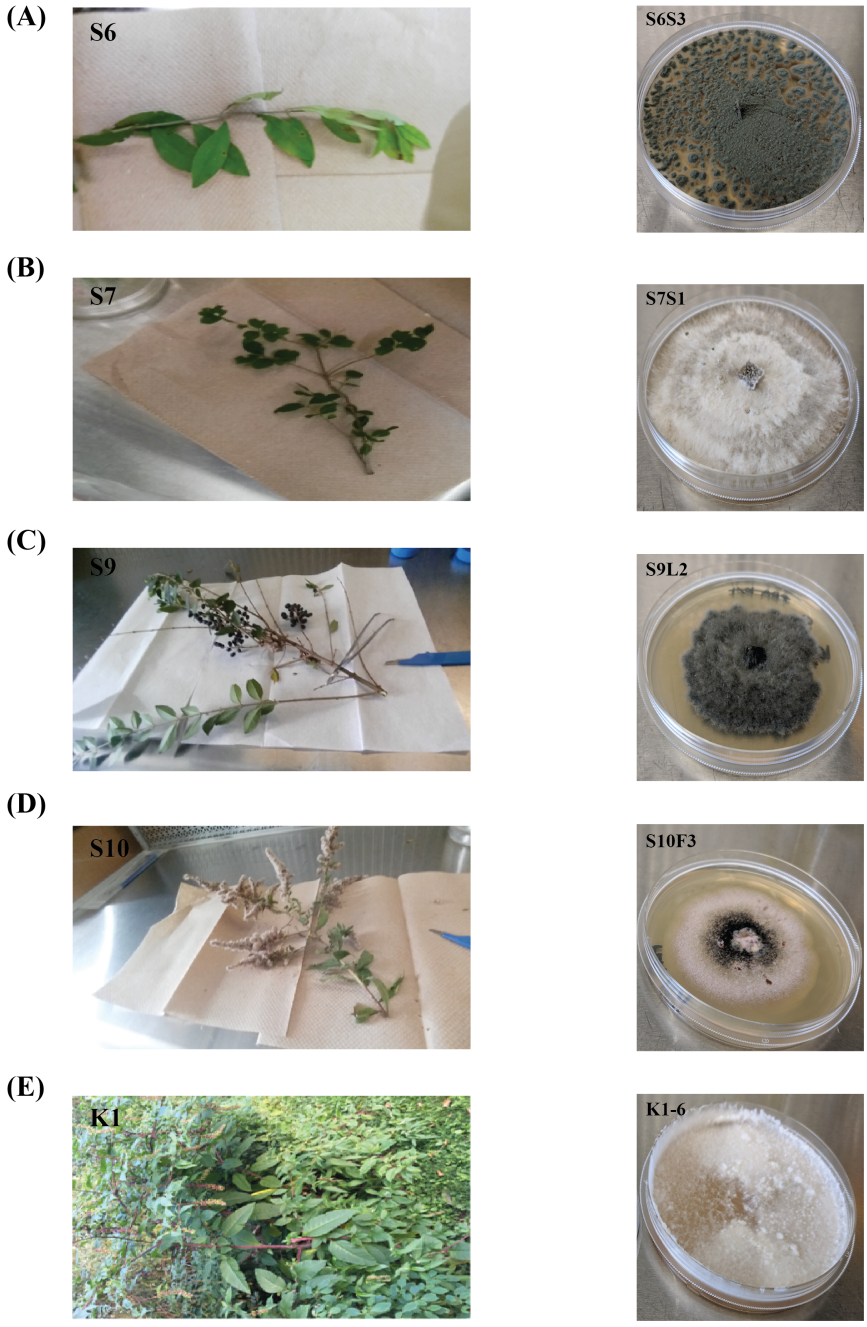

Figure 3.2: **Plants and their corresponding fungal endophytes with anti-cancer properties.** **(A)** Plant S6 and the third fungi isolated from the stem (S3). **(B)**Plant S7 and the first fungi isolated from the stem (S1).**(C)**Plant S9 and the second fungi isolated from the leaf (L2).**(D)**Plant S10 and the third fungi isolated from the flower(F3).**(E)**Plant K1 and and fungi isolated from an unknown part.

layer (****p<0.0001). However, all four fractions resulted in significantly higher cell death compared to paclitaxel. All the Fractions in Extract 40 (S10F3) resulted in significantly (fractions 1 and 4 (****p<0.0001), fraction 2 ((***p<0.001), fraction 3(**p<0.01)) fewer dead cells in the 3D model. However, while fraction 1 performed better than paclitaxel in the 2D monolayer culture, it did not in 3D. Fractions 2, 3, and 4 did not perform better than paclitaxel in either models. Fractions 2 and 4 in Extract 53 (K1-6) showed similar responses in 3D spheroids model (****p<0.0001). While fractions 1,2,and 3 resulted in significantly higher cell death compared to paclitaxel in both 2D and 3D models, fraction 4 did so only in the 2D model.

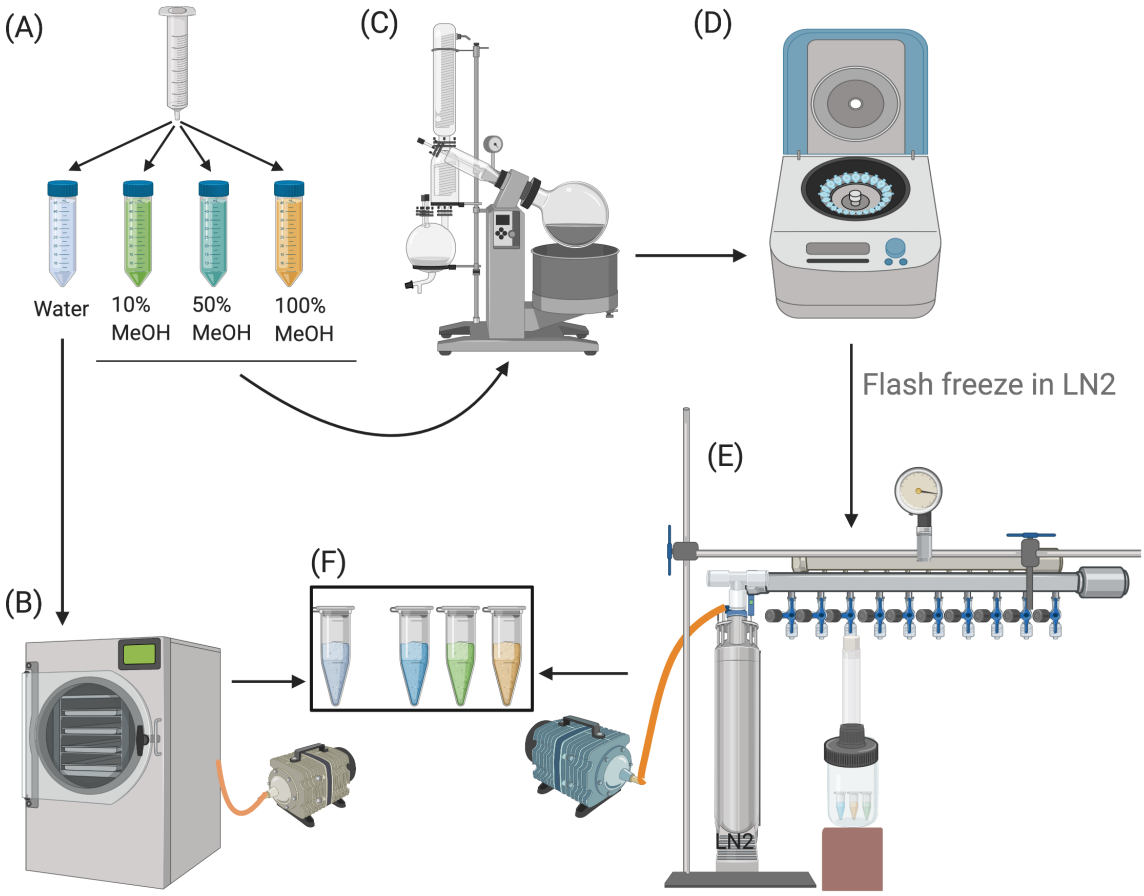

Figure 3.3: **Solid-phase extraction of fungal extracts. (A)** Oasis Prime HLB cartridges were primed with 1ml MeOH, followed by 1ml water using a hose vacuum and cartridge holder system. The fungal metabolites are slowly eluted through the cartridges and washed by water. This is fraction 1. The process is repeated with 10% MeOH (Fraction 2), 50% MeOH (Fraction 3), and 100% MeOH (Fraction 4) **(B)**The water fractions are flash frozen in LN2 and freeze dried overnight in a freeze drier.**(C)**The remaining fractions are concentrated down using a rotavapor to remove any MeOH.**(D)**Samples are further concentrated using a centrifugal vacuum concentrator.**(E)**The samples are then flash frozen in LN2 and evaporated to dryness using a high vacuum line.**(F)**All the dry samples and stored in -20°C until further use for assays.

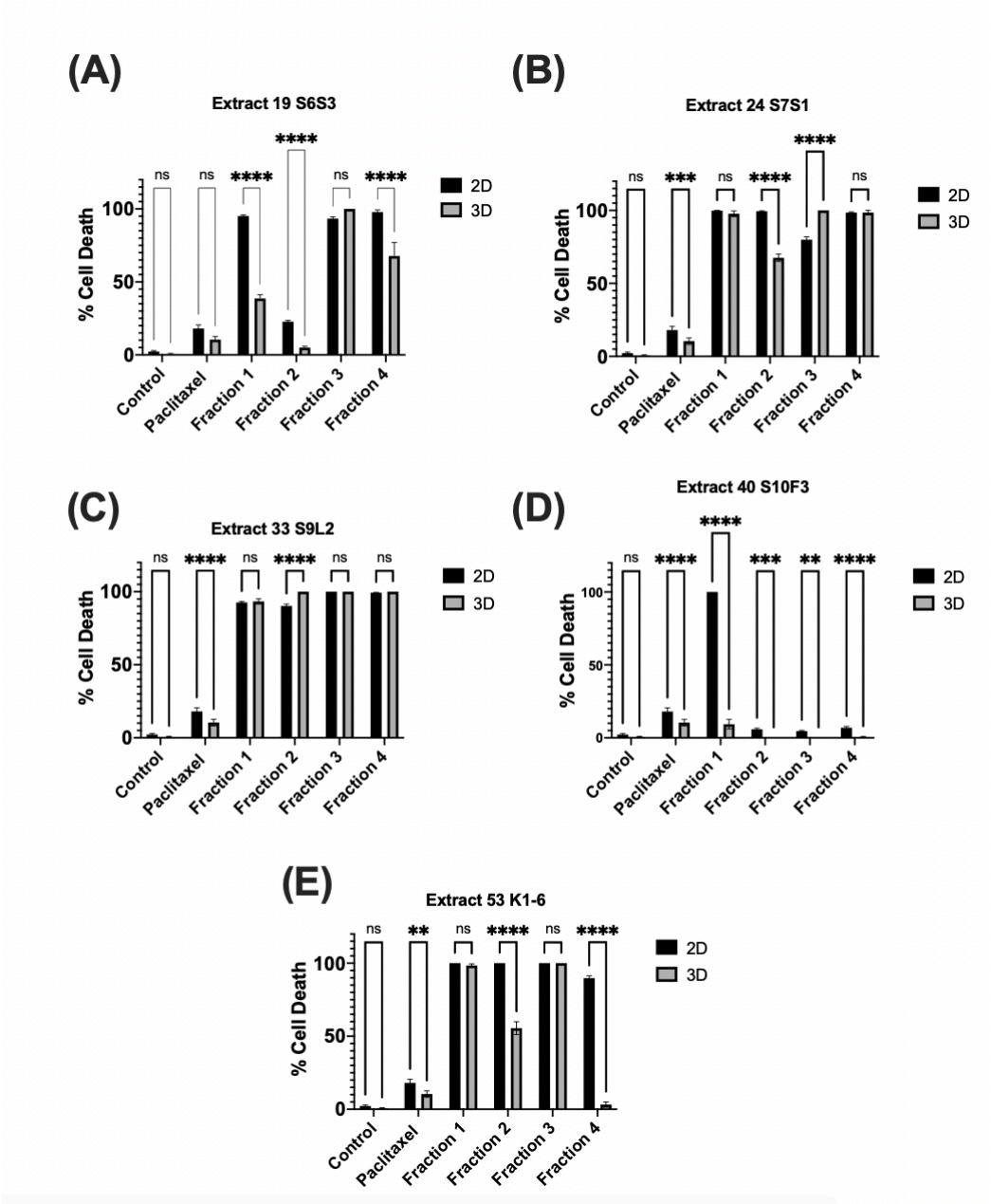

Figure 3.4: **Secondary metabolites from fungal endophytes show high cytotoxicity against breast cancer cells.** Solid-phase extraction in water (Fraction 1), 10% MeOH (Fraction 2), 50% MeOH (Fraction 3), and 100% MeOH (Fraction 4) were used to treat 2D and 3D models of TNBC cells. Some fractions were more active than others, and in several cases there were significant differences observed between 2D and 3D cell cultures.

3.5 Discussion

Secondary metabolites from fungal endophytes have shown promising anti-breast cancer activity. As of now, 34% of the drug used in cancer therapy are natural products or derivatives of natural products[125]. However, despite promising results, a very small percentage of fungal endophytes have been studied, with millions still left to be explored[126]. Furthermore, the potential of natural compounds goes beyond cancer, for applications in immunomodulation, antiviral, antibacterial and antiparasitic treatment, as well as treatment and control of a plethora of other disease states, with minimal adverse effects[127]. It is therefore critical to identify novel natural compounds and sources of these compounds that can be exploited for their properties.

With fungal endophytes cultured from different parts of the plants collected from the new river valley, we were able to demonstrate high levels of cytotoxicity toward anti-breast cancer cells in several of the extracts. Furthermore, we were able to identify the fractions with the active metabolites through solid-phase extraction. Using 2D monolayer and 3D spheroid models of the TNBC cell line, we were able to demonstrate the differences observed in cytoxicity due to morphological and transcriptomic changes in 3D matrix microenvironments.

Current efforts are being led to identify the active metabolites using Mass Spectrometry, as well as focused on using breast epithelial tissue to identify any adverse cytotoxicity. With the advent of automated high-throughput screening technologies, it is likely that more natural compounds will be screened for their medicinal properties. In order to expedite the process going from drug discovery to drug approval, there is a need to improve the screening process, by introducing better disease models in the preclinical research phase.

3.6 Future Directions

3.6.1 Mass Spectrometry

Mass Spectrometry has been widely used since its inception, and more frequently to identify novel natural compounds. Active and non-active metabolites can be profiled using liquid chromatography and mass spectrometry in each of the extract fractions. Obtaining the chemical structures of potentially novel secondary metabolites with cytotoxic properties against breast cancer, and possibly other types of cancers will allow further scrutiny of their therapeutic function, target(s) and mechanism of action.

3.7 Conclusions

In conclusion, we were able to isolate endophytic fungi and demonstrate the anticancer properties of the extracts by screening MDA-MB-231 and using as end-point live and dead cell staining. Further screening was carried out after solid-phase extraction of extracts into fractions, to narrow down the source of the active secondary metabolite. Additional studies will focus on mass spectrometry to analyze the compounds in the active fractions, in order to further test for toxicity and efficacy.

3.8 Acknowledgments

We would like to thank John Feeman, Dave Close, Dr. Alex Nimiera and Dr. Holly Scoggins at Virginia Tech for help with the identification of the plants from which the endophytes were possibly derived.

3.9 Conflicts of Interest

There are no conflicts to declare.

3.10 Supplementary Information

Table 3.1: **Identification of Plants from which endophytes were derived.**

Plant	Broad ID	Genus	Species
S6			
S7	Herbaceous	Thalictrum	
S9	Privet	Ligustrum	sinense
S10	Herbaceous		
K1	Pokeweed	Phytolacca	americana

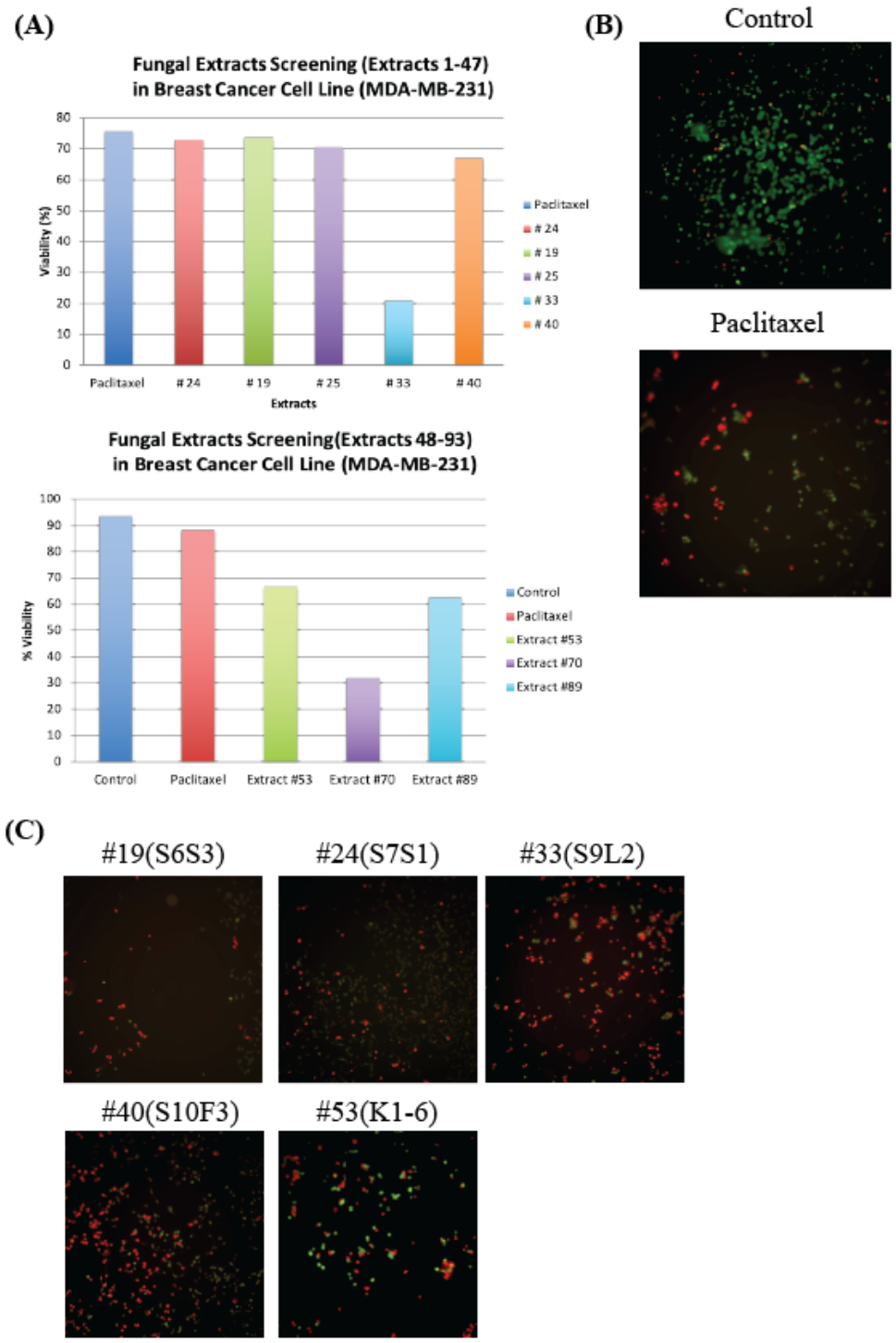

Figure 3.5: **Preliminary Screening of Fungal Extracts show anticancer properties.** **(A)** Fungal Extracts show higher cell death compared Paclitaxel. **(B)** Representative Images of MDA-MB-231 live (green) and dead(red) staining in Control and Paclitaxel treatments after 24 hours.**(C)**Representative Images of MDA-MB-231 live and dead staining for the fungal extracts chosen for further analysis in the study.

Chapter 4

Real-time sensing of ICAM1 and CD11b receptor expression using fluorescence resonance and nanometal surface energy transfer

4.1 Abstract

Conventional techniques for fluorescence-based assays include flow cytometry and immunofluorescence(IF). Flow cytometry gives the ability to use antibodies in conjunction in with live cells to visualize cell-surface protein expression. However, the information is limited to the surface expression without providing spatial or temporal value. Immunofluorescence is widely used to provide spatial context for protein expression, in both intracellular and extracellular proteins, but require the cells to be fixed, a process that kills the cells. Fluorescence-based assays in live-cell imaging have been rising over the last few years. However, there is a lack of a simple biosensor that can provide antigen-dependent fluorescence to offer spatiotemporal quantification of cell-surface proteins. Here, we aim to develop a quencher-fluorophore systems using gold nanoparticles and green fluorophore tagged antibody for the detection of

protein ectodomains in live cells. Bare gold nanoparticles are used for physical adsorption of the antibody on the surface, and results show successful binding based on the absorbance shift observed. In this study, ICAM1 and CD11b biosensors are developed and tested. CD11b is tested using primary neutrophils and leukocytes. In absence of the cells, and thus the target protein, quenching takes place via nonradiative energy transfer mechanisms. In the presence of cells expressing the target analyte, competitive binding of antibody to the antigen recovers the fluorescence, and can be observed under a fluorescent live-cell imaging.

4.2 Introduction

Spatiotemporal sensing of cell surface protein expression can be useful in studying cell behavior in various disease phenotypes. They are useful for measuring the expression and density of cell markers for applications in diagnosis and prognosis in clinics as well as for life science research. Unlike conventional techniques such as flow cytometry, immunohistochemistry (IHC) and enzyme linked immunosorbent assays (ELISA) that require a lot of reagents, time and labor, biosensors can be used for real-time and rapid point-of-care (POC) sensing[128, 129]. They can be integrated with live cell cultures to monitor dynamic changes while modulating *in vitro* microenvironments. Traditional cell-surface biosensors often require immobilization of cells, and despite providing rapid testing, they lack real-time monitoring capabilities, and do not always help biologists visualize the spatiotemporal changes. Moreover, some of these molecular beacons are complex to develop. There is need for a simple, yet effective approach to biosensing cell surface receptors.

Förster or fluorescent resonance energy transfer (FRET) is a nonradiative process in which energy is transferred from an excited donor fluorophore to an acceptor molecule by means of

intermolecular long-range dipole-dipole coupling. This is a distance-sensitive process wherein the energy transfer efficiency is dependent on the inverse sixth power of intermolecular separation[61, 130]. When the donor-acceptor separation is over the range of 1–10 nm, especially within the Förster radius, FRET is an accurate spectroscopic nano-ruler of molecular proximity which is able to quantitatively analyze biological phenomena well below the resolution of conventional optical microscopy. Currently, FRET has been widely used to investigate biomolecular interactions (e.g. protein-protein interactions, protein-DNA interactions, etc.), biomolecular dynamics and conformations (e.g. DNA folding, protein conformational change, etc.), drug and ligand screening, monitoring of cellular dynamics, and so on[71, 131].

To design a successful FRET probe, it first requires the donor fluorophore emission range, and the acceptor fluorophore excitation range to overlap by more than 30%. Many organic donor and acceptor fluorophore pairs have been developed for FRET, such as CFP and dsRED, BFP and GFP, Cy3 and Cy5, Alexa488 and Alexa555, Alexa488 and Cy3, and FITC and rhodamine.[132] With the emergence of nanobiosensors, nanoparticles (e.g. quantum dot, gold nanoparticles, upconversion nanoparticles, mesoporous silica nanoparticles, etc.) have been incorporated into the design of FRET systems[133]. Take gold nanoparticles (AuNPs) for example, they are excellent quenchers via FRET as well as nanometal surface energy transfer (NSET) because of their characteristic plasmon resonance, which results in extraordinary high molar extinction coefficients and broad energy bandwidth[77]. Nanobiosensors utilizing AuNPs with FRET have been applied for the detection of metal ions, small molecules, DNAs, proteins, pathogens, and mammalian cells[76]. Recent research also reported their applications in cancer cells, like targeted imaging and detection of matriptase expression in tumor cells, implying a great potential for disease diagnosis[63, 66, 134].

AuNPs can be functionalized with biomolecules via physical adsorption, usually via hydrophobic or electrostatic interactions, and Au-S bonding[135, 136]. This mechanism can

be applied specifically for bioconjugation of proteins (including antibodies) to AuNPs. The energy transfer mechanisms between fluorophores (conjugated to the antibody) are distance, fluorescent protein, and AuNP-size dependent[137, 138, 139]. Both FRET and NSET have been previously shown to play a role in nonradiative energy transfer, responsible for fluorescent quenching in these systems[140, 141, 142]. In case of FRET, the rate of energy transfer is proportional to $1/R^6$, wherein R is the distance between the donor and acceptor[143]. In NSET, however, it is proportional to $1/R^4$ [144]. The difference being NSET models the acceptor as a group of multiple point dipoles, as opposed to point dipoles in FRET[144]. More recent studies have shown fluorescent energy transfer to AuNP surfaces follows the NSET model[145]. Utilizing a simple physisorption technique, we evaluate the adsorption capability, stability, quenching and recovery of a fluorescence "on-off"-based AuNP-Antibody (Ab) biosensing system. This is depicted in the schematic within a live-cell system to enable real-time readouts in various cell-based assays, as shown in Figure 4.1. Additionally, Table 4.1 compares biosensing tools and their applications in cell-receptor sensing, outlining the advantages of the FRET system.

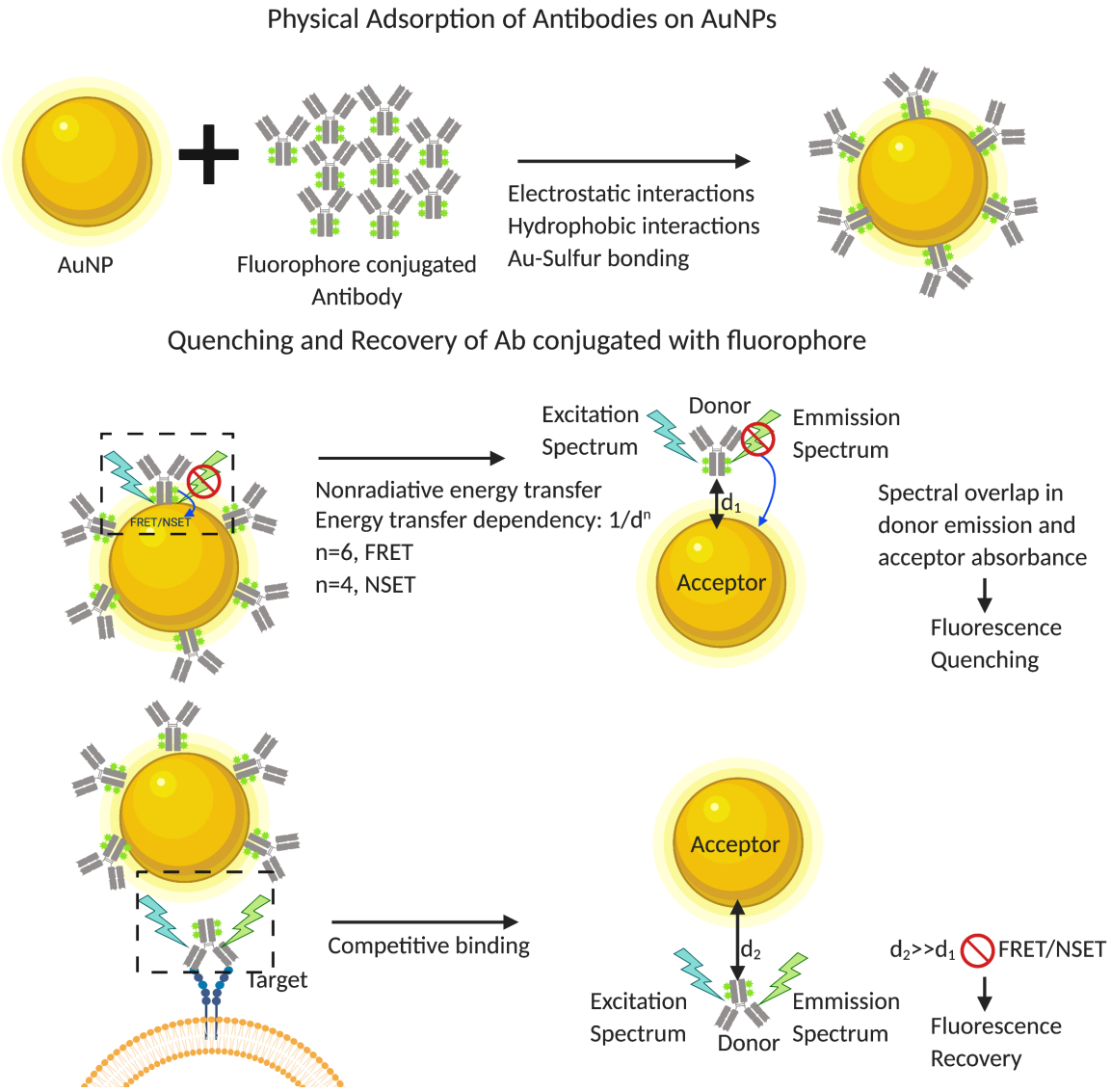

Figure 4.1: **Nonradiative energy transfer for application in real-time sensing.** Due to the energy transfer, fluorescence is quenched, and no fluorescence signal is interpreted.However, when the antibody with the tagged with the fluorophore comes into contact with the antigen on the cell surface, competitive binding increases the distance between the antibody and nanoparticle, causing the energy transfer to cease, thus recovering fluorescence. This mechanism can be applied for real-time sensing. Interactive forces between the gold nanoparticle and antibody also work to prevent unspecific binding, thereby making the sensing mechanism sensitive and reducing false readouts.

Table 4.1: **Antibody-based sensors for cell receptors.**

	IF	**FACS**	**Electrochemical**	**AuNP-Ab (FRET)**
Temporal quantification	✗	✗	✓	✓✓
Spatial quantification	✓✓	✗	✗	✓✓
Live Cells	✗	✓	✓	✓✓
Sensitivity	✓	✓	✓✓	✓
Specificity	✓	✓	✓	✓
Fast Response Time	✗	✓	✓✓	✓✓
Ease of Use	✗	✗	✗	✓

The cell surface receptors chosen for this study were ICAM1 and CD11b. Intercellular adhesion molecule (ICAM1) or CD54 expression can be induced via various cytokines in the cell's microenvironment, and plays a critical role in the inflammatory processes, and is associated with many pathological conditions[146]. Expression of ICAM1 on various cell surfaces have been correlated with a multitude of disease phenotypes, including cancer initiation, progression and metastasis, as well as polarization of tumor associated neutrophils and neutrophils in the context of sepsis[131, 132, 133, 147, 148]. Specifically, increased ICAM1 expression in several solid tumors is associated with poor survival, aggressive phenotypes, and increased transendothelial migration[119, 120, 124]. Additionally, elevated ICAM1 expression in neutrophils is known to induce the production of Neutrophil Extracellular Traps (NETs) and relates to a poor prognosis in sepsis[133].

Similarly, CD11b is also a transmembrane glycoprotein, and an important expression marker for leukocytes, and other immune cells[121, 123, 149]. CD11b expression and activation are involved in regulation of adhesion, migration, as well polarization of immune cells.Particularly, CD11b is an important receptor for lipopolysaccharide (LPS), an endotoxin on the outer walls of gram-negative bacteria[150]. CD11b expression in neutrophils provides both diagnostic and prognostic value in neonatal infection[123]. Furthermore, in adults with severe sepsis, neutrophil CD11b expression was found to be elevated compared to non-infectious

patients[151].

4.3 Materials and Methods

4.3.1 Ultraviolet-Visible (UV-Vis) Spectroscopy

To determine if the interactions between the AuNPs and Ab created stable AuNP-Ab conjugate, 10 nm and 20 nm bare (Sigma 752584) and citrate-stabilized (Sigma 741957) gold nanoparticles are incubated with ICAM1 (ThermoFisher #CL488-60299,) and CD11b (ThermoFisher # 53-0112-82) antibodies tagged with CoraLite488 and AlexaFluor488 respectively. The absorbance shift of bare AuNPs and AuNP-Ab conjugated are measured to evaluate the AuNP functionalization with Ab. This was done after diluting antibodies in PBS for a final concentration of 5 μgml^{-1}. Following which the stability of the functionalized AuNP is tested at 25°C and 37°C. The measurements were all taken using BioTek™ Cytation™ 3 Multimode Plate-reader.

4.3.2 Fluorescence Quenching

Quenching was observed using the end-point fluorescence measurement Ex/Em (485/520) of the green fluorophores upon sequential addition of 20μl AuNPs to 5μgml^{-1} of the antibody solution. The measurements were all taken using BioTek™ Cytation™ 3 Multimode Plate-reader. PBS (pH 7.4) was used as control to exclude the influence of volume change.

The interactions between AuNPs and Ab were further characterized by optical fluorescence measurement using a Nikon Ti-E light microscope. AuNPs were added into $5\mu gml^{-1}$ solution in $50\mu l$ increments, and images were taken after a 10 min incubation period after each addition. The ratio of Ab-AuNP was determined to ensure minimal background fluorescence and optimal recovery.

4.3.3 Cell Culture

Triple-negative breast cancer cell line MDA-MB-231 (American Type Cell Culture HTB-26) and Murine Macrophages (American Type Cell Culture RAW 264.7) were cultured in Gibco™ Dulbecco's Modified Eagle's Medium F-12 (DMEM/F-12) containing high glucose and GlutaMAX™, supplemented with 10% fetal bovine serum (FBS) and 100 units per ml penicillin and 0.1 mg ml^{-1} streptomycin. The cells were maintained in vented T-25 or T-75 flasks (corning) at 37°C and 5% CO2. Media was changed every 48 hours. Using 0.05% Trypsin-EDTA for detachment, cells were harvested for experiments at 80–90% confluency.

4.3.4 PBMC Isolation from Whole blood

Primary neutrophils were isolated from 10 mL whole blood, collected in EDTA tubes (shipped overnight) at ambient temperature using Phase 22 packaging. The EasySepTM human neutrophil isolation kit from STEMCELL Technologies (Catalog #17957) was used to isolate neutrophils whole blood via negative selection.

4.3.5 Cell-based Assays

The AuNP-Ab biosensor complex was prepared 30 mins prior to testing. Primary neutrophils were tested in 384-well plates, with 20 μl of media and 20 μl of the CD11B biosensor solution (containing 1% BSA).ND acquisition on Nikon Ti-E was used to measure fluorescence recovery at the cell surface. Fluorescence recovery was quantified and normalized relative to the background noise using Fiji/ImageJ[89].

4.3.6 Whole blood assay

Specificity of the sensor was studied using whole blood. BD contact-activated lancets (BD #366592) and microtainers (BD #365974) were used to collect blood via finger-pricking. The blood was centrifuged to remove excess RBCs. However, RBCs were incorporated in the solution being tested as a negative control. Additionally, Goat Anti-Rabbit secondary IgG tagged with Aelxaflour488 (Abcam #150077) was used as a negative control. CD11b sensor was used to to visualize CD11b expression on blood leukocytes.

4.4 Results

4.4.1 Physical functionalization of antibody on the gold nanoparticle surface produces a stable AuNP-Ab complex

Antibodies were initially tested for their functionalization of bare and citrate stabilized AuNPs. The surface plasmon resonance (SPR) peak for bare AuNPs was 515 nm whereas that of citrate-stabilized AuNPs was 520 nm. The SPR shift post the introduction of antibodies was by 10 nm for ICAM1(AF488) and ICAM1(CL488) for bare AuNPs and 5nm and no change for citrate stabilized AuNP respectively. The shift for CD11b was 5nm for bare AuNPs and no shift was observed in citrate-stabilized AuNPs (Figure 4.2). Functionalization was stronger on the surface of bare AuNPs compared to citrate stabilized AuNPs. Bare AuNPs were used going forward, and both 10nm and 20 nm AuNPs were used to test the functionalization. 10 nm AuNPs showed better functionalization as a measure of the absorbance shift (Figure 4.3) and was used moving forward. Stability of the AuNP-Ab complex remained unaffected by change in temperature to 37°C (Supplementary Figure 4.10).

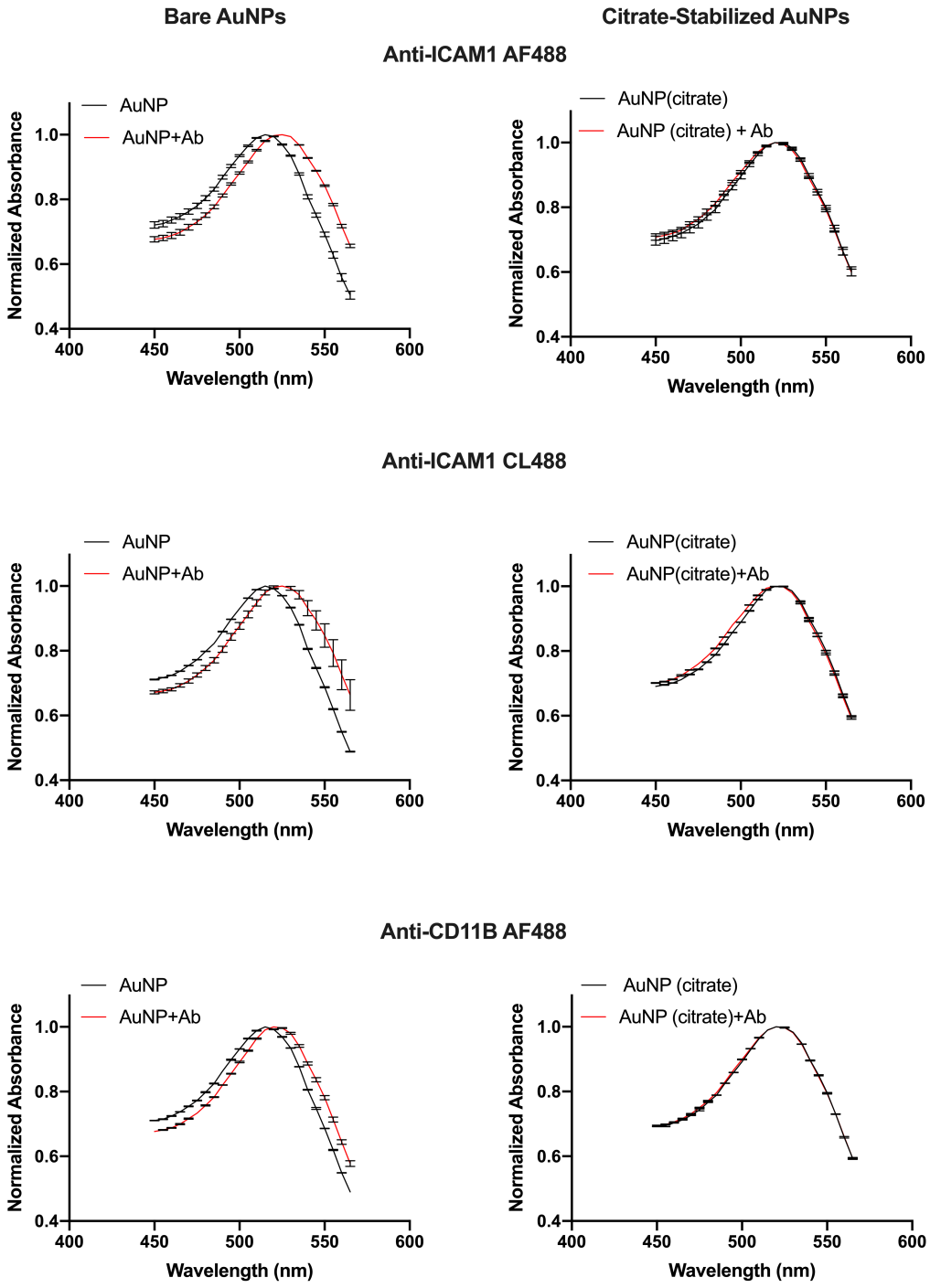

Figure 4.2: **SPR peak wavelength shift upon antibody adsorption.** Antibody adsorption on bare AuNPs produced better coverage (left) as indicated by the spectral shift, compared to citrate-stabilized AuNPs (right) for all the antibodies used.

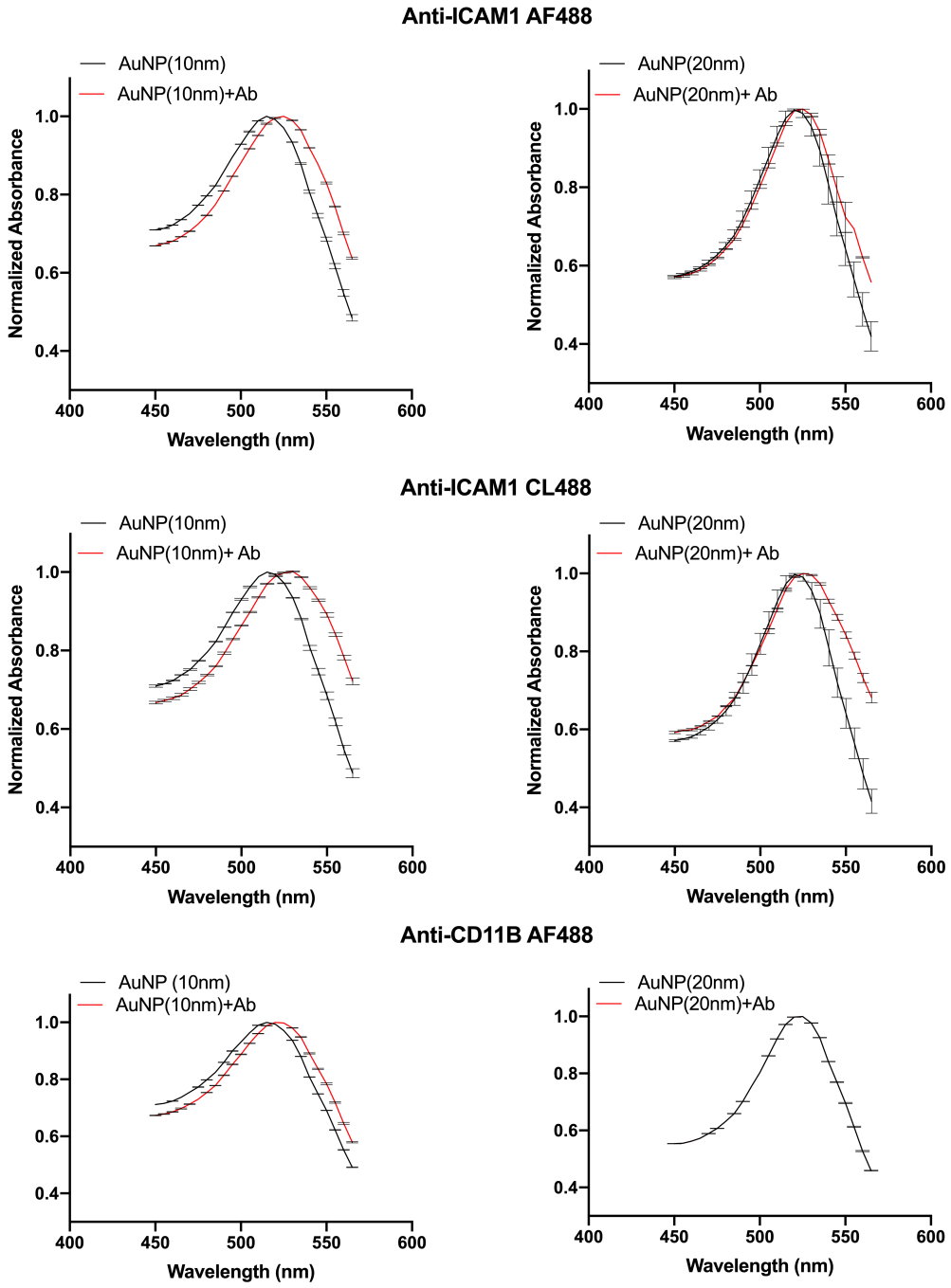

Figure 4.3: **AuNP size-dependent surface coverage of antibody.** 10 and 20 nm AuNPs were compared to optimize for coverage, quenching and recovery. Adsorption of both antibodies on 10nm AuNPs produced a larger spectral shift compared to 20nm AuNPs.

4.4.2 Fluorescence Quenching

The quenching effect of AuNPs was observed with increasing AuNPs in the solution and decreasing the ratio of Ab to AuNP (Figure 4.4). The relative fluorescence intensities were normalized to measure the decrease in fluorescence with decreasing Ab to AuNP ratio. After the addition of the total 100μl of AuNP for each Ab, at a ratio of 3.5 Ab particles to AuNP(10nm) nanoparticles, the quenching for anti-ICAM1 tagged with Alexafluor488 was 75%. For anti-ICAM1 tagged with CoraLite488, it was quenched by 84% . In the case of anti-CD11b tagged with Alexafluor488, it was much lower at 47%. Alternatively, addition of PBS to the Ab samples resulted in an average of 28% increase in fluorescence(not shown).

Fluorescence quenching by nonradiative energy transfer is visible under the light microscope, as shown in Figure 4.5. The molar ratio of Antibody to AuNP was determine based on the quenching properties of the AuNP to ensure all available Ab was bound to the AuNP surface and there was no fluorescent background visible. At a ratio of 3.5 Ab particles to AuNP, anti-ICAM1 tagged with Alexafluor488 showed an 87% decrease in fluorescence, anti-ICAM1 tagged with CoraLite488 showed an 88% decrease in fluorescence, and anti-CD11b tagged with Alexafluor488 showed a 63% reduction in fluorescence. Based on this, a 3 to 1 ratio of Ab to AuNP was considered to be optimal for the sensor.

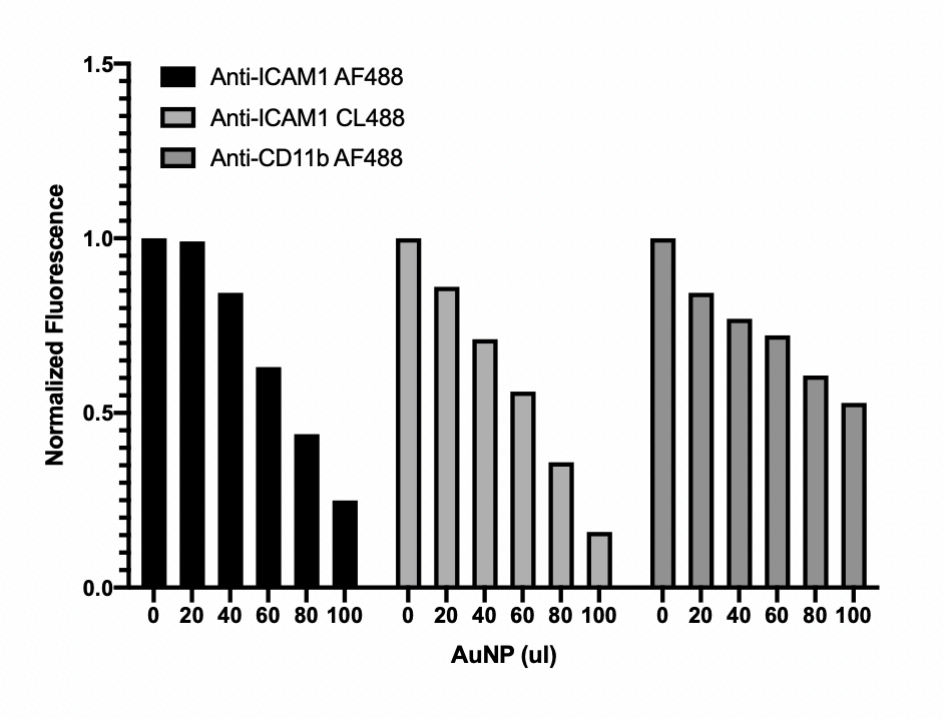

Figure 4.4: **Fluorescence Quenching of green fluorophore conjugated antibodies.** 10nm AuNPs were added in 20μl increments to measure the fluorescence quenching effects. ICAM1 antibodies tagged with Alexafluor488 and CoraLite488 showed effective quenching with increasing AuNPs in the solution.CD11b antibody tagged with Alexafluor488 demonstrated effective fluorescence quenching, however not as strongly as the ICAM1 antibodies.

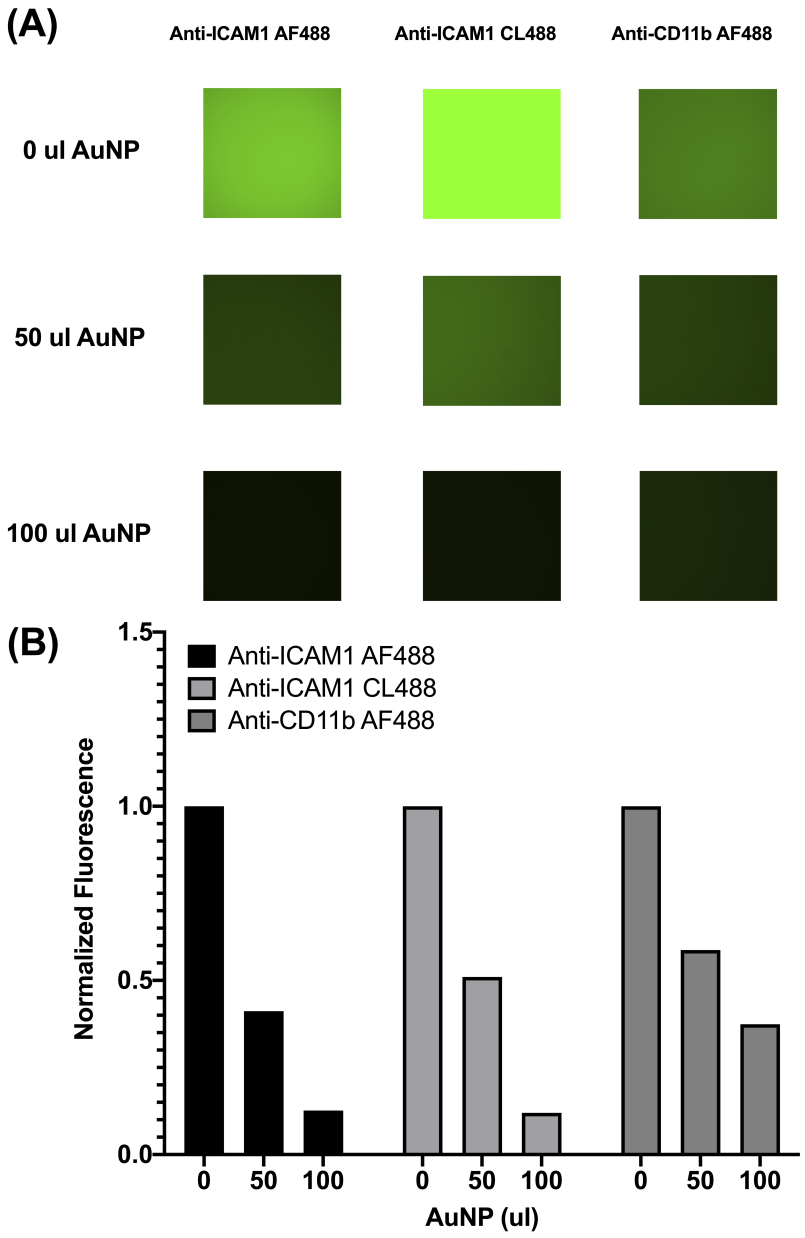

Figure 4.5: **Visual Quenching of green fluorophores conjugated to antibodies.** 10nm AuNPs were added in 50μl increments to measure the fluorescence quenching at a 300ms exposure time. **(A)** All the antibodies tagged with green fluorescent dyes showed decreasing fluorescence intensities with increasing AuNPs in the solution. **(B)**The corresponding normalized fluorescence intensities of the images demonstrate effective optical quenching of the green fluorophores.

4.4.3 Fluorescence Recovery using CD11b biosensor

Primary neutrophils were used to evaluate the recovery of AlexaFluor488 conjugated to CD11b. Antigen-dependent recovery of fluorescence was observed in isolated neutrophils (Figure 4.6). The fluorescence of the antibody on the neutrophil cell-surface was visualized over a period of 1 hour. Changes in fluorescence intensity can be observed spatiotemporally in Figure 4.7. The spatiotemporal fluorescence change can be quantified using a single neutrophil. Figure 4.8 shows the spatial and temporal changes in fluorescence of an individual neutrophil in a single frame. There are changes in the area of the cell as it moves in the physical space, as well as a change in the distribution of fluorescence intensity over time. Fluctuations in the changes are quantified using Fiji/ImageJ. Fluorescence intensity ranges from 74% of the initial fluorescence to 140%.

Further testing was done using whole blood. Primary leukocytes in the blood showed recovery using the CD11b biosensor (Figure 4.9). Red blood cells did not show any level of fluorescence. Similarly, negative control Goat Anti-Rabbit secondary IgG antibody tagged with Alexafluor488 did not have any recovery of fluorescence.

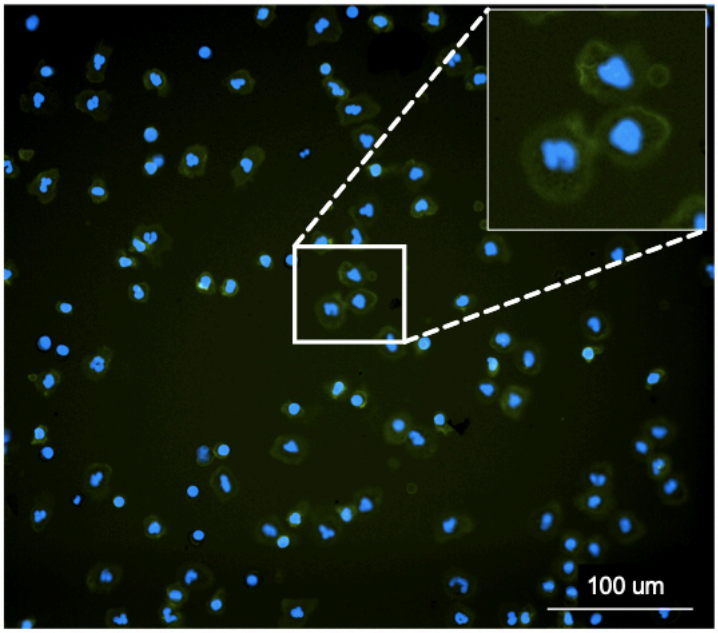

Figure 4.6: **Successful fluorescence recovery was observed using the CD11b biosensor with primary neutrophils.** Fluorescence recovery was observed with CD11b biosensor (green) using primary neutrophils (blue nuclei) (n=1).

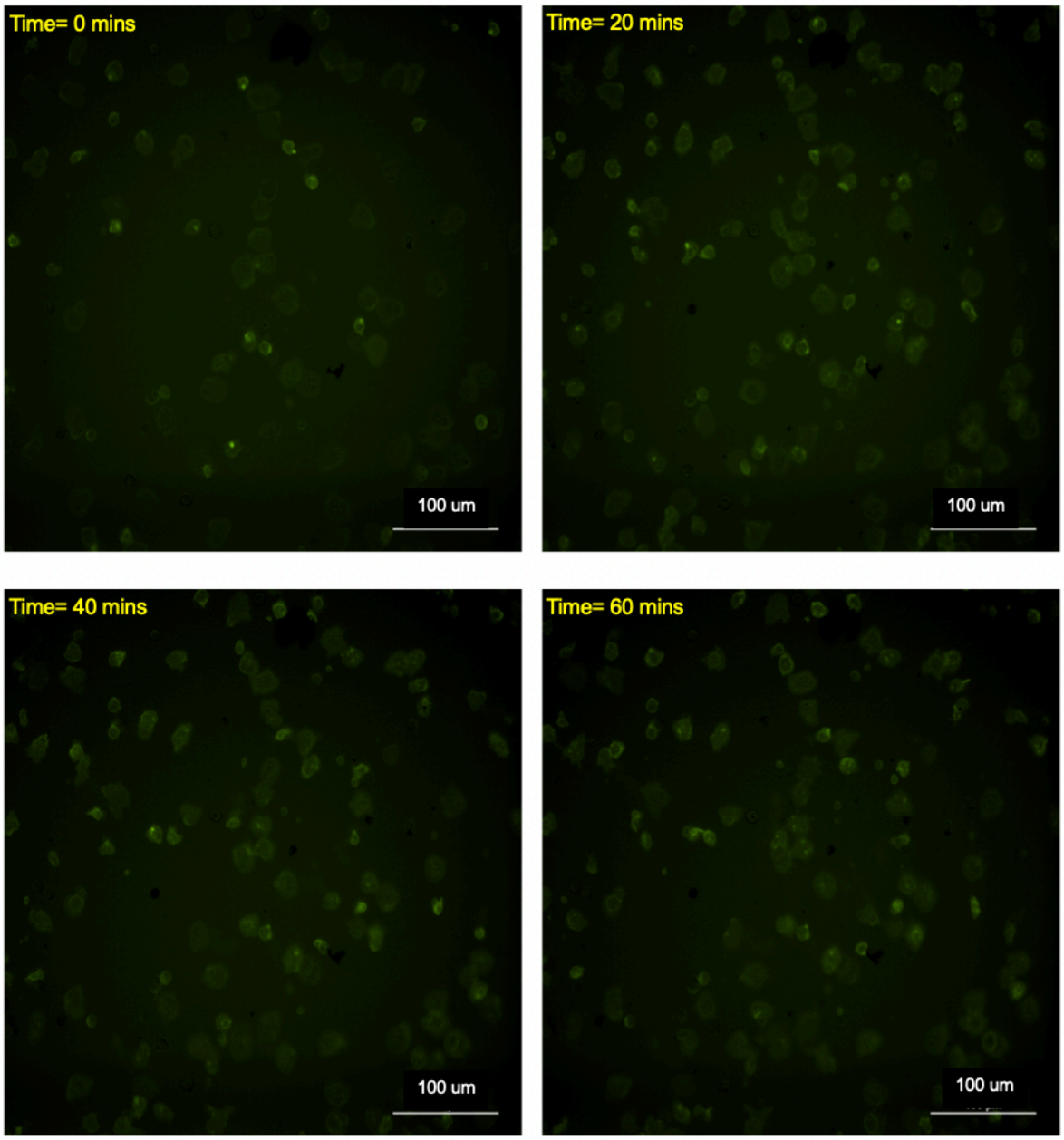

Figure 4.7: **Time-lapse image of the primary neutrophils shows active biosensing over a period of 1 hour.** The CD11b biosensor expression on neutrophil membrane surface can be seen over a period of 1 hr.

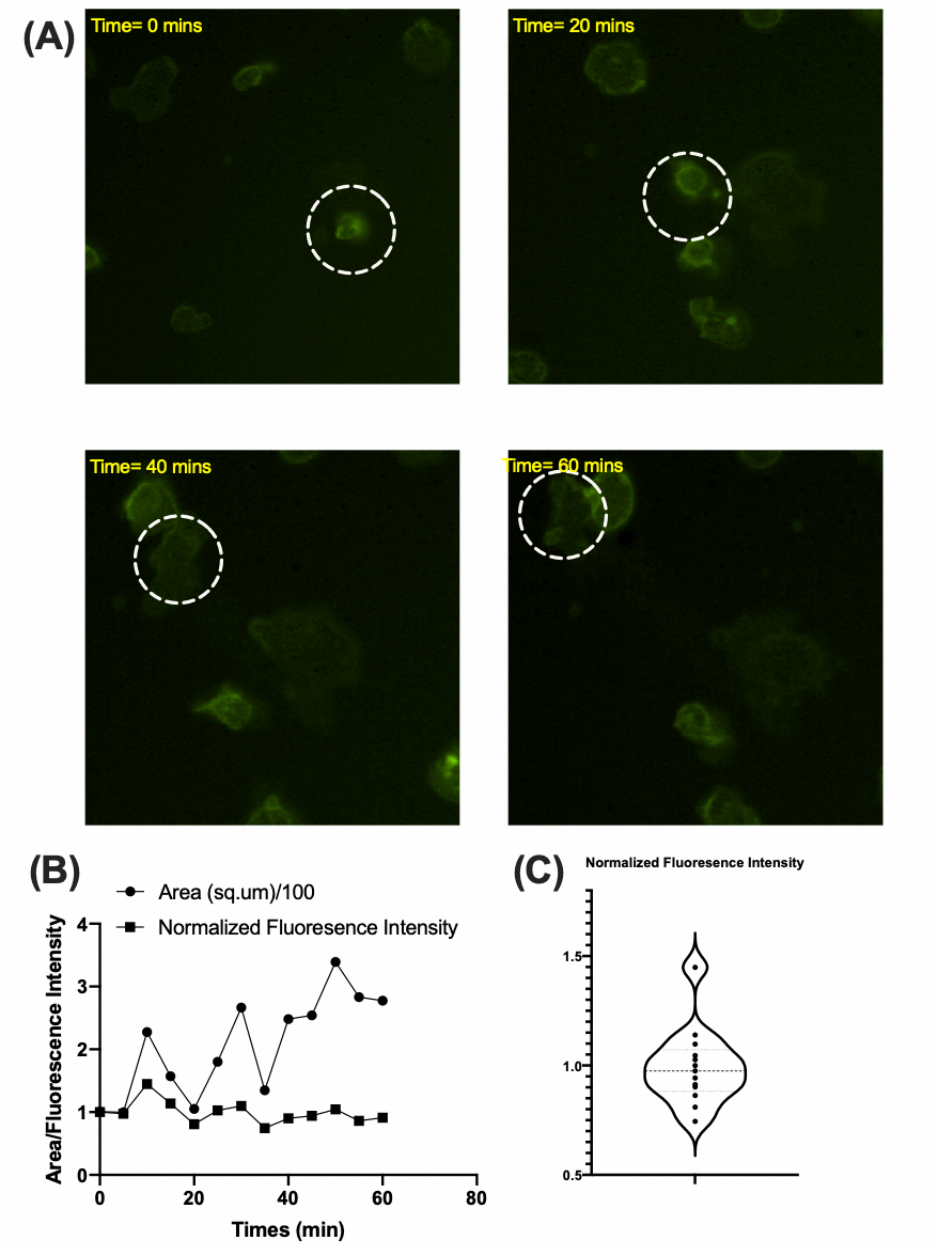

Figure 4.8: **Temporal quantification of fluorescence of the primary neutrophils. (A)** The CD11b biosensor expression on a single neutrophil membrane surface(green) can be seen over a period of 1 hr. Snapshots shown are taken 20 mins apart. **(B)** The plots shows the changes in cell area and normalized fluorescence intensity(with respect to the first time point) over a period of 60 mins, with 5 min intervals. **(C)** The violin plot shows the distribution of fluorescence intensity of a single neutrophil over 60 mins. Data plots are plotted for images that were taken every 5 mins.

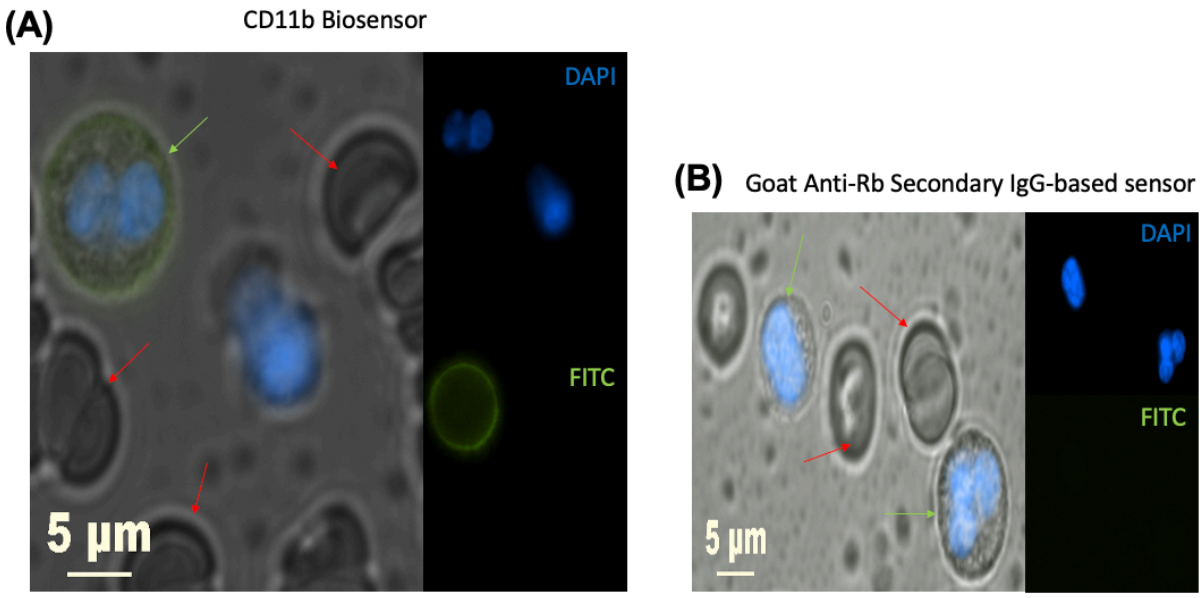

Figure 4.9: **Fluorescence recovery in primary leukocytes in whole blood. (A)**CD11b expression (green) on leukocytes(green arrow) is observed upon fluorescence recovery. No recovery is observed in RBCs(red arrow).**(B)** Goat Anti-Rabbit secondary IgG tagged with Alexafluor488 is used as a negative control and shows no recovery in leukocytes or RBCs in whole blood.

4.5 Discussion

In this study, we were able to present a simple, effective approach to quantify cell-surface receptor expression using gold nanoparticles and passive adsorption of fluorescent antibodies. The antibodies functionalized successfully on the gold nanoparticles as demonstrated, with effective energy transfer, resulting in quenching of antibodies prior to target introduction. The rapid sensing of cell-surface receptor could save labor and cost-intensive methods used in immunoassays and be especially useful in POC diagnostics. However, the applications go beyond clinical testing to applications in life sciences research and preclinical research for real-time quantification of cell phenotype.

The SPR peak wavelength shift upon binding was greater by a difference of 5nm for bare AuNPs compared to citrate-stabilized AuNPs, indicating a much better binding coverage. However, the balance between the various dipole-dipole interactions are distinctive, since it is dependent both on the specific type of protein and the AuNP surface chemistry[152]. Interestingly, the spectral shift was higher for 10 nm AuNPs compared to 20nm AuNPs when bound to the antibody. While this may be due to a lower concentration of antibody unable to provide the surface coverage required for a larger spectral shift. Further studies, such as investigating protein interactions using Raman Spectroscopy, are required to understand the binding chemistry in better depth.

Quenching of fluorescence using AuNPs was quantified and found to be efficient both using UV-Vis fluorescence quantification and using filter-based light microcope. Preliminary studies were able to show competitive binding of the receptor antigen to the CD11b antibody, disrupting the energy transfer, and recovering fluorescence. The live imaging of primary neutrophils was carried out over an hour and the spatiotemporal resolution of the receptor

expression is quantifiable via image processing tools.

4.6 Future Directions

4.6.1 Optimization of Protein Microarray Printing to develop a standard calibration curve

Ongoing studies are focused on optimizing microarray printing to develop a calibration curve and determine the range and sensitivity of the antibody for fluorescence recovery.

Protein microarray printing is carried out using Nexterion Slide H-3D hydrogel coated slide (SKU:1070936). An 8-pin handheld microarrayer is used to print different concentrations of the pure analyte to produce 500μm individual protein spots.

4.6.2 Additional Testing and Optimization of the Biosensor

MDA-MB-231 TNBC breast cancer cells and RAW264.7 murine macrophages are currently being tested for their ICAM1 expression using the biosensor.

Additional studies will focus on site-directed binding of antibody to AuNPs to ensure the right orientation for optimal recovery of fluorescence. The goal would be to carry forward the biosensing technology and translate it for the detection and temporal sensing of other prominent receptors in various other cell types.

4.7 Conclusions

In Conclusion, we were able to develop a simple, yet effective biosensor for real-time sensing of ICAM1 and CD11b receptor sensing. The results demonstrated effective binding and forming of a stable AuNP-Ab complex, with effective quenching of green fluorophores. Introducing the CD11b biosensor on primary neutrophils isolated from whole blood, we were able to show a recovery of fluorescence at the point of receptor expression. Further studies will focus on optimizing the printing of antigen microarrays for sensor calibration. Additionally, employing methods such as Raman Spectroscopy would enable further optimizing of antibody orientation on the nanoparticle surface for better and faster response. The applications of the biosensor would range from POC diagnostics in clinics to further enable spatiotemporal quantification of receptor-ligand interactions in various microphysiological systems *in vitro*.

4.8 Acknowledgments

Research reported in this publication was supported by The National Institute of General Medical Sciences of the National Institutes of Health under award number R35GM13361. Primary patient samples were obtained with written informed consent. IRB 2361 was approved by the Institutional Review Board at Virginia Tech as well as the Carilion Clinic in Roanoke, VA.

4.9 Conflicts of Interest

There are no conflicts to declare.

4.10 Supplementary Information

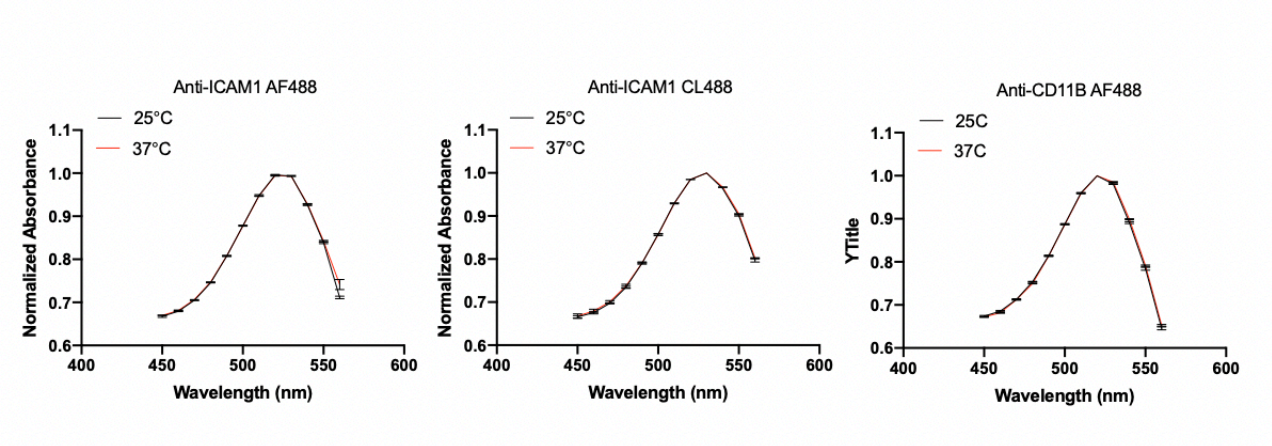

Figure 4.10: **Stability of AuNP-Ab complex.** Temperature stability the AuNP-antibody complex was tested at both 25°C and 37°C, and there was no change in spectral shift for over an hour.

Chapter 5

Future Directions

5.1 Microfluidic Devices

Microscale technologies like microfluidic devices allow patterning of complex designs to create functional platforms for a plethora of research needs, such as novel analytical methods to answering fundamental questions in cell biology[153, 154, 155, 156, 157]. The microscale nature allows better control, needs fewer reagents, and gives the ability to quantify changes at the single-cell level resolution[158, 159, 160]. Since the advent of new methods for fabricating microfluidic devices, it has been used widely to study spatiotemporal interactions of cells within engineered microenvironments in these systems. Specifically, it offers the benefit of being able to recapitulate the spatial intricacies to study the interactions between cells of the tumor stroma[161, 162, 163]. Silicone-elastomer based microfluidic devices, such as Polydimethylsiloxane (PDMS) have been used widely to incorporate 3D tumor models in the past for a diverse range of applications. These include studying interactions with the innate and adaptive immune cells, tissue-resident epithelial cells, and the vasculature[164, 165, 166]. Figure 5.1 shows the process of developing PDMS-based microfluidic devices using soft lithography.

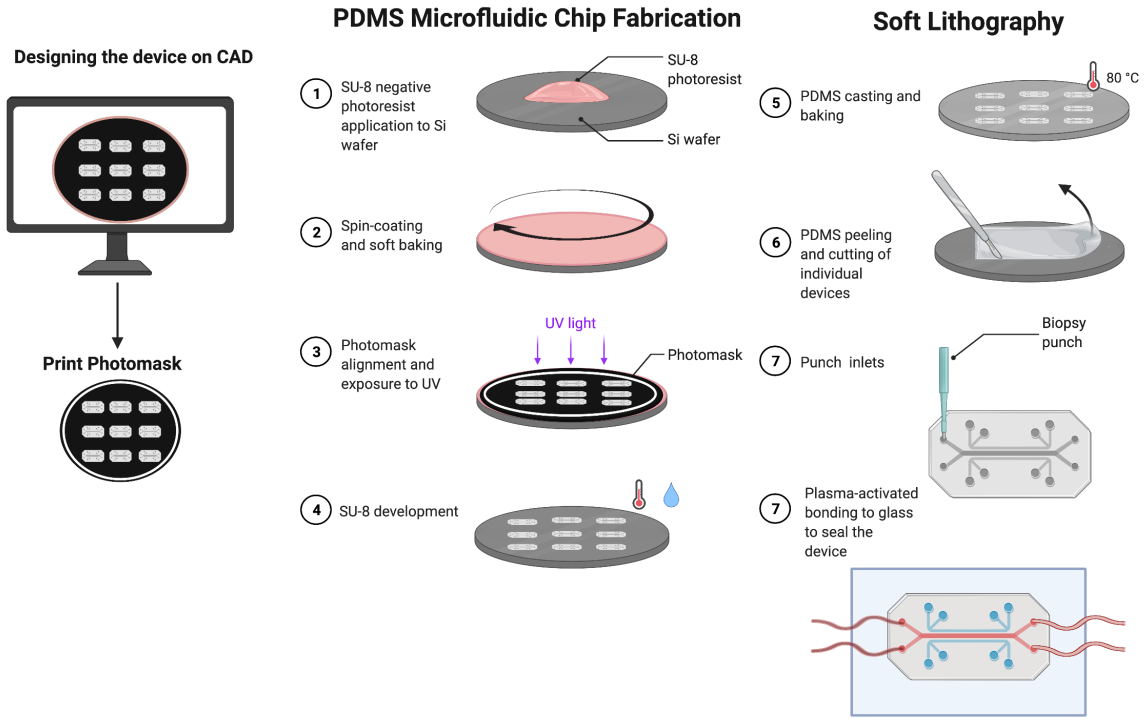

Figure 5.1: **Microfluidic Device Design and Fabrication** After designing the microfluidic device on a computer-aided design software, a photomask is printed. Photolithography is carried out to transfer the patterns on a silicon wafer, as the master mold. Soft Lithography is used to create patterned PDMS devices, which can be sealed after plasma-activation and thermal bonding to glass. Fluids can then be run through the channels for various applications.

5.2 Design and Development of a microfluidic platform to study neutrophil behavior in the tumor stroma

5.2.1 Neutrophils in the Tumor Microenvironment

Tumor-associated neutrophils (TANs) are known to contribute to the pathogenesis of cancer. Neutrophil heterogeneity in the tumor microenvironment, as anti-tumor(N1) or pro-tumor(N2) is modulated by cues from the tumor niche [167]. Cells of the immune system are a critical component of the tumor microenvironment. Systemic inflammation and evading the response of the innate and adaptive immune system is a hallmark of cancer[168, 169]. Previous studies have focused on the monocyte-macrophage lineage and their plasticity in the tumor microenvironment, displaying classical M1 and alternative M2 profiles. Neutrophils, on the contrary, were extensively studied as first responders in the fight against microbes[170]. Neutrophil plasticity has only recently been considered as a key contributor to tumor initiation, progression and metastasis. Early studies into neutrophil polarization in the tumor microenvironment has identified immunosuppressive cytokine, TGF-β, as a driver of N2 neutrophil phenotype. TGF-β depletion or blockage, was able to increase the recruitment of neutrophils and induce an N1 neutrophil phenotype. In addition to decreased TGF-β, elevated levels of type-1 interferons (IFN) were attributed to neutrophil polarization to the N1 subtype[171]. N1 polarization of neutrophils were able to inhibit tumor growth and their increased expression of cytokines such as CCL3 and TNF were responsible for driving the recruitment of CD8+ T cells to the tumor site [171, 172]. N1 TANs were found to have increased expression of ICAM1, IL-12, TNF and high Neutrophil-extracellular traps production compared to N2 neutrophils [172]. However, the anti-tumor role of ICAM1, an

adhesion molecule is not fully understood. Correlating migration of neutrophils and ICAM1 expression may provide more insight. The increasing interest in studying neutrophil function in the tumor microenvironment is hindered by the lack of an *in vitro* platform to study the interactions of TANs and their response to external stimuli.

5.2.2 Approach for studying neutrophil behavior in a novel microfluidic platform

Previous studies have focused on using animal models and primary neutrophils to study N1 and N2 phenotype. While this approach has increased understanding of neutrophil function in the tumor microenvironment, their function cannot be quantified in real-time, and heterogeneity cannot be measured at single-cell resolution. Designing and developing a microfluidic platform with a biomimetic tumor microenvironment allows us to study the plasticity and polarization of neutrophils in the tumor niche in real-time, and at a single-cell resolution. Additionally, incorporation of antigen-dependent biosensors will allow real-time quantification of specific biomarkers.

AutoCAD, a 2D design software, is used to design the device to reflect features similar to the *in vivo* tumor stroma, and the device is fabricated using photolithography techniques (Figure 5.2). Spheroid chambers are designed for the 3D tumor-model, and a pressure regulator is designed for the controlled introduction of the cells encapsulated within the hydrogel to be contained within the spheroid chamber. Also in the device is a channel for introducing neutrophils and smaller 10µm migration channels will allow for neutrophils to migrate to the tumor site. A small area around the spheroid is provided to study the influence of other cells of the tumor stroma in the context of neutrophil behavior, such

as tissue-resident macrophages. Initial analysis of the device on CFD software COMSOL shows that chemoattractant signals in the cell chamber should form a gradient to encourage neutrophil migration to the tumor site (Figure 5.3).

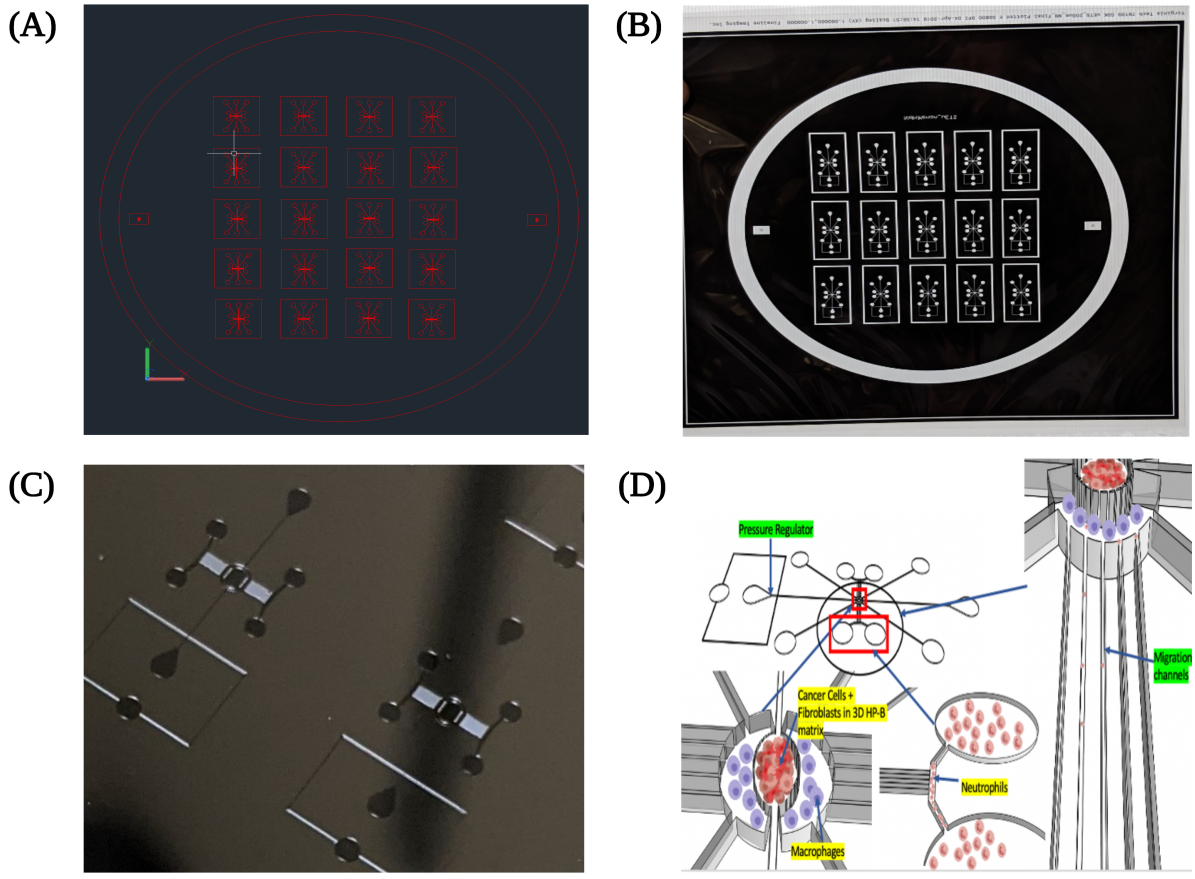

Figure 5.2: **Microfluidic platform to study neutrophil behavior in the tumor microenvironment.** **(A)** AutoCAD is used to make a 2D design of the device. **(B)** The corresponding photomask is printed. **(C)** Photolithography is carried out to transfer the patterns on a silicon wafer. The corresponding pattern is shown, zoomed in on two devices on the wafer.**(D)**The schematic outlines the individual features of the device, highlighting the concept behind the design.

The platform in will enable the culture of patient-derived cancer cells and incorporation of isolated primary neutrophils to study previously unexplored interactions *in vitro*. Recent studies have indicated that neutrophils have the potential to both inhibit and aggravate cancer progression based on microenvironmental cues. Our platform allows for ease of modula-

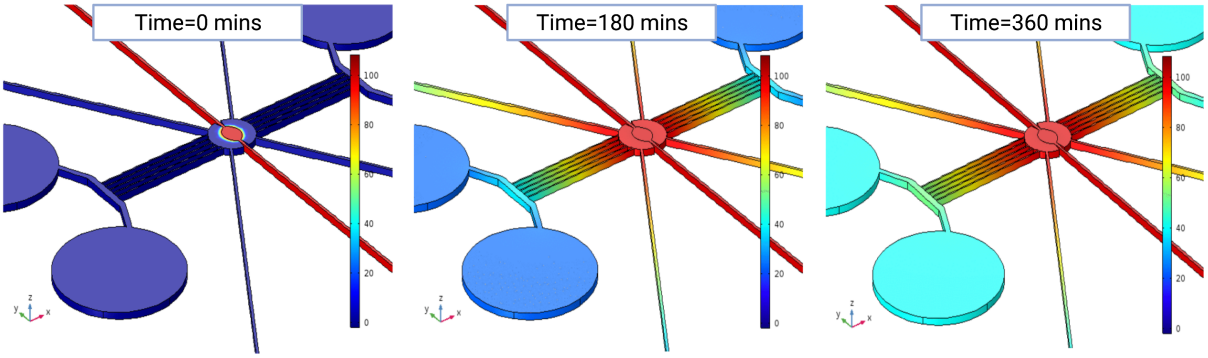

Figure 5.3: **CFD simulation showing the generation of chemoattractant gradients within the device.**

tion of environmental signals and immediate quantification of neutrophil response. Studying migration, NETosis and polarization of neutrophils will provide insight into novel targets for immunotherapy.Furthermore, our microfluidic chip can be used in translation, and will be able to open novel avenues in the field of personalized treatment.

Chapter 6

Conclusions

This dissertation has contributed to the development and understanding of microscale systems for applications in engineering the tumor microenvironment and quantifying cell phenotype. The goal is to eventually steer the platforms engineered and evaluated in these studies for applications in the culture of primary tumor samples *ex vivo* and to provide insight into phenotypic profiles that may be of diagnostic and prognostic value to the patient.

In chapter 2, we characterized the microscale architecture of heparin-based hydrogel scaffolding for engineering the tumor extracellular matrix. We emphasized on understanding the solid-phase GF presentation of EGF, an important growth factor overexpressed in several breast tumors. The composite mixture of thiolated collagen, hyaluronic acid, and heparin polymers, cross-linked with PEG-diacrylate was able to produce a hydrogel matrix with a stiffnes of 140 Pa. This was comparable to regular breast tissue and suitable for initial seeding of cancer cells. We were able to demonstrate the long-term solid-phase presentation of signals in the microenvironment due to the presence of GF-binding moieties, such as heparin and hyaluronic acid in the matrix. The influence of the engineered extracellular matrix on the cell morphology, viability, proliferation, and cell response to chemotherapy was compared to aqueous media. These were also quantified in 2D and 3D systems with EGF stimulation. The results showed the self-assembly of cells within the matrix into 3D MCSs compared to the epithelial morphology seen in 2D cultures. The viability was improved significantly in the microspheroids, also exhibiting significantly lower cell-death when treated with paclitaxel.

Ki-67 (marker of proliferation) stained nuclei had decreased in the 3D environment, but EGF stimulation in aqueous media increased proliferation. Through further RNA-sequencing using Next-Gen Sequencing, we were able to shed light on the hallmark pathways in cancer that were differentially regulated in these systems. Specific pathway changes in MCSs indicated cross-talk that might confer adaptive responses to chemotherapies. Additionally, we noticed significant changes in pathways regulating immune-cell responses. The GF stimulation in aqeuous media had a different expression profile compared to solid-phase stimulation. We were able to show the biocompatibility of the scaffold for cultivating breast cancer cells through the characteristic changes in phenotypic expression, which closely mimicked the expression profiles of early tumor formation *in vivo* .

In Chapter 3, we aimed the platform evaluated in Chapter 2 for screening natural compounds derived for endophytic fungi in a preliminary drug discovery process. Endophytic fungi were isolated from plants around the New River Valley in Virginia, USA. Individual fungi were grown and their extracts were filtered for an initial screening with 2D breast cancer cells. Results were compared against Paclitaxel, and the extracts were found to have high cytotoxicity against triple-negative breast cancer cells. Of the 25 hits that performed better than the standard Paclitaxel treatment, the first five were chosen to be further analyzed after solid-phase extraction to narrow down the active secondary metabolite. Further screening with the fractions in a 2D platform was able to highlight the active fractions. Once this was observed, fungal culture was scaled-up to produce larger quantities of fractions to be tested in both 2D and 3D platforms. While several of the fractions were active and induced cell death, 3D spheroid model of the TNBC cells showed significantly different responses, often resulting in lower cell death compared to the cells in 2D monolayer.

In Chapter 4, the goal was to develop a metal quencher-fluorophore pair for effective nonradiative energy transfer either via Förster Resonance Energy Transfer (FRET) or Nanometal

Surface Energy Transfer(NSET) for cell-surface receptor biosensing. Citrate-stabilized and bare AuNPs were used to observe the physical adsorption of CD11b and ICAM1 antibodies(Ab) tagged with green fluorophores. We were able to see a better surface coverage of antibodies in bare AuNPs, indicated by the absorbance shift in the SPR peak of AuNPs. 10 nm and 20nm bare AuNPs were both tested to compare Ab coverage. 10 nm AuNPs provided a better surface for physical adsorption in all the Abs that were tested. Quenching of the fluorophore was observed through the FITC filter on the microscope. Increasing amounts of AuNPs resulted in visible quenching of the fluorophore conjugated to the antibodies. To test antigen-dependent recovery of fluorophores, cells expressing ICAM1 (MDA-MB-231 and RAW 264.7) and CD11b (primary neutrophils) were chosen. Upon introducing the previously non-fluorescing biosensor consisting of AuNP-Ab complex, into wells with cells expressing the antigen, we observed the recovery of fluorescence. The fluorescence was observed in live cells over a period of 1 hour. Using an image analysis software, we were able to quantify fluorescence expression changes in a single cell over a period of time. The spatiotemporal quantification of cell phenotype via the expression of cell-surface proteins can be used in conjunction with 3D cell-based assays and microscale platforms like microfluidic devices to scrutinize single-cell heterogeneity of various cells in the tumor-microenvironment.

Bibliography

[1] S. Mittal, N. J. Brown, and I. Holen. The breast tumor microenvironment: role in cancer development, progression and response to therapy. *Expert Rev Mol Diagn*, 18 (3):227–243, 2018. ISSN 1744-8352 (Electronic) 1473-7159 (Linking). doi: 10.1080/14737159.2018.1439382. URL https://www.ncbi.nlm.nih.gov/pubmed/29424261.

[2] F. Balkwill and A. Mantovani. Inflammation and cancer: back to virchow? *Lancet*, 357(9255):539–45, 2001. ISSN 0140-6736 (Print) 0140-6736 (Linking). doi: 10.1016/S0140-6736(00)04046-0. URL https://www.ncbi.nlm.nih.gov/pubmed/11229684.

[3] I. P. Witz. The tumor microenvironment: the making of a paradigm. *Cancer Microenviron*, 2 Suppl 1:9–17, 2009. ISSN 1875-2292 (Print) 1875-2284 (Linking). doi: 10.1007/s12307-009-0025-8. URL https://www.ncbi.nlm.nih.gov/pubmed/19701697.

[4] T. L. Whiteside. The tumor microenvironment and its role in promoting tumor growth. *Oncogene*, 27(45):5904–12, 2008. ISSN 1476-5594 (Electronic) 0950-9232 (Linking). doi: 10.1038/onc.2008.271. URL https://www.ncbi.nlm.nih.gov/pubmed/18836471.

[5] M. Allinen, R. Beroukhim, L. Cai, C. Brennan, J. Lahti-Domenici, H. Huang, D. Porter, M. Hu, L. Chin, A. Richardson, S. Schnitt, W. R. Sellers, and K. Polyak. Molecular characterization of the tumor microenvironment in breast cancer. *Cancer Cell*, 6(1):17–32, 2004. ISSN 1535-6108 (Print) 1535-6108 (Linking). doi: 10.1016/j.ccr.2004.06.010. URL https://www.ncbi.nlm.nih.gov/pubmed/15261139.

[6] A. Ben-Baruch. Host microenvironment in breast cancer development: inflammatory cells, cytokines and chemokines in breast cancer progression: reciprocal tumor-

microenvironment interactions. *Breast Cancer Res*, 5(1):31–6, 2003. ISSN 1465-542X (Electronic) 1465-5411 (Linking). doi: 10.1186/bcr554. URL https://www.ncbi.nlm.nih.gov/pubmed/12559043.

[7] D. Hanahan and L. M. Coussens. Accessories to the crime: functions of cells recruited to the tumor microenvironment. *Cancer Cell*, 21(3):309–22, 2012. ISSN 1878-3686 (Electronic) 1535-6108 (Linking). doi: 10.1016/j.ccr.2012.02.022. URL https://www.ncbi.nlm.nih.gov/pubmed/22439926.

[8] G. Lorusso and C. Ruegg. The tumor microenvironment and its contribution to tumor evolution toward metastasis. *Histochem Cell Biol*, 130(6):1091–103, 2008. ISSN 0948-6143 (Print) 0948-6143 (Linking). doi: 10.1007/s00418-008-0530-8. URL https://www.ncbi.nlm.nih.gov/pubmed/18987874.

[9] M. Giussani, G. Merlino, V. Cappelletti, E. Tagliabue, and M. G. Daidone. Tumor-extracellular matrix interactions: Identification of tools associated with breast cancer progression. *Semin Cancer Biol*, 35:3–10, 2015. ISSN 1096-3650 (Electronic) 1044-579X (Linking). doi: 10.1016/j.semcancer.2015.09.012. URL https://www.ncbi.nlm.nih.gov/pubmed/26416466.

[10] J. Insua-Rodriguez and T. Oskarsson. The extracellular matrix in breast cancer. *Adv Drug Deliv Rev*, 97:41–55, 2016. ISSN 1872-8294 (Electronic) 0169-409X (Linking). doi: 10.1016/j.addr.2015.12.017. URL https://www.ncbi.nlm.nih.gov/pubmed/26743193.

[11] M. K. Jena and J. Janjanam. Role of extracellular matrix in breast cancer development: a brief update. *F1000Res*, 7:274, 2018. ISSN 2046-1402 (Print) 2046-1402 (Linking). doi: 10.12688/f1000research.14133.2. URL https://www.ncbi.nlm.nih.gov/pubmed/29983921.

[12] A. Kadar, A. M. Tokes, J. Kulka, and L. Robert. Extracellular matrix components in breast carcinomas. *Semin Cancer Biol*, 12(3):243–57, 2002. ISSN 1044-579X (Print) 1044-579X (Linking). doi: 10.1016/s1044-579x(02)00027-5. URL https://www.ncbi.nlm.nih.gov/pubmed/12083854.

[13] R. T. Kao, J. Hall, and R. Stern. Collagen and elastin synthesis in human stroma and breast carcinoma cell lines: modulation by the extracellular matrix. *Connect Tissue Res*, 14(4):245–55, 1986. ISSN 0300-8207 (Print) 0300-8207 (Linking). doi: 10.3109/03008208609017468. URL https://www.ncbi.nlm.nih.gov/pubmed/2938880.

[14] A. S. Hoffman. Hydrogels for biomedical applications. *Ann N Y Acad Sci*, 944:62–73, 2001. ISSN 0077-8923 (Print) 0077-8923 (Linking). doi: 10.1111/j.1749-6632.2001.tb03823.x. URL https://www.ncbi.nlm.nih.gov/pubmed/11797696.

[15] W. Hu, Z. Wang, Y. Xiao, S. Zhang, and J. Wang. Advances in crosslinking strategies of biomedical hydrogels. *Biomater Sci*, 7(3):843–855, 2019. ISSN 2047-4849 (Electronic) 2047-4830 (Linking). doi: 10.1039/c8bm01246f. URL https://www.ncbi.nlm.nih.gov/pubmed/30648168.

[16] W. Hu, Z. Wang, Y. Xiao, S. Zhang, and J. Wang. Advances in crosslinking strategies of biomedical hydrogels. *Biomater Sci*, 7(3):843–855, 2019. ISSN 2047-4849 (Electronic) 2047-4830 (Linking). doi: 10.1039/c8bm01246f. URL https://www.ncbi.nlm.nih.gov/pubmed/30648168.

[17] Cindy J. Farino, Shantanu Pradhan, and John H. Slater. The influence of matrix-induced dormancy on metastatic breast cancer chemoresistance. *ACS Applied Bio Materials*, 3(9):5832–5844, 2020. doi: 10.1021/acsabm.0c00549. URL https://doi.org/10.1021/acsabm.0c00549.

[18] S. Pradhan and J. H. Slater. Tunable hydrogels for controlling phenotypic cancer cell states to model breast cancer dormancy and reactivation. *Biomaterials*, 215:119177, 2019. ISSN 1878-5905 (Electronic) 0142-9612 (Linking). doi: 10.1016/j.biomaterials.2019.04.022. URL https://www.ncbi.nlm.nih.gov/pubmed/31176804.

[19] M. C. Catoira, L. Fusaro, D. Di Francesco, M. Ramella, and F. Boccafoschi. Overview of natural hydrogels for regenerative medicine applications. *J Mater Sci Mater Med*, 30(10):115, 2019. ISSN 1573-4838 (Electronic) 0957-4530 (Linking). doi: 10.1007/s10856-019-6318-7. URL https://www.ncbi.nlm.nih.gov/pubmed/31599365.

[20] M. W. Tibbitt and K. S. Anseth. Hydrogels as extracellular matrix mimics for 3d cell culture. *Biotechnol Bioeng*, 103(4):655–63, 2009. ISSN 1097-0290 (Electronic) 0006-3592 (Linking). doi: 10.1002/bit.22361. URL https://www.ncbi.nlm.nih.gov/pubmed/19472329.

[21] H. K. Kleinman and G. R. Martin. Matrigel: basement membrane matrix with biological activity. *Semin Cancer Biol*, 15(5):378–86, 2005. ISSN 1044-579X (Print) 1044-579X (Linking). doi: 10.1016/j.semcancer.2005.05.004. URL https://www.ncbi.nlm.nih.gov/pubmed/15975825.

[22] N. A. Peppas, J. Z. Hilt, A. Khademhosseini, and R. Langer. Hydrogels in biology and medicine: From molecular principles to bionanotechnology. *Advanced Materials*, 18 (11):1345–1360, 2006. ISSN 0935-9648. doi: https://doi.org/10.1002/adma.200501612. URL https://onlinelibrary.wiley.com/doi/abs/10.1002/adma.200501612.

[23] Buddy D. Ratner and Allan S. Hoffman. *Synthetic Hydrogels for Biomedical Applications*, volume 31 of *ACS Symposium Series*, book section 1, pages 1–36. AMERICAN CHEMICAL SOCIETY, 1976. ISBN 9780841203389. doi: doi:10.1021/bk-1976-0031.

ch00110.1021/bk-1976-0031.ch001. URL https://doi.org/10.1021/bk-1976-0031.ch001.

[24] Desireé Alesa Gyles, Lorena Diniz Castro, José Otávio Carréra Silva, and Roseane Maria Ribeiro-Costa. A review of the designs and prominent biomedical advances of natural and synthetic hydrogel formulations. *European Polymer Journal*, 88:373–392, 2017. ISSN 0014-3057. doi: https://doi.org/10.1016/j.eurpolymj.2017.01.027. URL https://www.sciencedirect.com/science/article/pii/S0014305716312502.

[25] E. A. Aisenbrey and W. L. Murphy. Synthetic alternatives to matrigel. *Nat Rev Mater*, 5(7):539–551, 2020. ISSN 2058-8437 (Print) 2058-8437 (Linking). doi: 10.1038/s41578-020-0199-8. URL https://www.ncbi.nlm.nih.gov/pubmed/32953138.

[26] T. Chanmee, P. Ontong, and N. Itano. Hyaluronan: A modulator of the tumor microenvironment. *Cancer Lett*, 375(1):20–30, 2016. ISSN 1872-7980 (Electronic) 0304-3835 (Linking). doi: 10.1016/j.canlet.2016.02.031. URL https://www.ncbi.nlm.nih.gov/pubmed/26921785.

[27] P. P. Provenzano, D. R. Inman, K. W. Eliceiri, J. G. Knittel, L. Yan, C. T. Rueden, J. G. White, and P. J. Keely. Collagen density promotes mammary tumor initiation and progression. *BMC Med*, 6:11, 2008. ISSN 1741-7015 (Electronic) 1741-7015 (Linking). doi: 10.1186/1741-7015-6-11. URL https://www.ncbi.nlm.nih.gov/pubmed/18442412.

[28] R. K. Okolicsanyi, A. J. van Wijnen, S. M. Cool, G. S. Stein, L. R. Griffiths, and L. M. Haupt. Heparan sulfate proteoglycans and human breast cancer epithelial cell tumorigenicity. *J Cell Biochem*, 115(5):967–76, 2014. ISSN 1097-4644 (Electronic)

0730-2312 (Linking). doi: 10.1002/jcb.24746. URL https://www.ncbi.nlm.nih.gov/pubmed/24357546.

[29] M. Hay, D. W. Thomas, J. L. Craighead, C. Economides, and J. Rosenthal. Clinical development success rates for investigational drugs. *Nat Biotechnol*, 32(1):40–51, 2014. ISSN 1546-1696 (Electronic) 1087-0156 (Linking). doi: 10.1038/nbt.2786. URL https://www.ncbi.nlm.nih.gov/pubmed/24406927.

[30] Y. Imamura, T. Mukohara, Y. Shimono, Y. Funakoshi, N. Chayahara, M. Toyoda, N. Kiyota, S. Takao, S. Kono, T. Nakatsura, and H. Minami. Comparison of 2d- and 3d-culture models as drug-testing platforms in breast cancer. *Oncol Rep*, 33(4):1837–43, 2015. ISSN 1791-2431 (Electronic) 1021-335X (Linking). doi: 10.3892/or.2015.3767. URL https://www.ncbi.nlm.nih.gov/pubmed/25634491.

[31] X. Yan, L. Zhou, Z. Wu, X. Wang, X. Chen, F. Yang, Y. Guo, M. Wu, Y. Chen, W. Li, J. Wang, and Y. Du. High throughput scaffold-based 3d micro-tumor array for efficient drug screening and chemosensitivity testing. *Biomaterials*, 198:167–179, 2019. ISSN 1878-5905 (Electronic) 0142-9612 (Linking). doi: 10.1016/j.biomaterials.2018.05.020. URL https://www.ncbi.nlm.nih.gov/pubmed/29807624.

[32] M. R. Carvalho, D. Lima, R. L. Reis, V. M. Correlo, and J. M. Oliveira. Evaluating biomaterial- and microfluidic-based 3d tumor models. *Trends Biotechnol*, 33(11):667–678, 2015. ISSN 1879-3096 (Electronic) 0167-7799 (Linking). doi: 10.1016/j.tibtech.2015.09.009. URL https://www.ncbi.nlm.nih.gov/pubmed/26603572.

[33] Qi Sun, Say Hwa Tan, Qiushui Chen, Rui Ran, Yue Hui, Dong Chen, and Chun-Xia Zhao. Microfluidic formation of coculture tumor spheroids with stromal cells as a novel 3d tumor model for drug testing. *ACS Biomaterials Science Engineering*, 4(12):

4425–4433, 2018. doi: 10.1021/acsbiomaterials.8b00904. URL https://doi.org/10.1021/acsbiomaterials.8b00904.

[34] Kolin C. Hribar, Christopher J. Wheeler, Alexey Bazarov, Kunal Varshneya, Ryosuke Yamada, Padraig Buckley, and Chirag G. Patil. A simple three-dimensional hydrogel platform enables ex vivo cell culture of patient and pdx tumors for assaying their response to clinically relevant therapies. *Molecular Cancer Therapeutics*, 18(3):718–725, 2019. doi: 10.1158/1535-7163.Mct-18-0359. URL https://mct.aacrjournals.org/content/molcanther/18/3/718.full.pdf.

[35] D. J. Newman and G. M. Cragg. Natural products as sources of new drugs over the nearly four decades from 01/1981 to 09/2019. *J Nat Prod*, 83(3):770–803, 2020. ISSN 1520-6025 (Electronic) 0163-3864 (Linking). doi: 10.1021/acs.jnatprod.9b01285. URL https://www.ncbi.nlm.nih.gov/pubmed/32162523.

[36] J. Sharifi-Rad, A. Ozleyen, T. Boyunegmez Tumer, C. Oluwaseun Adetunji, N. El Omari, A. Balahbib, Y. Taheri, A. Bouyahya, M. Martorell, N. Martins, and W. C. Cho. Natural products and synthetic analogs as a source of antitumor drugs. *Biomolecules*, 9(11), 2019. ISSN 2218-273x. doi: 10.3390/biom9110679.

[37] R. X. Tan and W. X. Zou. Endophytes: a rich source of functional metabolites. *Nat Prod Rep*, 18(4):448–59, 2001. ISSN 0265-0568 (Print) 0265-0568 (Linking). doi: 10.1039/b100918o. URL https://www.ncbi.nlm.nih.gov/pubmed/11548053.

[38] Agata Staniek, Herman J. Woerdenbag, and Oliver Kayser. Endophytes: exploiting biodiversity for the improvement of natural product-based drug discovery. *Journal of Plant Interactions*, 3(2):75–93, 2008. ISSN 1742-9145. doi: 10.1080/17429140801886293. URL https://doi.org/10.1080/17429140801886293.

[39] R. N. Kharwar, A. Mishra, S. K. Gond, A. Stierle, and D. Stierle. Anticancer compounds derived from fungal endophytes: their importance and future challenges. *Nat Prod Rep*, 28(7):1208–28, 2011. ISSN 0265-0568. doi: 10.1039/c1np00008j.

[40] A. Stierle, G. Strobel, and D. Stierle. Taxol and taxane production by taxomyces andreanae, an endophytic fungus of pacific yew. *Science*, 260(5105):214–6, 1993. ISSN 0036-8075 (Print) 0036-8075 (Linking). doi: 10.1126/science.8097061. URL https://www.ncbi.nlm.nih.gov/pubmed/8097061.

[41] S. P. Mohanty and E. Kougianos. Biosensors: a tutorial review. *IEEE Potentials*, 25 (2):35–40, 2006. ISSN 1558-1772. doi: 10.1109/MP.2006.1649009.

[42] A. Makaraviciute and A. Ramanaviciene. Site-directed antibody immobilization techniques for immunosensors. *Biosens Bioelectron*, 50:460–71, 2013. ISSN 1873-4235 (Electronic) 0956-5663 (Linking). doi: 10.1016/j.bios.2013.06.060. URL https://www.ncbi.nlm.nih.gov/pubmed/23911661.

[43] H. H. Nguyen, S. H. Lee, U. J. Lee, C. D. Fermin, and M. Kim. Immobilized enzymes in biosensor applications. *Materials (Basel)*, 12(1), 2019. ISSN 1996-1944 (Print) 1996-1944 (Linking). doi: 10.3390/ma12010121. URL https://www.ncbi.nlm.nih.gov/pubmed/30609693.

[44] X. Sun, P. He, S. Liu, J. Ye, and Y. Fang. Immobilization of single-stranded deoxyribonucleic acid on gold electrode with self-assembled aminoethanethiol monolayer for dna electrochemical sensor applications. *Talanta*, 47(2):487–95, 1998. ISSN 0039-9140 (Print) 0039-9140 (Linking). doi: 10.1016/s0039-9140(98)00108-8. URL https://www.ncbi.nlm.nih.gov/pubmed/18967350.

[45] M. Strianese, M. Staiano, G. Ruggiero, T. Labella, C. Pellecchia, and S. D'Auria. Fluorescence-based biosensors. *Methods Mol Biol*, 875:193–216, 2012. ISSN 1940-6029

(Electronic) 1064-3745 (Linking). doi: 10.1007/978-1-61779-806-1_9. URL https://www.ncbi.nlm.nih.gov/pubmed/22573441.

[46] E. A. Jares-Erijman and T. M. Jovin. Fret imaging. *Nat Biotechnol*, 21(11):1387–95, 2003. ISSN 1087-0156 (Print) 1087-0156 (Linking). doi: 10.1038/nbt896. URL https://www.ncbi.nlm.nih.gov/pubmed/14595367.

[47] A. W. Nguyen and P. S. Daugherty. Evolutionary optimization of fluorescent proteins for intracellular fret. *Nat Biotechnol*, 23(3):355–60, 2005. ISSN 1087-0156 (Print) 1087-0156 (Linking). doi: 10.1038/nbt1066. URL https://www.ncbi.nlm.nih.gov/pubmed/15696158.

[48] D. W. Piston and G. J. Kremers. Fluorescent protein fret: the good, the bad and the ugly. *Trends Biochem Sci*, 32(9):407–14, 2007. ISSN 0968-0004 (Print) 0968-0004 (Linking). doi: 10.1016/j.tibs.2007.08.003. URL https://www.ncbi.nlm.nih.gov/pubmed/17764955.

[49] J. Shi, C. Chan, Y. Pang, W. Ye, F. Tian, J. Lyu, Y. Zhang, and M. Yang. A fluorescence resonance energy transfer (fret) biosensor based on graphene quantum dots (gqds) and gold nanoparticles (aunps) for the detection of meca gene sequence of staphylococcus aureus. *Biosens Bioelectron*, 67:595–600, 2015. ISSN 1873-4235 (Electronic) 0956-5663 (Linking). doi: 10.1016/j.bios.2014.09.059. URL https://www.ncbi.nlm.nih.gov/pubmed/25288044.

[50] Ryoji Abe, Hiroyuki Ohashi, Issei Iijima, Masaki Ihara, Hiroaki Takagi, Takahiro Hohsaka, and Hiroshi Ueda. "quenchbodies": Quench-based antibody probes that show antigen-dependent fluorescence. *Journal of the American Chemical Society*, 133 (43):17386–17394, 2011. ISSN 0002-7863. doi: 10.1021/ja205925j. URL https://doi.org/10.1021/ja205925j.

[51] John Nebu, J. S. Anjali Devi, R. S. Aparna, B. Aswathy, G. M. Lekha, and George Sony. Fluorescence turn-on detection of fenitrothion using gold nanoparticle quenched fluorescein and its separation using superparamagnetic iron oxide nanoparticle. *Sensors and Actuators B: Chemical*, 277:271–280, 2018. ISSN 0925-4005. doi: https://doi.org/10.1016/j.snb.2018.08.153. URL https://www.sciencedirect.com/science/article/pii/S0925400518315910.

[52] F. Chen, X. Zhuang, L. Lin, P. Yu, Y. Wang, Y. Shi, G. Hu, and Y. Sun. New horizons in tumor microenvironment biology: challenges and opportunities. *BMC Med*, 13:45, 2015. ISSN 1741-7015 (Electronic) 1741-7015 (Linking). doi: 10.1186/s12916-015-0278-7. URL https://www.ncbi.nlm.nih.gov/pubmed/25857315.

[53] E. L. Fong, D. A. Harrington, M. C. Farach-Carson, and H. Yu. Heralding a new paradigm in 3d tumor modeling. *Biomaterials*, 108:197–213, 2016. ISSN 1878-5905 (Electronic) 0142-9612 (Linking). doi: 10.1016/j.biomaterials.2016.08.052. URL https://www.ncbi.nlm.nih.gov/pubmed/27639438.

[54] K. C. Valkenburg, A. E. de Groot, and K. J. Pienta. Targeting the tumour stroma to improve cancer therapy. *Nat Rev Clin Oncol*, 15(6):366–381, 2018. ISSN 1759-4782 (Electronic) 1759-4774 (Linking). doi: 10.1038/s41571-018-0007-1. URL https://www.ncbi.nlm.nih.gov/pubmed/29651130.

[55] T. L. Whiteside. The tumor microenvironment and its role in promoting tumor growth. *Oncogene*, 27(45):5904–12, 2008. ISSN 1476-5594 (Electronic) 0950-9232 (Linking). doi: 10.1038/onc.2008.271. URL https://www.ncbi.nlm.nih.gov/pubmed/18836471.

[56] E. W. Young and D. J. Beebe. Fundamentals of microfluidic cell culture in controlled microenvironments. *Chem Soc Rev*, 39(3):1036–48, 2010. ISSN 1460-4744 (Electronic)

0306-0012 (Linking). doi: 10.1039/b909900j. URL https://www.ncbi.nlm.nih.gov/pubmed/20179823.

[57] H. Maeda and M. Khatami. Analyses of repeated failures in cancer therapy for solid tumors: poor tumor-selective drug delivery, low therapeutic efficacy and unsustainable costs. *Clin Transl Med*, 7(1):11, 2018. ISSN 2001-1326 (Print). doi: 10.1186/s40169-018-0185-6. URL https://www.ncbi.nlm.nih.gov/pubmed/29541939.

[58] N. E. Timmins and L. K. Nielsen. Generation of multicellular tumor spheroids by the hanging-drop method. *Methods Mol Med*, 140:141–51, 2007. ISSN 1543-1894 (Print) 1543-1894 (Linking). doi: 10.1007/978-1-59745-443-8_8. URL https://www.ncbi.nlm.nih.gov/pubmed/18085207.

[59] O. Costachel, L. Fadei, and E. Badea. Tumor cell suspension culture on non adhesive substratum. *Z Krebsforsch*, 72(1):24–31, 1969. ISSN 0301-1585 (Print) 0301-1585 (Linking). doi: 10.1007/bf00524788. URL https://www.ncbi.nlm.nih.gov/pubmed/4240338.

[60] W. Shi, J. Kwon, Y. Huang, J. Tan, C. G. Uhl, R. He, C. Zhou, and Y. Liu. Facile tumor spheroids formation in large quantity with controllable size and high uniformity. *Sci Rep*, 8(1):6837, 2018. ISSN 2045-2322 (Electronic) 2045-2322 (Linking). doi: 10.1038/s41598-018-25203-3. URL https://www.ncbi.nlm.nih.gov/pubmed/29717201.

[61] S. R. Caliari and J. A. Burdick. A practical guide to hydrogels for cell culture. *Nat Methods*, 13(5):405–14, 2016. ISSN 1548-7105 (Electronic) 1548-7091 (Linking). doi: 10.1038/nmeth.3839. URL https://www.ncbi.nlm.nih.gov/pubmed/27123816.

[62] F. Del Bufalo, T. Manzo, V. Hoyos, S. Yagyu, I. Caruana, J. Jacot, O. Benavides, D. Rosen, and M. K. Brenner. 3d modeling of human cancer: A peg-fibrin hydrogel

system to study the role of tumor microenvironment and recapitulate the in vivo effect of oncolytic adenovirus. *Biomaterials*, 84:76–85, 2016. ISSN 1878-5905 (Electronic) 0142-9612 (Linking). doi: 10.1016/j.biomaterials.2016.01.030. URL https://www.ncbi.nlm.nih.gov/pubmed/26826297.

[63] R. C. Hooper, A. Jacoby, O. Asanbe, H. L. Osoria, K. A. Morrison, K. Hernandez, T. Boyko, J. Joyce, W. Landford, and J. A. Spector. A novel three-dimensional platform to investigate neoangiogenesis, transendothelial migration, and metastasis of mdamb-231 breast cancer cells. *Plast Reconstr Surg*, 138(3):472e–82e, 2016. ISSN 1529-4242 (Electronic) 0032-1052 (Linking). doi: 10.1097/PRS.0000000000002470. URL https://www.ncbi.nlm.nih.gov/pubmed/27556622.

[64] C. B. Khatiwala, S. R. Peyton, and A. J. Putnam. Intrinsic mechanical properties of the extracellular matrix affect the behavior of pre-osteoblastic mc3t3-e1 cells. *Am J Physiol Cell Physiol*, 290(6):C1640–50, 2006. ISSN 0363-6143 (Print) 0363-6143 (Linking). doi: 10.1152/ajpcell.00455.2005. URL https://www.ncbi.nlm.nih.gov/pubmed/16407416.

[65] S. Pradhan, J. M. Clary, D. Seliktar, and E. A. Lipke. A three-dimensional spheroidal cancer model based on peg-fibrinogen hydrogel microspheres. *Biomaterials*, 115: 141–154, 2017. ISSN 1878-5905 (Electronic) 0142-9612 (Linking). doi: 10.1016/j.biomaterials.2016.10.052. URL https://www.ncbi.nlm.nih.gov/pubmed/27889665.

[66] Mark W. Tibbitt and Kristi S. Anseth. Hydrogels as extracellular matrix mimics for 3d cell culture. *Biotechnology and bioengineering*, 103(4):655–663, 2009. ISSN 1097-0290 0006-3592. doi: 10.1002/bit.22361. URL https://www.ncbi.nlm.nih.gov/pubmed/19472329https://www.ncbi.nlm.nih.gov/pmc/PMC2997742/.

[67] Danh Truong, Julieann Puleo, Alison Llave, Ghassan Mouneimne, Roger D. Kamm,

and Mehdi Nikkhah. Breast cancer cell invasion into a three dimensional tumor-stroma microenvironment. *Scientific Reports*, 6:34094, 2016. doi: 10.1038/srep34094https://www.nature.com/articles/srep34094#supplementary-information. URL https://doi.org/10.1038/srep34094.

[68] X. Xu, L. A. Gurski, C. Zhang, D. A. Harrington, M. C. Farach-Carson, and X. Jia. Recreating the tumor microenvironment in a bilayer, hyaluronic acid hydrogel construct for the growth of prostate cancer spheroids. *Biomaterials*, 33(35):9049–60, 2012. ISSN 1878-5905 (Electronic) 0142-9612 (Linking). doi: 10.1016/j.biomaterials.2012.08.061. URL https://www.ncbi.nlm.nih.gov/pubmed/22999468.

[69] Jordi Cabanas-Danés, Jurriaan Huskens, and Pascal Jonkheijm. Chemical strategies for the presentation and delivery of growth factors. *Journal of Materials Chemistry B*, 2(17):2381–2394, 2014. ISSN 2050-750X. doi: 10.1039/C3TB20853B. URL http://dx.doi.org/10.1039/C3TB20853B.

[70] Elena Foster, Jungmok You, Christian Siltanen, Dipali Patel, Amranul Haque, Leif Anderson, and Alexander Revzin. Heparin hydrogel sandwich cultures of primary hepatocytes. *European Polymer Journal*, 72:726–735, 2015. ISSN 0014-3057. doi: https://doi.org/10.1016/j.eurpolymj.2014.12.033. URL http://www.sciencedirect.com/science/article/pii/S0014305714004741.

[71] Mihye Kim, Yang-Jung Kim, Kihak Gwon, and Giyoong Tae. Modulation of cell adhesion of heparin-based hydrogel by efficient physisorption of adhesive proteins. *Macromolecular Research*, 20(3):271–276, 2012. ISSN 2092-7673. doi: 10.1007/s13233-012-0058-6. URL https://doi.org/10.1007/s13233-012-0058-6.

[72] Mihye Kim, Young Ha Kim, and Giyoong Tae. Human mesenchymal stem cell culture on heparin-based hydrogels and the modulation of interactions by gel elas-

ticity and heparin amount. *Acta Biomaterialia*, 9(8):7833–7844, 2013. ISSN 1742-7061. doi: https://doi.org/10.1016/j.actbio.2013.04.041. URL http://www.sciencedirect.com/science/article/pii/S1742706113002225.

[73] Mihye Kim, Ji Youn Lee, Caroline N. Jones, Alexander Revzin, and Giyoong Tae. Heparin-based hydrogel as a matrix for encapsulation and cultivation of primary hepatocytes. *Biomaterials*, 31(13):3596–3603, 2010. ISSN 1878-5905 0142-9612. doi: 10.1016/j.biomaterials.2010.01.068. URL https://www.ncbi.nlm.nih.gov/pubmed/20153045https://www.ncbi.nlm.nih.gov/pmc/PMC2837121/.

[74] Y. S. Kim, D. K. Sung, W. H. Kong, H. Kim, and S. K. Hahn. Synergistic effects of hyaluronate - epidermal growth factor conjugate patch on chronic wound healing. *Biomater Sci*, 6(5):1020–1030, 2018. ISSN 2047-4849 (Electronic) 2047-4830 (Linking). doi: 10.1039/c8bm00079d. URL https://www.ncbi.nlm.nih.gov/pubmed/29616250.

[75] Mikaël M. Martino, Priscilla S. Briquez, Adrian Ranga, Matthias P. Lutolf, and Jeffrey A. Hubbell. Heparin-binding domain of fibrin(ogen) binds growth factors and promotes tissue repair when incorporated within a synthetic matrix. *Proceedings of the National Academy of Sciences*, 110(12):4563, 2013. URL http://www.pnas.org/content/110/12/4563.abstract.

[76] Daniel B. Pike, Shenshen Cai, Kyle R. Pomraning, Matthew A. Firpo, Robert J. Fisher, Xiao Zheng Shu, Glenn D. Prestwich, and Robert A. Peattie. Heparin-regulated release of growth factors in vitro and angiogenic response in vivo to implanted hyaluronan hydrogels containing vegf and bfgf. *Biomaterials*, 27(30):5242–5251, 2006. ISSN 0142-9612. doi: https://doi.org/10.1016/j.biomaterials.2006.05.018. URL http://www.sciencedirect.com/science/article/pii/S014296120600456X.

[77] Zhenming Wang, Zhefeng Wang, William Weijia Lu, Wanxin Zhen, Dazhi Yang, and Songlin Peng. Novel biomaterial strategies for controlled growth factor delivery for biomedical applications. *Npg Asia Materials*, 9:e435, 2017. doi: 10.1038/am.2017.171https://www.nature.com/articles/am2017171#supplementary-information. URL https://doi.org/10.1038/am.2017.171.

[78] Xian Xu, Amit K. Jha, Randall L. Duncan, and Xinqiao Jia. Heparin-decorated, hyaluronic acid-based hydrogel particles for the controlled release of bone morphogenetic protein 2. *Acta biomaterialia*, 7(8):3050–3059, 2011. ISSN 1878-7568 1742-7061. doi: 10.1016/j.actbio.2011.04.018. URL https://www.ncbi.nlm.nih.gov/pubmed/21550426https://www.ncbi.nlm.nih.gov/pmc/PMC3188452/.

[79] Ronald N. Buick, Jorge Filmus, and Jon G. Church. *The role of epidermal growth factor receptors in breast cancer*, pages 159–170. Springer US, Boston, MA, 1991. ISBN 978-1-4615-3940-7. doi: 10.1007/978-1-4615-3940-7_7. URL https://doi.org/10.1007/978-1-4615-3940-7_7.

[80] C. A. Hudis and L. Gianni. Triple-negative breast cancer: an unmet medical need. *Oncologist*, 16 Suppl 1:1–11, 2011. ISSN 1549-490X (Electronic) 1083-7159 (Linking). doi: 10.1634/theoncologist.2011-S1-01. URL https://www.ncbi.nlm.nih.gov/pubmed/21278435.

[81] Huey-En Tzeng, Lixin Yang, Kemin Chen, Yafan Wang, Yun-Ru Liu, Shiow-Lin Pan, Shikha Gaur, Shuya Hu, and Yun Yen. The pan-pi3k inhibitor gdc-0941 activates canonical wnt signaling to confer resistance in tnbc cells: resistance reversal with wnt inhibitor. *Oncotarget*, 6(13):11061–11073, 2015. ISSN 1949-2553. doi: 10.18632/oncotarget.3568. URL https://www.ncbi.nlm.nih.gov/pubmed/25857298https://www.ncbi.nlm.nih.gov/pmc/PMC4484439/.

[82] M. S. Shin, P. Shinghirunnusorn, Y. Sugishima, M. Nishimura, S. Suzuki, K. Koizumi, I. Saiki, and H. Sakurai. Cross interference with tnf-alpha-induced tak1 activation via egfr-mediated p38 phosphorylation of tak1-binding protein 1. *Biochim Biophys Acta*, 1793(7):1156–64, 2009. ISSN 0006-3002 (Print) 0006-3002 (Linking). doi: 10.1016/j.bbamcr.2009.04.005. URL https://www.ncbi.nlm.nih.gov/pubmed/19393267.

[83] A. Dahmani and J. S. Delisle. Tgf-beta in t cell biology: Implications for cancer immunotherapy. *Cancers (Basel)*, 10(6), 2018. ISSN 2072-6694 (Print) 2072-6694 (Linking). doi: 10.3390/cancers10060194. URL https://www.ncbi.nlm.nih.gov/pubmed/29891791.

[84] D. A. Thomas and J. Massague. Tgf-beta directly targets cytotoxic t cell functions during tumor evasion of immune surveillance. *Cancer Cell*, 8(5):369–80, 2005. ISSN 1535-6108 (Print) 1535-6108 (Linking). doi: 10.1016/j.ccr.2005.10.012. URL https://www.ncbi.nlm.nih.gov/pubmed/16286245.

[85] T. Jiang, C. Zhou, and S. Ren. Role of il-2 in cancer immunotherapy. *Oncoimmunology*, 5(6):e1163462, 2016. ISSN 2162-4011 (Print) 2162-4011 (Linking). doi: 10.1080/2162402X.2016.1163462. URL https://www.ncbi.nlm.nih.gov/pubmed/27471638.

[86] J. D. Campbell, G. Cook, S. E. Robertson, A. Fraser, K. S. Boyd, J. A. Gracie, and I. M. Franklin. Suppression of il-2-induced t cell proliferation and phosphorylation of stat3 and stat5 by tumor-derived tgf beta is reversed by il-15. *J Immunol*, 167(1):553–61, 2001. ISSN 0022-1767 (Print) 0022-1767 (Linking). doi: 10.4049/jimmunol.167.1.553. URL https://www.ncbi.nlm.nih.gov/pubmed/11418694.

[87] G. Bhakta, B. Rai, Z. X. Lim, J. H. Hui, G. S. Stein, A. J. van Wijnen, V. Nurcombe, G. D. Prestwich, and S. M. Cool. Hyaluronic acid-based hydrogels functionalized with heparin that support controlled release of bioactive bmp-2. *Biomaterials*, 33

(26):6113–22, 2012. ISSN 1878-5905 (Electronic) 0142-9612 (Linking). doi: 10.1016/j.biomaterials.2012.05.030. URL https://www.ncbi.nlm.nih.gov/pubmed/22687758.

[88] Christie Geankoplis. *Transport processes and separation process principles (includes unit operations) fourth edition*. Prentice Hall Press, 2003. ISBN 013101367X.

[89] Johannes Schindelin, Ignacio Arganda-Carreras, Erwin Frise, Verena Kaynig, Mark Longair, Tobias Pietzsch, Stephan Preibisch, Curtis Rueden, Stephan Saalfeld, Benjamin Schmid, Jean-Yves Tinevez, Daniel James White, Volker Hartenstein, Kevin Eliceiri, Pavel Tomancak, and Albert Cardona. Fiji: an open-source platform for biological-image analysis. *Nature Methods*, 9:676, 2012. doi: 10.1038/nmeth.2019https://www.nature.com/articles/nmeth.2019#supplementary-information. URL https://doi.org/10.1038/nmeth.2019.

[90] Daehwan Kim, Ben Langmead, and Steven L. Salzberg. Hisat: a fast spliced aligner with low memory requirements. *Nature methods*, 12(4):357–360, 2015. ISSN 1548-7105 1548-7091. doi: 10.1038/nmeth.3317. URL https://www.ncbi.nlm.nih.gov/pubmed/25751142https://www.ncbi.nlm.nih.gov/pmc/PMC4655817/.

[91] Ben Langmead and Steven L. Salzberg. Fast gapped-read alignment with bowtie 2. *Nature methods*, 9(4):357–359, 2012. ISSN 1548-7105 1548-7091. doi: 10.1038/nmeth.1923. URL https://www.ncbi.nlm.nih.gov/pubmed/22388286https://www.ncbi.nlm.nih.gov/pmc/PMC3322381/.

[92] Yang Liao, Gordon K. Smyth, and Wei Shi. The subread aligner: fast, accurate and scalable read mapping by seed-and-vote. *Nucleic acids research*, 41(10):e108–e108, 2013. ISSN 1362-4962 0305-1048. doi: 10.1093/nar/gkt214. URL https://www.ncbi.nlm.nih.gov/pubmed/23558742https://www.ncbi.nlm.nih.gov/pmc/PMC3664803/.

[93] Adam Frankish, Mark Diekhans, Anne-Maud Ferreira, Rory Johnson, Irwin Jungreis, Jane Loveland, Jonathan M. Mudge, Cristina Sisu, James Wright, Joel Armstrong, If Barnes, Andrew Berry, Alexandra Bignell, Silvia Carbonell Sala, Jacqueline Chrast, Fiona Cunningham, Tomás Di Domenico, Sarah Donaldson, Ian T. Fiddes, Carlos García Girón, Jose Manuel Gonzalez, Tiago Grego, Matthew Hardy, Thibaut Hourlier, Toby Hunt, Osagie G. Izuogu, Julien Lagarde, Fergal J. Martin, Laura Martínez, Shamika Mohanan, Paul Muir, Fabio C. P. Navarro, Anne Parker, Baikang Pei, Fernando Pozo, Magali Ruffier, Bianca M. Schmitt, Eloise Stapleton, Marie-Marthe Suner, Irina Sycheva, Barbara Uszczynska-Ratajczak, Jinuri Xu, Andrew Yates, Daniel Zerbino, Yan Zhang, Bronwen Aken, Jyoti S. Choudhary, Mark Gerstein, Roderic Guigó, Tim J. P. Hubbard, Manolis Kellis, Benedict Paten, Alexandre Reymond, Michael L. Tress, and Paul Flicek. Gencode reference annotation for the human and mouse genomes. *Nucleic Acids Research*, pages gky955–gky955, 2018. ISSN 0305-1048. doi: 10.1093/nar/gky955. URL http://dx.doi.org/10.1093/nar/gky955.

[94] Mark D. Robinson, Davis J. McCarthy, and Gordon K. Smyth. edger: a bioconductor package for differential expression analysis of digital gene expression data. *Bioinformatics (Oxford, England)*, 26(1):139–140, 2010. ISSN 1367-4811 1367-4803. doi: 10.1093/bioinformatics/btp616. URL https://www.ncbi.nlm.nih.gov/pubmed/19910308https://www.ncbi.nlm.nih.gov/pmc/PMC2796818/.

[95] Aravind Subramanian, Pablo Tamayo, Vamsi K. Mootha, Sayan Mukherjee, Benjamin L. Ebert, Michael A. Gillette, Amanda Paulovich, Scott L. Pomeroy, Todd R. Golub, Eric S. Lander, and Jill P. Mesirov. Gene set enrichment analysis: a knowledge-based approach for interpreting genome-wide expression profiles. *Proceedings of the National Academy of Sciences of the United States of America*, 102(43):15545–15550, 2005. ISSN 0027-8424 1091-6490. doi: 10.1073/pnas.

0506580102. URL https://www.ncbi.nlm.nih.gov/pubmed/16199517https://www.ncbi.nlm.nih.gov/pmc/PMC1239896/.

[96] R Core Team (2018). R: A language and environment for statistical computing. 2018. URL https://www.R-project.org/.

[97] Arthur Liberzon, Chet Birger, Helga Thorvaldsdóttir, Mahmoud Ghandi, Jill P. Mesirov, and Pablo Tamayo. The molecular signatures database (msigdb) hallmark gene set collection. *Cell systems*, 1(6):417–425, 2015. ISSN 2405-4712 2405-4720. doi: 10.1016/j.cels.2015.12.004. URL https://www.ncbi.nlm.nih.gov/pubmed/26771021https://www.ncbi.nlm.nih.gov/pmc/PMC4707969/.

[98] Britta Weigelt, Alvin T. Lo, Catherine C. Park, Joe W. Gray, and Mina J. Bissell. Her2 signaling pathway activation and response of breast cancer cells to her2-targeting agents is dependent strongly on the 3d microenvironment. *Breast cancer research and treatment*, 122(1):35–43, 2010. ISSN 1573-7217 0167-6806. doi: 10.1007/s10549-009-0502-2. URL https://www.ncbi.nlm.nih.gov/pubmed/19701706https://www.ncbi.nlm.nih.gov/pmc/PMC2935800/.

[99] Ken M. Cadigan and Marian L. Waterman. Tcf/lefs and wnt signaling in the nucleus. *Cold Spring Harbor perspectives in biology*, 4(11):a007906. ISSN 1943-0264. doi: 10.1101/cshperspect.a007906. URL https://www.ncbi.nlm.nih.gov/pubmed/23024173https://www.ncbi.nlm.nih.gov/pmc/PMC3536346/.

[100] Larion Santiago, Garrett Daniels, Dongwen Wang, Fang-Ming Deng, and Peng Lee. Wnt signaling pathway protein lef1 in cancer, as a biomarker for prognosis and a target for treatment. *American journal of cancer research*, 7(6):1389–1406, 2017. ISSN 2156-6976. URL https://www.ncbi.nlm.nih.gov/pubmed/28670499https://www.ncbi.nlm.nih.gov/pmc/PMC5489786/.

[101] Samantha J. Paluck, Thi H. Nguyen, and Heather D. Maynard. Heparin-mimicking polymers: Synthesis and biological applications. *Biomacromolecules*, 17(11):3417–3440, 2016. ISSN 1525-7797. doi: 10.1021/acs.biomac.6b01147. URL https://doi.org/10.1021/acs.biomac.6b01147.

[102] J. Y. Fang, S. J. Tan, Y. C. Wu, Z. Yang, B. X. Hoang, and B. Han. From competency to dormancy: a 3d model to study cancer cells and drug responsiveness. *J Transl Med*, 14:38, 2016. ISSN 1479-5876 (Electronic) 1479-5876 (Linking). doi: 10.1186/s12967-016-0798-8. URL https://www.ncbi.nlm.nih.gov/pubmed/26847768.

[103] M. Perez, B. Haschke, and N. J. Donato. Differential expression and translocation of protein tyrosine phosphatase 1b-related proteins in me-180 tumor cells expressing apoptotic sensitivity and resistance to tumor necrosis factor: potential interaction with epidermal growth factor receptor. *Oncogene*, 18(4):967–78, 1999. ISSN 0950-9232 (Print) 0950-9232 (Linking). doi: 10.1038/sj.onc.1202368. URL https://www.ncbi.nlm.nih.gov/pubmed/10023672.

[104] K. Gong, G. Guo, D. E. Gerber, B. Gao, M. Peyton, C. Huang, J. D. Minna, K. J. Hatanpaa, K. Kernstine, L. Cai, Y. Xie, H. Zhu, F. J. Fattah, S. Zhang, M. Takahashi, B. Mukherjee, S. Burma, J. Dowell, K. Dao, V. A. Papadimitrakopoulou, V. Olivas, T. G. Bivona, D. Zhao, and A. A. Habib. Tnf-driven adaptive response mediates resistance to egfr inhibition in lung cancer. *J Clin Invest*, 128(6):2500–2518, 2018. ISSN 1558-8238 (Electronic) 0021-9738 (Linking). doi: 10.1172/JCI96148. URL https://www.ncbi.nlm.nih.gov/pubmed/29613856.

[105] Ilaria Elia, Ginevra Doglioni, and Sarah-Maria Fendt. Metabolic hallmarks of metastasis formation. *Trends in Cell Biology*, 28(8):673–684, 2018. ISSN 0962-8924. doi: 10.1016/j.tcb.2018.04.002. URL https://doi.org/10.1016/j.tcb.2018.04.002.

[106] Waseem Asghar, Rami El Assal, Hadi Shafiee, Sharon Pitteri, Ramasamy Paulmurugan, and Utkan Demirci. Engineering cancer microenvironments for in vitro 3-d tumor models. *Materials Today*, 18(10):539–553, 2015. ISSN 1369-7021. doi: https://doi.org/10.1016/j.mattod.2015.05.002. URL http://www.sciencedirect.com/science/article/pii/S1369702115001625.

[107] O. I. Abdel-Wahab, R. P. Rosovsky, and J. A. Warth. Warfarin-induced skin necrosis in a patient with heparin-induced thrombocytopenia: two diseases or one? *Acta Haematol*, 120(2):117–22, 2008. ISSN 1421-9662 (Electronic) 0001-5792 (Linking). doi: 10.1159/000174756. URL https://www.ncbi.nlm.nih.gov/pubmed/19018128.

[108] B. J. Miriovsky and T. L. Ortel. Heparin-induced thrombocytopenia in cancer. *J Natl Compr Canc Netw*, 9(7):781–7, 2011. ISSN 1540-1413 (Electronic) 1540-1405 (Linking). doi: 10.6004/jnccn.2011.0063. URL https://www.ncbi.nlm.nih.gov/pubmed/21715724.

[109] R. H. Cosgrove, L. R. Zacharski, E. Racine, and J. C. Andersen. Improved cancer mortality with low-molecular-weight heparin treatment: a review of the evidence. *Semin Thromb Hemost*, 28(1):79–87, 2002. ISSN 0094-6176 (Print) 0094-6176 (Linking). doi: 10.1055/s-2002-20566. URL https://www.ncbi.nlm.nih.gov/pubmed/11885028.

[110] F. Macbeth, S. Noble, J. Evans, S. Ahmed, D. Cohen, K. Hood, D. Knoyle, S. Linnane, M. Longo, B. Moore, P. J. Woll, W. Appel, J. Dickson, D. Ferry, C. Brammer, and G. Griffiths. Randomized phase iii trial of standard therapy plus low molecular weight heparin in patients with lung cancer: Fragmatic trial. *J Clin Oncol*, 34(5):488–94, 2016. ISSN 1527-7755 (Electronic) 0732-183X (Linking). doi: 10.1200/JCO.2015.64.0268. URL https://www.ncbi.nlm.nih.gov/pubmed/26700124.

[111] N. Zhang, W. Lou, F. Ji, L. Qiu, B. K. Tsang, and W. Di. Low molecular weight

heparin and cancer survival: clinical trials and experimental mechanisms. *J Cancer Res Clin Oncol*, 142(8):1807–16, 2016. ISSN 1432-1335 (Electronic) 0171-5216 (Linking). doi: 10.1007/s00432-016-2131-6. URL https://www.ncbi.nlm.nih.gov/pubmed/26912316.

[112] K. Aysola, A. Desai, C. Welch, J. Xu, Y. Qin, V. Reddy, R. Matthews, C. Owens, J. Okoli, D. J. Beech, C. J. Piyathilake, S. P. Reddy, and V. N. Rao. Triple negative breast cancer - an overview. *Hereditary Genet*, 2013(Suppl 2), 2013. ISSN 2161-1041 (Print) 2161-1041 (Linking). doi: 10.4172/2161-1041.S2-001. URL https://www.ncbi.nlm.nih.gov/pubmed/25285241.

[113] L. A. Carey, E. C. Dees, L. Sawyer, L. Gatti, D. T. Moore, F. Collichio, D. W. Ollila, C. I. Sartor, M. L. Graham, and C. M. Perou. The triple negative paradox: primary tumor chemosensitivity of breast cancer subtypes. *Clin Cancer Res*, 13(8): 2329–34, 2007. ISSN 1078-0432 (Print) 1078-0432 (Linking). doi: 10.1158/1078-0432.CCR-06-1109. URL https://www.ncbi.nlm.nih.gov/pubmed/17438091.

[114] M. C. Wani, H. L. Taylor, M. E. Wall, P. Coggon, and A. T. McPhail. Plant antitumor agents. vi. the isolation and structure of taxol, a novel antileukemic and antitumor agent from taxus brevifolia. *J Am Chem Soc*, 93(9):2325–7, 1971. ISSN 0002-7863 (Print) 0002-7863 (Linking). doi: 10.1021/ja00738a045. URL https://www.ncbi.nlm.nih.gov/pubmed/5553076.

[115] A. Stierle, G. Strobel, and D. Stierle. Taxol and taxane production by taxomyces andreanae, an endophytic fungus of pacific yew. *Science*, 260(5105):214–6, 1993. ISSN 0036-8075 (Print) 0036-8075 (Linking). doi: 10.1126/science.8097061. URL https://www.ncbi.nlm.nih.gov/pubmed/8097061.

[116] F. A. S. Alasmary, A. S. Awaad, M. Kamal, S. I. Alqasoumi, and M. E. Zain. Antitumor

activity of extract and isolated compounds from drechslera rostrata and eurotium tonophilum. *Saudi Pharm J*, 26(2):279–285, 2018. ISSN 1319-0164 (Print) 1319-0164 (Linking). doi: 10.1016/j.jsps.2017.11.011. URL https://www.ncbi.nlm.nih.gov/pubmed/30166929.

[117] A. Matuszewska, M. Jaszek, D. Stefaniuk, T. Ciszewski, and L. Matuszewski. Anticancer, antioxidant, and antibacterial activities of low molecular weight bioactive subfractions isolated from cultures of wood degrading fungus cerrena unicolor. *PLoS One*, 13(6):e0197044, 2018. ISSN 1932-6203 (Electronic) 1932-6203 (Linking). doi: 10.1371/journal.pone.0197044. URL https://www.ncbi.nlm.nih.gov/pubmed/29874240.

[118] B. Zaferanloo, S. A. Pepper, S. A. Coulthard, C. P. F. Redfern, and E. A. Palombo. Metabolites of endophytic fungi from australian native plants as potential anticancer agents. *FEMS Microbiol Lett*, 365(9), 2018. ISSN 1574-6968 (Electronic) 0378-1097 (Linking). doi: 10.1093/femsle/fny078. URL https://www.ncbi.nlm.nih.gov/pubmed/29590360.

[119] S. J. Nass, M. L. Rothenberg, R. Pentz, H. Hricak, A. Abernethy, K. Anderson, A. W. Gee, R. D. Harvey, S. Piantadosi, M. M. Bertagnolli, D. Schrag, and R. L. Schilsky. Accelerating anticancer drug development - opportunities and trade-offs. *Nat Rev Clin Oncol*, 15(12):777–786, 2018. ISSN 1759-4782 (Electronic) 1759-4774 (Linking). doi: 10.1038/s41571-018-0102-3. URL https://www.ncbi.nlm.nih.gov/pubmed/30275514.

[120] M. Hay, D. W. Thomas, J. L. Craighead, C. Economides, and J. Rosenthal. Clinical development success rates for investigational drugs. *Nat Biotechnol*, 32(1):40–51, 2014. ISSN 1546-1696 (Electronic) 1087-0156 (Linking). doi: 10.1038/nbt.2786. URL https://www.ncbi.nlm.nih.gov/pubmed/24406927.

[121] Ana S. Nunes, Andreia S. Barros, Elisabete C. Costa, André F. Moreira, and Ilídio J. Correia. 3d tumor spheroids as in vitro models to mimic in vivo human solid tumors resistance to therapeutic drugs. *Biotechnology and Bioengineering*, 116 (1):206–226, 2019. ISSN 0006-3592. doi: https://doi.org/10.1002/bit.26845. URL https://onlinelibrary.wiley.com/doi/abs/10.1002/bit.26845.

[122] K. Stock, M. F. Estrada, S. Vidic, K. Gjerde, A. Rudisch, V. E. Santo, M. Barbier, S. Blom, S. C. Arundkar, I. Selvam, A. Osswald, Y. Stein, S. Gruenewald, C. Brito, W. van Weerden, V. Rotter, E. Boghaert, M. Oren, W. Sommergruber, Y. Chong, R. de Hoogt, and R. Graeser. Capturing tumor complexity in vitro: Comparative analysis of 2d and 3d tumor models for drug discovery. *Sci Rep*, 6:28951, 2016. ISSN 2045-2322 (Electronic) 2045-2322 (Linking). doi: 10.1038/srep28951. URL https://www.ncbi.nlm.nih.gov/pubmed/27364600.

[123] X. Xu, M. C. Farach-Carson, and X. Jia. Three-dimensional in vitro tumor models for cancer research and drug evaluation. *Biotechnol Adv*, 32(7):1256–1268, 2014. ISSN 1873-1899 (Electronic) 0734-9750 (Linking). doi: 10.1016/j.biotechadv.2014.07.009. URL https://www.ncbi.nlm.nih.gov/pubmed/25116894.

[124] N. Menon, H. X. Dang, U. S. Datla, M. Moarefian, C. B. Lawrence, C. A. Maher, and C. N. Jones. Heparin-based hydrogel scaffolding alters the transcriptomic profile and increases the chemoresistance of mda-mb-231 triple-negative breast cancer cells. *Biomater Sci*, 8(10):2786–2796, 2020. ISSN 2047-4849 (Electronic) 2047-4830 (Linking). doi: 10.1039/c9bm01481k. URL https://www.ncbi.nlm.nih.gov/pubmed/32091043.

[125] D. J. Newman and G. M. Cragg. Natural products as sources of new drugs over the

last 25 years. *J Nat Prod*, 70(3):461–77, 2007. ISSN 0163-3864 (Print) 0163-3864. doi: 10.1021/np068054v.

[126] Nilesh Rai, Priyanka Kumari Keshri, Ashish Verma, Swapnil C. Kamble, Pradeep Mishra, Suvakanta Barik, Santosh Kumar Singh, and Vibhav Gautam. Plant associated fungal endophytes as a source of natural bioactive compounds. *Mycology*, pages 1–21, 2021. ISSN 2150-1203. doi: 10.1080/21501203.2020.1870579. URL https://doi.org/10.1080/21501203.2020.1870579.

[127] Sanjana Kaul, Suruchi Gupta, Maroof Ahmed, and Manoj K. Dhar. Endophytic fungi from medicinal plants: a treasure hunt for bioactive metabolites. *Phytochemistry Reviews*, 11(4):487–505, 2012. ISSN 1572-980X. doi: 10.1007/s11101-012-9260-6. URL https://doi.org/10.1007/s11101-012-9260-6.

[128] J. Pena-Bahamonde, H. N. Nguyen, S. K. Fanourakis, and D. F. Rodrigues. Recent advances in graphene-based biosensor technology with applications in life sciences. *J Nanobiotechnology*, 16(1):75, 2018. ISSN 1477-3155 (Electronic) 1477-3155 (Linking). doi: 10.1186/s12951-018-0400-z. URL https://www.ncbi.nlm.nih.gov/pubmed/30243292.

[129] M. Pirzada and Z. Altintas. Nanomaterials for healthcare biosensing applications. *Sensors (Basel)*, 19(23), 2019. ISSN 1424-8220 (Electronic) 1424-8220 (Linking). doi: 10.3390/s19235311. URL https://www.ncbi.nlm.nih.gov/pubmed/31810313.

[130] E. A. Jares-Erijman and T. M. Jovin. Fret imaging. *Nature Biotechnology*, 21(11): 1387–1395, 2003. ISSN 1087-0156. doi: 10.1038/nbt896. URL <GotoISI>://WOS:000186320000042.

[131] S. L. Figenschau, E. Knutsen, I. Urbarova, C. Fenton, B. Elston, M. Perander, E. S. Mortensen, and K. A. Fenton. Icam1 expression is induced by proinflammatory cy-

tokines and associated with tls formation in aggressive breast cancer subtypes. *Sci Rep*, 8(1):11720, 2018. ISSN 2045-2322 (Electronic) 2045-2322 (Linking). doi: 10.1038/s41598-018-29604-2. URL https://www.ncbi.nlm.nih.gov/pubmed/30082828.

[132] Z. G. Fridlender, J. Sun, S. Kim, V. Kapoor, G. Cheng, L. Ling, G. S. Worthen, and S. M. Albelda. Polarization of tumor-associated neutrophil phenotype by tgf-beta: "n1" versus "n2" tan. *Cancer Cell*, 16(3):183–94, 2009. ISSN 1878-3686 (Electronic) 1535-6108 (Linking). doi: 10.1016/j.ccr.2009.06.017. URL https://www.ncbi.nlm.nih.gov/pubmed/19732719.

[133] N. T. Chen, S. H. Cheng, C. P. Liu, J. S. Souris, C. T. Chen, C. Y. Mou, and L. W. Lo. Recent advances in nanoparticle-based forster resonance energy transfer for biosensing, molecular imaging and drug release profiling. *International Journal of Molecular Sciences*, 13(12):16598–16623, 2012. ISSN 1422-0067. doi: 10.3390/ijms131216598. URL <GotoISI>://WOS:000312608100066.

[134] T. R. Kuang, L. Q. Chang, X. F. Peng, X. L. Hu, and D. Gallego-Perez. Molecular beacon nano-sensors for probing livinc cancer cells. *Trends in Biotechnology*, 35(4):347–359, 2017. ISSN 0167-7799. doi: 10.1016/j.tibtech.2016.09.003. URL <GotoISI>://WOS:000398870500010.

[135] Khlebtsov N. Dykman, L. Gold nanoparticles in biomedical applications (1st ed.). page 352, 2017. doi: https://doi.org/10.1201/b22465.

[136] Mir Hadi Jazayeri, Hamed Amani, Ali Akbar Pourfatollah, Hamidreza Pazoki-Toroudi, and Bijan Sedighimoghaddam. Various methods of gold nanoparticles (gnps) conjugation to antibodies. *Sensing and Bio-Sensing Research*, 9:17–22, 2016. ISSN 2214-1804. doi: https://doi.org/10.1016/j.sbsr.2016.04.002. URL https://www.sciencedirect.com/science/article/pii/S2214180416300344.

[137] S. Chatterjee, J. B. Lee, N. V. Valappil, D. Luo, and V. M. Menon. Investigating the distance limit of a metal nanoparticle based spectroscopic ruler. *Biomed Opt Express*, 2(6):1727–33, 2011. ISSN 2156-7085 (Electronic) 2156-7085 (Linking). doi: 10.1364/BOE.2.001727. URL https://www.ncbi.nlm.nih.gov/pubmed/21698032.

[138] J. Griffin, A. K. Singh, D. Senapati, P. Rhodes, K. Mitchell, B. Robinson, E. Yu, and P. C. Ray. Size- and distance-dependent nanoparticle surface-energy transfer (nset) method for selective sensing of hepatitis c virus rna. *Chemistry*, 15(2):342–51, 2009. ISSN 1521-3765 (Electronic) 0947-6539 (Linking). doi: 10.1002/chem.200801812. URL https://www.ncbi.nlm.nih.gov/pubmed/19035615.

[139] J. Liu and Q. Peng. Protein-gold nanoparticle interactions and their possible impact on biomedical applications. *Acta Biomater*, 55:13–27, 2017. ISSN 1878-7568 (Electronic) 1742-7061 (Linking). doi: 10.1016/j.actbio.2017.03.055. URL https://www.ncbi.nlm.nih.gov/pubmed/28377307.

[140] D. Deng, D. Zhang, Y. Li, S. Achilefu, and Y. Gu. Gold nanoparticles based molecular beacons for in vitro and in vivo detection of the matriptase expression on tumor. *Biosens Bioelectron*, 49:216–21, 2013. ISSN 1873-4235 (Electronic) 0956-5663 (Linking). doi: 10.1016/j.bios.2013.05.018. URL https://www.ncbi.nlm.nih.gov/pubmed/23770391.

[141] T. L. Jennings, M. P. Singh, and G. F. Strouse. Fluorescent lifetime quenching near d = 1.5 nm gold nanoparticles: probing nset validity. *J Am Chem Soc*, 128(16):5462–7, 2006. ISSN 0002-7863 (Print) 0002-7863 (Linking). doi: 10.1021/ja0583665. URL https://www.ncbi.nlm.nih.gov/pubmed/16620118.

[142] T. Pons, I. L. Medintz, K. E. Sapsford, S. Higashiya, A. F. Grimes, D. S. English, and H. Mattoussi. On the quenching of semiconductor quantum dot photoluminescence by

proximal gold nanoparticles. *Nano Lett*, 7(10):3157–64, 2007. ISSN 1530-6984 (Print) 1530-6984 (Linking). doi: 10.1021/nl071729+. URL https://www.ncbi.nlm.nih.gov/pubmed/17845066.

[143] Niko Hildebrandt Igor Medintz. *FRET – Förster Resonance Energy Transfer*. Wiley, 4 october 2013 edition, 2013. ISBN 9783527656028. doi: 10.1002/9783527656028.

[144] Chi Chen and Niko Hildebrandt. Resonance energy transfer to gold nanoparticles: Nset defeats fret. *TrAC Trends in Analytical Chemistry*, 123:115748, 2020. ISSN 0165-9936. doi: https://doi.org/10.1016/j.trac.2019.115748. URL https://www.sciencedirect.com/science/article/pii/S0165993619305084.

[145] Huilin Tao, Xiufen Liao, Mingze Xu, Xiangli Xie, Fuxin Zhong, and Zhongsheng Yi. Detection of immunoglobulin g based on nanoparticle surface energy transfers from fluorescein isothiocyanate to gold nanoparticles. *Analytical Methods*, 6(8):2560–2565, 2014. ISSN 1759-9660. doi: 10.1039/C3AY41957F. URL http://dx.doi.org/10.1039/C3AY41957F.

[146] A. van de Stolpe and P. T. van der Saag. Intercellular adhesion molecule-1. *J Mol Med (Berl)*, 74(1):13–33, 1996. ISSN 0946-2716 (Print) 0946-2716 (Linking). doi: 10.1007/BF00202069. URL https://www.ncbi.nlm.nih.gov/pubmed/8834767.

[147] P. Guo, J. Huang, L. Wang, D. Jia, J. Yang, D. A. Dillon, D. Zurakowski, H. Mao, M. A. Moses, and D. T. Auguste. Icam-1 as a molecular target for triple negative breast cancer. *Proc Natl Acad Sci U S A*, 111(41):14710–5, 2014. ISSN 1091-6490 (Electronic) 0027-8424 (Linking). doi: 10.1073/pnas.1408556111. URL https://www.ncbi.nlm.nih.gov/pubmed/25267626.

[148] C. Rosette, R. B. Roth, P. Oeth, A. Braun, S. Kammerer, J. Ekblom, and M. F. Denissenko. Role of icam1 in invasion of human breast cancer cells. *Carcinogenesis*, 26

(5):943–50, 2005. ISSN 0143-3334 (Print) 0143-3334 (Linking). doi: 10.1093/carcin/bgi070. URL https://www.ncbi.nlm.nih.gov/pubmed/15774488.

[149] J. Erbo Christensen, S. Ørding Andreasen, J. Pravsgaard Christensen, and A. Randrup Thomsen. Cd11b expression as a marker to distinguish between recently activated effector cd8+ t cells and memory cells. *International Immunology*, 13(4):593–600, 2001. ISSN 0953-8178. doi: 10.1093/intimm/13.4.593. URL https://doi.org/10.1093/intimm/13.4.593.

[150] W. A. Lynn, C. R. Raetz, N. Qureshi, and D. T. Golenbock. Lipopolysaccharide-induced stimulation of cd11b/cd18 expression on neutrophils. evidence of specific receptor-based response and inhibition by lipid a-based antagonists. *J Immunol*, 147(9):3072–9, 1991. ISSN 0022-1767 (Print) 0022-1767 (Linking). URL https://www.ncbi.nlm.nih.gov/pubmed/1717586.

[151] J. Jamsa, V. Huotari, E. R. Savolainen, H. Syrjala, and T. Ala-Kokko. Kinetics of leukocyte cd11b and cd64 expression in severe sepsis and non-infectious critical care patients. *Acta Anaesthesiol Scand*, 59(7):881–91, 2015. ISSN 1399-6576 (Electronic) 0001-5172 (Linking). doi: 10.1111/aas.12515. URL https://www.ncbi.nlm.nih.gov/pubmed/25866876.

[152] S. Khan, A. Gupta, N. C. Verma, and C. K. Nandi. Kinetics of protein adsorption on gold nanoparticle with variable protein structure and nanoparticle size. *J Chem Phys*, 143(16):164709, 2015. ISSN 1089-7690 (Electronic) 0021-9606 (Linking). doi: 10.1063/1.4934605. URL https://www.ncbi.nlm.nih.gov/pubmed/26520545.

[153] D. N. Breslauer, P. J. Lee, and L. P. Lee. Microfluidics-based systems biology. *Mol Biosyst*, 2(2):97–112, 2006. ISSN 1742-206X (Print) 1742-2051 (Linking). doi: 10.1039/b515632g. URL https://www.ncbi.nlm.nih.gov/pubmed/16880927.

[154] Amy E. Herr, Anson V. Hatch, Daniel J. Throckmorton, Huu M. Tran, James S. Brennan, William V. Giannobile, and Anup K. Singh. Microfluidic immunoassays as rapid saliva-based clinical diagnostics. *Proceedings of the National Academy of Sciences*, 104(13):5268, 2007. doi: 10.1073/pnas.0607254104. URL http://www.pnas.org/content/104/13/5268.abstract.

[155] D. Kim, X. Wu, A. T. Young, and C. L. Haynes. Microfluidics-based in vivo mimetic systems for the study of cellular biology. *Acc Chem Res*, 47(4):1165–73, 2014. ISSN 1520-4898 (Electronic) 0001-4842 (Linking). doi: 10.1021/ar4002608. URL https://www.ncbi.nlm.nih.gov/pubmed/24555566.

[156] I. M. Lazar, P. Trisiripisal, and H. A. Sarvaiya. Microfluidic liquid chromatography system for proteomic applications and biomarker screening. *Anal Chem*, 78(15):5513–24, 2006. ISSN 0003-2700 (Print) 0003-2700 (Linking). doi: 10.1021/ac060434y. URL https://www.ncbi.nlm.nih.gov/pubmed/16878890.

[157] J. S. Marcus, W. F. Anderson, and S. R. Quake. Microfluidic single-cell mrna isolation and analysis. *Anal Chem*, 78(9):3084–9, 2006. ISSN 0003-2700 (Print) 0003-2700 (Linking). doi: 10.1021/ac0519460. URL https://www.ncbi.nlm.nih.gov/pubmed/16642997.

[158] A. D. Hargis, J. P. Alarie, and J. M. Ramsey. Characterization of cell lysis events on a microfluidic device for high-throughput single cell analysis. *Electrophoresis*, 32(22):3172–9, 2011. ISSN 1522-2683 (Electronic) 0173-0835 (Linking). doi: 10.1002/elps.201100229. URL https://www.ncbi.nlm.nih.gov/pubmed/22025127.

[159] A. M. Streets, X. Zhang, C. Cao, Y. Pang, X. Wu, L. Xiong, L. Yang, Y. Fu, L. Zhao, F. Tang, and Y. Huang. Microfluidic single-cell whole-transcriptome sequencing. *Proc Natl Acad Sci U S A*, 111(19):7048–53, 2014. ISSN 1091-6490 (Electronic) 0027-8424

(Linking). doi: 10.1073/pnas.1402030111. URL https://www.ncbi.nlm.nih.gov/pubmed/24782542.

[160] A. R. Wheeler, W. R. Throndset, R. J. Whelan, A. M. Leach, R. N. Zare, Y. H. Liao, K. Farrell, I. D. Manger, and A. Daridon. Microfluidic device for single-cell analysis. *Anal Chem*, 75(14):3581–6, 2003. ISSN 0003-2700 (Print) 0003-2700 (Linking). doi: 10.1021/ac0340758. URL https://www.ncbi.nlm.nih.gov/pubmed/14570213.

[161] M. Chung, J. Ahn, K. Son, S. Kim, and N. L. Jeon. Biomimetic model of tumor microenvironment on microfluidic platform. *Adv Healthc Mater*, 6(15), 2017. ISSN 2192-2659 (Electronic) 2192-2640 (Linking). doi: 10.1002/adhm.201700196. URL https://www.ncbi.nlm.nih.gov/pubmed/28544639.

[162] S. Y. Jeong, J. H. Lee, Y. Shin, S. Chung, and H. J. Kuh. Co-culture of tumor spheroids and fibroblasts in a collagen matrix-incorporated microfluidic chip mimics reciprocal activation in solid tumor microenvironment. *PLoS One*, 11(7):e0159013, 2016. ISSN 1932-6203 (Electronic) 1932-6203 (Linking). doi: 10.1371/journal.pone.0159013. URL https://www.ncbi.nlm.nih.gov/pubmed/27391808.

[163] R. Michna, M. Gadde, A. Ozkan, M. DeWitt, and M. Rylander. Vascularized microfluidic platforms to mimic the tumor microenvironment. *Biotechnol Bioeng*, 115(11):2793–2806, 2018. ISSN 1097-0290 (Electronic) 0006-3592 (Linking). doi: 10.1002/bit.26778. URL https://www.ncbi.nlm.nih.gov/pubmed/29940072.

[164] S. Chung, R. Sudo, V. Vickerman, I. K. Zervantonakis, and R. D. Kamm. Microfluidic platforms for studies of angiogenesis, cell migration, and cell-cell interactions. sixth international bio-fluid mechanics symposium and workshop march 28-30, 2008 pasadena, california. *Ann Biomed Eng*, 38(3):1164–77, 2010. ISSN 1573-

9686 (Electronic) 0090-6964 (Linking). doi: 10.1007/s10439-010-9899-3. URL https://www.ncbi.nlm.nih.gov/pubmed/20336839.

[165] Huipeng Ma, Tingjiao Liu, Jianhua Qin, and Bingcheng Lin. Characterization of the interaction between fibroblasts and tumor cells on a microfluidic co-culture device. *ELECTROPHORESIS*, 31(10):1599–1605, 2010. ISSN 0173-0835. doi: https://doi.org/10.1002/elps.200900776. URL https://analyticalsciencejournals.onlinelibrary.wiley.com/doi/abs/10.1002/elps.200900776.

[166] M. Rothbauer, H. Zirath, and P. Ertl. Recent advances in microfluidic technologies for cell-to-cell interaction studies. *Lab Chip*, 18(2):249–270, 2018. ISSN 1473-0189 (Electronic) 1473-0189 (Linking). doi: 10.1039/c7lc00815e. URL https://www.ncbi.nlm.nih.gov/pubmed/29143053.

[167] D. R. Powell and A. Huttenlocher. Neutrophils in the tumor microenvironment. *Trends Immunol*, 37(1):41–52, 2016. ISSN 1471-4981 (Electronic) 1471-4906 (Linking). doi: 10.1016/j.it.2015.11.008. URL https://www.ncbi.nlm.nih.gov/pubmed/26700397.

[168] A. Mantovani. The yin-yang of tumor-associated neutrophils. *Cancer Cell*, 16(3):173–4, 2009. ISSN 1878-3686 (Electronic) 1535-6108 (Linking). doi: 10.1016/j.ccr.2009.08.014. URL https://www.ncbi.nlm.nih.gov/pubmed/19732714.

[169] A. Mantovani, P. Allavena, A. Sica, and F. Balkwill. Cancer-related inflammation. *Nature*, 454(7203):436–44, 2008. ISSN 1476-4687 (Electronic) 0028-0836 (Linking). doi: 10.1038/nature07205. URL https://www.ncbi.nlm.nih.gov/pubmed/18650914.

[170] M. R. Galdiero, E. Bonavita, I. Barajon, C. Garlanda, A. Mantovani, and S. Jaillon. Tumor associated macrophages and neutrophils in cancer. *Immunobiology*, 218(11):1402–10, 2013. ISSN 1878-3279 (Electronic) 0171-2985 (Linking). doi: 10.1016/j.imbio.2013.06.003. URL https://www.ncbi.nlm.nih.gov/pubmed/23891329.

[171] M. A. Giese, L. E. Hind, and A. Huttenlocher. Neutrophil plasticity in the tumor microenvironment. *Blood*, 133(20):2159–2167, 2019. ISSN 1528-0020 (Electronic) 0006-4971 (Linking). doi: 10.1182/blood-2018-11-844548. URL https://www.ncbi.nlm.nih.gov/pubmed/30898857.

[172] M. E. Shaul, L. Levy, J. Sun, I. Mishalian, S. Singhal, V. Kapoor, W. Horng, G. Fridlender, S. M. Albelda, and Z. G. Fridlender. Tumor-associated neutrophils display a distinct n1 profile following tgfbeta modulation: A transcriptomics analysis of pro- vs. antitumor tans. *Oncoimmunology*, 5(11):e1232221, 2016. ISSN 2162-4011 (Print) 2162-4011 (Linking). doi: 10.1080/2162402X.2016.1232221. URL https://www.ncbi.nlm.nih.gov/pubmed/27999744.